

Dynamic Optimization of Integrated Active-Passive Strategies for Building Enthalpy Control

Dissertation

submitted in partial fulfillment of the requirements for
the degree of

Doctor of Philosophy

in

Building Performance and Diagnostics
School of Architecture

Rongpeng Zhang

B.S., Mechanical Engineering, Tongji University, 2006

M.S., Mechanical Engineering, Tongji University, 2009

Carnegie Mellon University
Pittsburgh, PA, USA

May 2014

CARNEGIE MELLON UNIVERSITY

College of Fine Arts
School of Architecture

Dissertation

Submitted in Partial Fulfillment of the requirements for the degree of

DOCTOR OF PHILOSOPHY

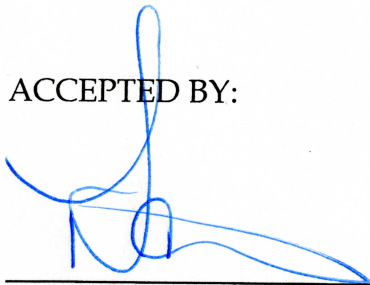
TITLE:

**Dynamic Optimization of Integrated Active-Passive Strategies for
Building Enthalpy Control**

PRESENTED BY:

Rongpeng Zhang

ACCEPTED BY:

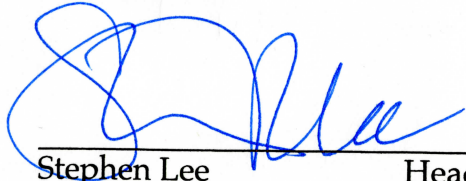


Dan Martin

Dean

5/13/2014

DATE



Stephen Lee

Head of School

2014.05.13

DATE

CARNEGIE MELLON UNIVERSITY

School of Architecture
College of Fine Arts

Dissertation

Submitted in Partial Fulfillment of the requirements for the degree of

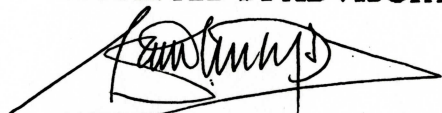
Doctor of Philosophy

TITLE:

**Dynamic Optimization of Integrated Active-Passive Strategies for
Building Enthalpy Control**

PRESENTED BY: Rongpeng Zhang

ACCEPTED BY ADVISORY COMMITTEE:



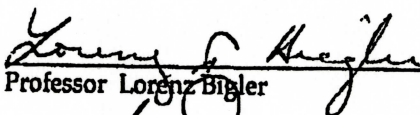
Professor Khee Poh Lam Principal Advisor

May 9, 2014
DATE



Professor Laura Schaefer Advisor

May 9, 2014
DATE



Professor Lorenz Bigler Advisor

May 9, 2014
DATE



Dr. Trevor Bailey Advisor

May 9, 2014
DATE

Dynamic Optimization of Integrated Active-Passive Strategies for Building Enthalpy Control

By

Rongpeng Zhang

School of Architecture, Carnegie Mellon University
Pittsburgh, PA, USA

Advisory Committee

Khee Poh Lam (Chair)

Ph.D., RIBA, Professor of Architecture
Carnegie Mellon University
Pittsburgh, PA, USA

Laura A. Schaefer

Ph.D., Professor of Mechanical Engineering
University of Pittsburgh
Pittsburgh, PA, USA

Lorenz T. Biegler

Ph.D., Bayer University Professor of Chemical Engineering
Carnegie Mellon University
Pittsburgh, PA, USA

Trevor E. Bailey

Ph.D., Climate Controls & Security Program Lead
United Technologies Research Center
East Hartford, CT, USA

May 2014

A dissertation submitted in partial fulfillment of the requirements for the Degree of Doctor of Philosophy
in Building Performance and Diagnostics
School of Architecture, Carnegie Mellon University

Copyright Declaration

I hereby declare that I am the sole author of this thesis.

I authorize Carnegie Mellon University, Pittsburgh, PA, USA to lend this thesis to other institutions or individuals for the purpose of scholarly research.

I authorize Carnegie Mellon University, Pittsburgh, PA, USA to reproduce this thesis by photocopying or by other means, in total or in part, at the request of other institutions or individuals for the purpose of scholarly research.

Copyright© Rongpeng Zhang, 2014. All rights reserved.

Dedicate to my mother and my motherland!



Rongpeng Zhang

School of Architecture, Carnegie Mellon University

Pittsburgh, PA, USA May 2014

Acknowledgements

I would like to express my great gratitude to Prof. Khee Poh Lam, for all the academic guidance, financial support, and life suggestions. I learnt from him not only the professional knowledge but also the method and attitude to conduct research. He also provided me extensive opportunities to be involved in various types of projects, which greatly broadened my horizons and enriched my experience. I feel very lucky to be a member in his group for five years. Moreover, I appreciate all the New-Year-Eve parties and Thanksgiving dinners held in his lovely house.

I would also like to express my sincere appreciations to my co-advisors, Prof. Laura Schaefer, Prof. Lorenz Biegler, and Dr. Trevor Bailey. Prof. Schaefer provided me with valuable comments and advice on the physical model development part of the thesis, with her deep understanding of building mechanical systems and heat and moisture transfer. Prof. Biegler introduced me to the wonderful world of dynamic optimization, which played a key role in analyzing and solving the thesis problem. I really appreciate his patience and insight in guiding my work. Dr. Trevor provided critical guidance on the selection of this research topic and the formulation of the methods. His unique industry experience on building energy systems and intelligent buildings has highly improved my understanding of the current market demands. Without their diverse professional advice, inspiring comments and continuous support, the completion of this multi-disciplinary research would be impossible.

My special thanks are given to Dr. Yisu Nie for working with me on the formulation and implementation of the dynamic optimization in the thesis. I also quite cherish all the joyous hours we shared on the tennis and squash courts! My deep thanks also go to Dr. Omer Karaguzel, for our cooperation on the building energy system modeling and co-simulations, as well as all the impressive career, political and life discussions!

I thank all the other good friends at Carnegie Mellon University, especially those in the Intelligent Workplace (IW) and Center for Advanced Decision-making (CAPD). Without our friendship, the picnics, spring travels and hot-pot parties that we enjoyed together, my PhD life cannot be that vivid and colorful! I will store all the wonderful time we experienced together in my heart!

I owe my deepest gratitude to my parents, who have always brought me endless courage and motivations and stood beside me in both the sunny and rainy days. Words are not enough to express my appreciation.

Abstract

The building sector has become the largest consumer of end use energy in the world, exceeding both the industry and the transportation sectors. Extensive types of energy saving techniques have been developed in the past two decades to mitigate the impact of buildings on the environment. Instead of the conventional active building environmental control approaches that solely rely on the mechanical air conditioning systems, increasing attention is given to the passive and mixed-mode approaches in buildings.

This thesis aims to explore the integration of passive cooling approaches and active air conditioning approaches with different dehumidification features, by making effective use of the information on: 1) various dynamic response properties of the building system and mechanical plants, 2) diverse variations of the building boundary conditions over the whole operation process, 3) coupling effect and synergistic influence of the key operational parameters, and 4) numerous parameter conflicts in the integrated active-passive operation. These issues make the proposed integration a complex multifaceted process operation problem. In order to deal with these challenges, a systematic approach is developed by integrating a number of advanced building/system physical models and implementing well-established advanced dynamic optimization algorithms.

Firstly, a reduced-order model development and calibration framework is presented to generate differential-algebraic equations (DAE) based physical building models, by coupling with the high-order building energy simulations (i.e., EnergyPlus) and implementing MLE+

co-simulation programs in the Matlab platform. The reduced-order building model can describe the dynamic building thermal behaviors and address substantial time delay effects intrinsic in the building heat transfer and moisture migration. A calibration procedure is developed to balance the modelling complexity and the simulation accuracy. By making use of the advanced modeling and simulation features of EnergyPlus, the developed computational platform is able to handle real buildings with various geometric configurations, and offers the potential to cooperate with the dominant commercial building modeling software existing in the current AEC industry.

Secondly, the physical model for the active air conditioning systems is developed, which is the other critical part for the dynamic optimization. By introducing and integrating a number of sub-models developed for specific building components, the model is able to specify the dynamic hygrothermal behavior and energy performance of the system under various operating conditions. Two representative air conditioning systems are investigated as the study cases: variable air volume systems (VAV) with mechanical dehumidification, and the desiccant wheel system (DW) with chemical dehumidification. The control variables and constraints representing the system operational characteristics are specified for the dynamic optimization.

Thirdly, the integrated active-passive operations are formulated as dynamic optimization problems based on the above building and system physical models. The simultaneous collocation method is used in the solution algorithm to discretize the state and control variables, translating the optimization formulation into a nonlinear program (NLP). After collocation, the translated NLP problems for the daily integrated VAV/DW operation for a

case zone have 1605/2181 variables, 1485/2037 equality constraints and 280/248 inequality constraints, respectively. It is found that IPOPT is able to provide the optimal solution within minutes using an 8-core 64-bit desktop, which illustrates the efficiency of the problem formulation.

The case study results indicate that the approach can effectively improve the energy performance of the integrated active-passive operations, while maintaining acceptable indoor thermal comfort. Compared to the conventional local control strategies, the optimized strategies lead to remarkable energy saving percentages in different climate conditions: 29.77~48.76% for VAV and 27.85~41.33% for DW. The energy saving is contributed by the improvement of both the passive strategies (around 33%) and active strategies (around 67%). It is found that the thermal comfort constraint defined in the optimization also affects the energy saving. The total optimal energy consumption drops by around 3% if the value of the predicted percentage dissatisfied (PPD) limit is increased by one unit between 5~15%. It is also found that the fitted periodic weather data can lead to similar operation strategies in the dynamic optimization as the realistic data, and therefore can be a reasonable alternative when the more detailed realistic weather data is not available. The method described in the thesis can be generalized to supervise the operation design of building systems with different configurations.

Keywords:

Building Energy Efficiency, Building Enthalpy Control, Integrated Active-Passive Strategies, Air Conditioning and Dehumidification, Dynamic Optimization, Simultaneous Collocation.

Table of Contents

Acknowledgements	iv
Abstract.....	vi
Table of Contents.....	ix
List of Figures	xiv
List of Tables.....	xviii
Nomenclature	xix
CHAPTER 1 INTRODUCTION.....	1
1.1 Research Backgrounds.....	1
1.1.1 Building, energy and environment	1
1.1.2 Green building investigation	2
1.2 Passive Cooling Approaches for Building Energy Saving	3
1.2.1 Internal building mass: a passive indoor environment dampening system	4
1.2.2 Mechanical ventilation with passive cooling sources	5
1.2.3 Literature review of passive cooling approaches	6
1.3 Active Air Conditioning Approaches with Dehumidification Features	9
1.3.1 Building enthalpy control.....	9
1.3.2 Mechanical dehumidification and chemical dehumidification	10

1.3.3	Literature review of active dehumidification approaches	14
1.4	Research Motivations and Purposes	16
1.4.1	Research motivation	16
1.4.2	Research objectives	17
1.5	Challenges of the Integrated Operation Optimization	18
1.5.1	Complexity of the dynamic operation process analysis	18
1.5.2	Coupling effect and synergistic influence of the key parameters	19
1.5.3	Balancing of a large quantity of potential operational conflicts	21
1.5.4	Summary of the Challenges	24
1.6	Proposed Methodology	25
1.6.1	Physical model development	25
1.6.2	Dynamic optimization for process system operation	27
1.7	Thesis Organization	28

CHAPTER 2 REDUCED-ORDER PHYSICAL MODELS FOR BUILDING THERMAL PERFORMANCE EVALUATION.....30

2.1	Overview of the Building Thermal Performance Evaluation	30
2.1.1	Challenges for reduced-order building model development	31
2.1.2	Introduction to high-order building energy simulation	35
2.2	Framework of the Reduced-Order Model Development	39
2.3	Model Reduction for the Cooling Load Components.....	42
2.3.1	Radiative heat gain conversion to building cooling loads.....	42
2.3.2	Heat and moisture migration through external envelopes	48
2.3.3	Thermal storage and moisture buffering in the internal building mass.....	57

2.3.4	Energy and moisture balances for the building zone air	62
2.4	Reduced-order Building Model Calibration by Integrated Simulation	65
2.4.1	Configurations of the case building.....	65
2.4.2	Procedure for the reduced-order model calibration and simulation	69
2.4.3	Optimization formulation for the calibration	73
2.4.4	Calibration results and discussions.....	74
2.4.5	Parameter Sensitivity Analysis and Ranking	79
 CHAPTER 3 PHYSICAL MODELS FOR AIR CONDITIONING SYSTEMS WITH DEHUMIDIFICATION FEATURES		83
3.1	Modeling of Variable Air Volume System: Mechanical Dehumidification.....	83
3.1.1	Introduction to the VAV system operation	83
3.1.2	Performance modeling of the VAV system	85
3.1.3	Control variables in the dynamic optimization for VAV	89
3.1.4	Summary of the key parameters in the VAV system operation	90
3.2	Modeling of Desiccant Wheel System: Chemical Dehumidification.....	91
3.2.1	Introduction to the DW system operation	91
3.2.2	Desiccant wheel performance modeling	94
3.2.3	Performance modeling of the active desiccant wheel	95
3.2.4	Performance modeling of the enthalpy recovery wheel	98
3.2.5	Control variables in the dynamic optimization for DW	101
3.2.6	Summary of the key parameters in the DW system operation	102

**CHAPTER 4 DYNAMIC OPTIMIZATION FORMULATION AND
IMPLEMENTATION..... 104**

4.1	Dynamic Optimization Formulation.....	104
4.1.1	Objectives of the process optimization	104
4.1.2	Constraints for the integrated system operation	105
4.1.3	General form of the dynamic optimization	108
4.2	Solution Approaches for Dynamic Optimization	109
4.2.1	Comparison of methods for dynamic optimization	109
4.2.2	Problem transformation using simultaneous collocation method	111
4.2.3	Selection of nonlinear programming algorithms.....	115
4.3	Optimization Implementation in the GAMS Platform	116
4.4	Summary of the Implementation Configurations	118

**CHAPTER 5 OPTIMAL INTEGRATED OPERATION STRATEGIES AND
ENERGY SAVING POTENTIAL ANALYSIS..... 120**

5.1	Energy Saving Potentials by Dynamic Optimization	121
5.1.1	Steady periodic outdoor condition	121
5.1.2	Energy saving in the VAV air conditioning system.....	123
5.1.3	Energy saving in the DW air conditioning system.....	125
5.2	Optimal Strategies for the Integrated Operation.....	127
5.3	Analysis on the Indoor Temperature and Humidity Profiles.....	131
5.4	Distribution of Predicted Percentage Dissatisfied (PPD) Index	136
5.5	Contribution Analysis for Passive Strategy and Active Strategy	138

5.6	Integrated Operation Strategy Formulation using Realistic Weather Data	140
5.7	Optimization Potential under Various Weather Conditions	143
CHAPTER 6 CONCLUSIONS		148
6.1	Contributions	148
6.2	Summary of Findings	150
6.3	Future Work.....	152
APPENDICES		154
Appendix 1 Empirical model coefficients of the implemented active desiccant wheel		154
Appendix 2 Empirical model coefficients of the implemented enthalpy recovery wheel ...		155
REFERENCES		156

List of Figures

Fig. 1.1 Overview of the energy consumption in the U.S. buildings sector.....	1
Fig. 1.2 Relationship between passive cooling approaches and building indoor environment..	3
Fig. 1.3 Thermal storage and moisture buffering effects of internal building mass	5
Fig. 1.4 Psychrometric comparison of mechanical and chemical dehumidification.....	12
Fig. 1.5 Schematic figure of a typical desiccant wheel	13
Fig. 1.6 Relationship between various aspects involved in the integrated active-passive thermal conditioning system operation	24
Fig. 1.7 Overview of the physical models implemented in the study	26
Fig. 2.1 Major elements related to building thermal performance.....	31
Fig. 2.2 Schematic description of EnergyPlus modeling structure for transparent fenestration definitions.....	34
Fig. 2.3 EnergyPlus integrated simulation manager: correlation between program modules..	36
Fig. 2.4 EnergyPlus interoperability: building modeling information from various supporting tools	38
Fig. 2.5 Flow diagram of reduced-order model development.....	39
Fig. 2.6 Radiation components in the surface heat balance analysis	43
Fig. 2.7 Overview of the procedure for RTS based reduced-order model for radiation cooling load evaluation	47
Fig. 2.8 RTS values corresponding to a group of representative constructions.....	48
Fig. 2.9 Moisture transfer phenomena in the pores of capillary porous materials	50

Fig. 2.10 Illustration of the relationship between various hygrothermal properties	51
Fig. 2.11 Schematic chart of combined heat and moisture transfer in capillary porous materials	53
Fig. 2.12 Overview of the procedure for developing the CTS based reduced-order model for conductive cooling load evaluation through external envelopes.....	54
Fig. 2.13 CTS values corresponding to a group of representative constructions	57
Fig. 2.14 Schematic chart of the Effective Moisture Penetration Depth Model	58
Fig. 2.15 Exterior view (l) and plan layout (r) of the case building	66
Fig. 2.16 Hourly internal occupancy schedule for the building case	68
Fig. 2.17 Hourly internal lighting schedule for the building case	68
Fig. 2.18 Hourly internal equipment schedule for the building case	68
Fig. 2.19 Calibration and simulation procedure for the reduced-order model development ...	69
Fig. 2.20 Relative error distribution of the reduced-order model simulations for one month (July).....	75
Fig. 2.21 Comparison of the cooling load predictions by the EnergyPlus and reduced-order model simulation	76
Fig. 2.22 Comparison of the daily cooling load profiles for four zones	77
Fig. 2.23 Recovered CTS and RTS values in the calibration for one month (July).....	78
Fig. 2.24 Variance contribution of CTS and RTS values for parameter sensitivity analysis and ranking.....	82
Fig. 3.1 Schematic figure of a typical VAV system.....	84
Fig. 3.2 Psychrometric representations of the VAV system operation	85

Fig. 3.3 Flow diagram of the SEMCO FVR 2000 and REV 2250 desiccant wheel system installed in the IW at Carnegie Mellon	93
Fig. 3.4 Schematic charts of the FVR 2000 and REV 2250 desiccant wheel system	93
Fig. 3.5 Psychrometric representations of the DW system operation	94
Fig. 4.1 Summary of solution approaches for dynamic optimization	110
Fig. 4.2 Orthogonal polynomial representations at collocation points on finite elements	113
Fig. 4.3 Programming environment in the GAMS platform	116
Fig. 4.4 Problem solving process in the GAMS platform	117
Fig. 5.1 Schematic illustration of the iterative approach for the initial model condition determination.....	122
Fig. 5.2 Energy consumption of the optimized and conventional operations for VAV	124
Fig. 5.3 Energy consumption distribution by system component within VAV	124
Fig. 5.4 Energy consumption of the optimized and conventional operations for DW	126
Fig. 5.5 Energy consumption distribution by system component within DW	126
Fig. 5.6 Dynamic profiles of air flow rates in the optimized operation strategy for VAV	129
Fig. 5.7 Resulting temperature profiles in the optimized and conventional operations for VAV	132
Fig. 5.8 Resulting humidity ratio profiles in the optimized and conventional operations for VAV	134
Fig. 5.9 Resulting relative humidity profiles in the optimized and conventional operations for VAV	135
Fig. 5.10 Daily PPD distributions during office hours for the VAV operations.....	136
Fig. 5.11 Daily PPD distributions during office hours for the DW operations.....	137

Fig. 5.12 Comparison of energy saving contributed by passive and active strategies in VAV operation.....	139
Fig. 5.13 Comparison of energy saving contributed by passive and active strategies in DW operation.....	139
Fig. 5.14 Comparison of the realistic TMY3 weather data and the fitted periodic weather data	141
Fig. 5.15 Time-step relative error of the simulations using realistic TMY3 and fitted periodic weather data.....	142
Fig. 5.16 Energy consumption of the optimized operation under different climate conditions	145
Fig. 5.17 Energy saving potential of the optimized operation under different climate conditions	145
Fig. 5.18 Optimal air flow rate profiles for the VAV operations in different climate regions	146

List of Tables

Table 1.1 Comparison between the proposed thesis work and related studies	16
Table 2.1 Summary of the physical and operational configurations of the building case	66
Table 2.2 Summary of the external wall configurations of the building case.....	67
Table 2.3 Summary of the fenestration configurations of the building case.....	67
Table 2.4 List of parameters transferred between models/components during the model calibration and simulation	70
Table 3.1 List of the key parameters in the VAV system operation	90
Table 3.2 List of the key parameters in the DW system operation	102
Table 4.1 Interpolation locations of Radau roots as collocation points for various degrees..	111
Table 4.2 Collocation coefficients of three-point Radau roots	118
Table 4.3 Summary of the implementation configurations for daily optimizations for a zone	119
Table 5.1 Comparison of the internal mass temperatures under different strategies	133
Table 5.2 Control parameters corresponding to the improvement of the passive and active strategies.....	138
Table 5.3 Temperature and relative humidity levels for different climate types	144

Nomenclature

A	surface area of the internal mass [m^2]
A_{face}	heat exchanger face area [m^2]
A_T	isothermal moisture capacity [m^3/kg]
$a \sim d$	parameters describing the hygrothermal properties of the material [–]
BE_i	empirical coefficients [–]
B_p	thermal gradient coefficient [K^{-1}]
CE_i	empirical coefficients [–]
C_h	moisture dependent heat storage capacity of the control volume [$\text{J}/\text{m}^3 \cdot \text{K}$]
C_w	moisture dependent moisture capacitance of the control volume [kg/m^3]
$c_0 \dots c_N$	conduction time factors for the surface [–]
c_p	specific heat of air [$\text{J}/\text{kg} \cdot \text{K}$]
D_w	liquid diffusivity [m^2/s]
e_{tol}	fan total efficiency [–]
e_{motor}	motor efficiency [–]
E_t	total solar radiation incident on the external surface [$\text{W}/\text{m}^2 \cdot \text{K}$]
FC_i	empirical coefficients [–]

h_0	convection heat transfer coefficient at the external surface [$\text{W}/\text{m}^2\cdot\text{K}$]
h_M	convective moisture transfer coefficient [$\text{kg} / \text{m}^2\cdot\text{s}$]
h_T	convective heat transfer coefficient [$\text{W}/\text{m}^2\cdot\text{K}$]
h_v	evaporation enthalpy [J/kg]
k^w	thermal conductivity [$\text{W}/(\text{m}\cdot\text{K})$]
M	mass of the internal thermal mass [kg]
\dot{m}_0	mass flow rate of OA [kg/s]
\dot{m}_p	volumetric flow rate of the regeneration air stream [m^3/s]
\dot{m}_r	mass flow rate of RA [kg/s]
\dot{m}_s	mass flow rate of SA [kg/s]
\dot{m}_{inf}	mass flow rate of infiltration [kg/s]
\dot{m}_{vent}	mass flow rate of ventilation [kg/s]
\dot{m}_{sys}	mass flow rate of supply air from air conditioning [kg/s]
N	number of hours that the effect of a radiant/ conductive energy pulse last [h]
N_s	number of time steps in the calibration period [--]
N_z	number of building thermal zones [--]
OA	outdoor air [--]
p	partial vapor pressure [Pa]
$Q_{c,\theta}$	conductive heat gain of the zone for the current hour (θ) [W]

Q_{elec}	electric power corresponding to a certain amount of process air [W]
Q_{nom}	nominal electric power [W]
$Q_{cooling}$	energy consumption rate in the cooling coil [W]
Q_{dw}	energy consumption rate in the desiccant wheels [W]
Q_{fan}	energy consumption rate by fans [W]
Q_r	energy consumption rate by regeneration [W]
$Q_{reheating}$	energy consumption rate in the reheating coil [W]
$Q_{r,\theta}$	radiant cooling load for the current hour (θ) [W]
Q_{shaft}	fan shaft power [W]
Q_{tot}	is the fan power [W]
\dot{Q}_c	conductive cooling load of the zone [W]
\dot{Q}_i	zone internal cooling load [W]
\dot{Q}_r	radiant cooling load of the zone [W]
$\dot{Q}_{h,i,j}$	cooling load at time step i for zone j by the EnergyPlus simulations [W]
$\dot{Q}_{r,i,j}$	cooling load at time step i for zone j by the reduced-order simulations [W]
$\overline{\dot{Q}_j}$	average cooling load during the office hours of the day for zone j [W]
q_c	conductive heat input of the external surface [W]
q_{coil}	coil refrigeration load [kW]

$q_{c,\theta-n}$ conductive heat input of the external surface n hour ago [W]

q_r specific regeneration energy consumption rate [J/kg]

$q_{r,\theta-n}$ radiant heat gain n hour ago [W]

r_0, \dots, r_N radiant time factors for the heat source [--]

RA return air [--]

R_v ideal gas constant [461.52 J/kg·K]

SA supply air [--]

t_1, \dots, t_N the time-step points [--]

T temperature [°C]

T_a temperature of the surrounding air [K]

TC_i empirical coefficients [--]

T_i temperature of the indoor environment [K]

T_m temperature of the internal thermal mass [K]

T_o temperature of the outdoor environment [K]

T_s temperature of the supply air from air conditioning [K]

T_{su} temperature of the air at the material surface [K]

$T_{sol-air}$ sol-air temperature for the external surface [K]

T_{ei} exhaust air inlet dry-bulb temperature [°C]

T_{pi} process air inlet dry-bulb temperature [°C]

T_{po}	process air outlet dry-bulb temperature [$^{\circ}\text{C}$]
U	moisture content of the material [$\text{kg}_w/\text{kg}_{\text{material}}$]
U_o	overall heat transfer coefficient for the surface [$\text{W}/\text{m}^2\cdot\text{K}$]
V_p	process air velocity [m/s]
V_p	face velocity of the regeneration (and process) air stream [m/s]
V_{nom}	nominal volumetric flow rate of process air [m^3/s]
V_z	zone space volume [m^3]
W_a	humidity ratio of the surrounding air [$\text{kg}_w/\text{kg}_{\text{air}}$]
W_{ei}	exhaust air inlet humidity ratio [$\text{kg}_w/\text{kg}_{\text{air}}$]
W_i	humidity ratio of the indoor environment [$\text{kg}_w/\text{kg}_{\text{air}}$]
W_m	humidity ratio of the internal thermal mass [$\text{kg}_w/\text{kg}_{\text{air}}$]
W_o	humidity ratio of the outdoor environment [$\text{kg}_w/\text{kg}_{\text{air}}$]
W_{pi}	process air inlet humidity ratio [$\text{kg}_w/\text{kg}_{\text{air}}$]
W_{po}	process air outlet humidity ratio [$\text{kg}_w/\text{kg}_{\text{air}}$]
W_s	humidity ratio of the supply air from air conditioning [$\text{kg}_w/\text{kg}_{\text{air}}$]
W_{su}	humidity ratio of the air at the material surface [$\text{kg}_w/\text{kg}_{\text{air}}$]
$W_{su,sat}$	saturated humidity ratio of the air the material surface [$\text{kg}_w/\text{kg}_{\text{air}}$]
w	moisture content [kg/m^3]
w_r	moisture removal rate [kg/s]

\dot{w}_i	moisture addition into zone due to internal operational activities [kg/s]
y	responses, i.e., time-step cooling load [W]
y^*	the cooling loads corresponding to the recovered RTS and CTS values [W]
α	solar absorptance of the external surface [--]
δ	vapor permeability [kg/(m·s·Pa)]
δ_M	effective moisture penetration depth of the material[m]
ε	hemispherical emittance of the external surface [--]
ΔP	design pressure increase [Pa]
μ	vapor diffusion resistance factor [–]
ρ	material/air density [kg/m ³]
$\theta_1, \dots, \theta_P$	parameters to be estimated, i.e., RTS and CTS values [--]
θ_i^*	the recovered RTS and CTS values in the calibration [--]
Σ_θ	covariance matrix of the estimated parameters [--]
Σ_y, σ_y	covariance matrix of the responses [--]
τ	time [s]
φ	relative humidity [–]

CHAPTER 1 INTRODUCTION

1.1 Research Backgrounds

1.1.1 Building, energy and environment

The building sector has become the largest consumer of end use energy in the world exceeding both the industry and the transportation sectors. According to the US Department of Energy and the European Parliament and Council, buildings, both commercial and residential, account for about 40% of the total energy consumption in US and Europe (DOE 2011; EPC 2010). Fig. 1.1 shows the detailed composition of the U.S. energy consumption.

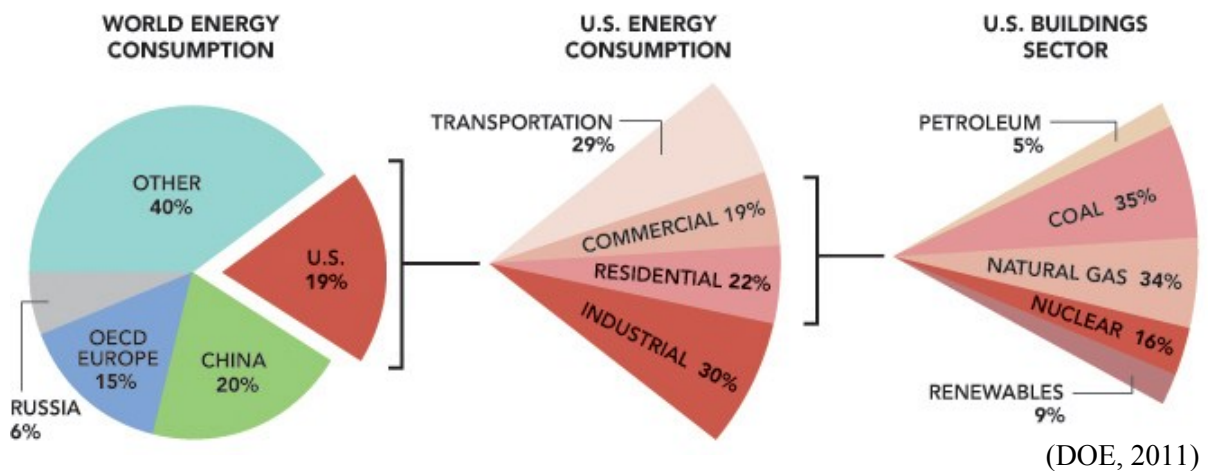


Fig. 1.1 Overview of the energy consumption in the U.S. buildings sector

The huge amount of energy consumption by buildings not only leads to enormous consumption of fossil fuel resources, but also produces severe environmental impacts such as

ozone layer depletion and global warming. It is believed that buildings contribute to almost 40% of the current carbon dioxide emissions in US (DOE 2011) and 36% in Europe (EPC 2010). Moreover, the increasing trend will continue in the next two decades: by 2035, world energy-related carbon dioxide emissions would reach 42.4 billion metric tons, an increase of 43% compared to that in 2007 (EIA 2010).

1.1.2 Green building investigation

In order to mitigate the impact of buildings on the environment, the concept of green building has gradually gained increasing attentions and become the flagship of sustainable development in the past decade. The concept offers an unprecedented opportunity to create energy efficient buildings by using an integrated approach of design and technology (Ali and Al Nsairat 2009; Zhai 2008). It may significantly contribute to the environment and public health, as well as reduce the operating costs, enhance building indoor thermal environment, and increase the indoor air quality and occupant productivity (Fowler and Rauch 2006).

Energy efficiency is one dominant aspect of green buildings, which indicates the quality of buildings in energy use (Poel, van Cruchten, and Balaras 2007). It is highly dependent on the performance of the building heating, ventilation and air conditioning systems (HVAC), the purpose of which is to provide good thermal comfort and acceptable air quality in the indoor environment. According to the research by World Business Council for Sustainable Development, HVAC systems usually present the highest impact on commercial building energy consumption among all the building systems (WBCSD 2009).

In order to achieve higher building energy efficiency, engineers and scientists have paid extensive attention to the building HVAC system, and a variety of energy saving techniques

have been developed in the past two decades to improve its performance. Instead of the conventional building environmental control approaches that solely rely on the mechanical systems to provide the desired indoor thermal conditions, increasing attention is given to the passive and mixed-mode approaches to gain further energy efficiency (Ma et al. 2012).

1.2 Passive Cooling Approaches for Building Energy Saving

In the study, the investigated passive cooling approach comprises (1) Internal building mass as a passive indoor environment dampening system, and (2) Mechanical ventilation with passive cooling sources. Fig. 1.2 shows the general relationship of the investigated approaches and the building indoor environment.

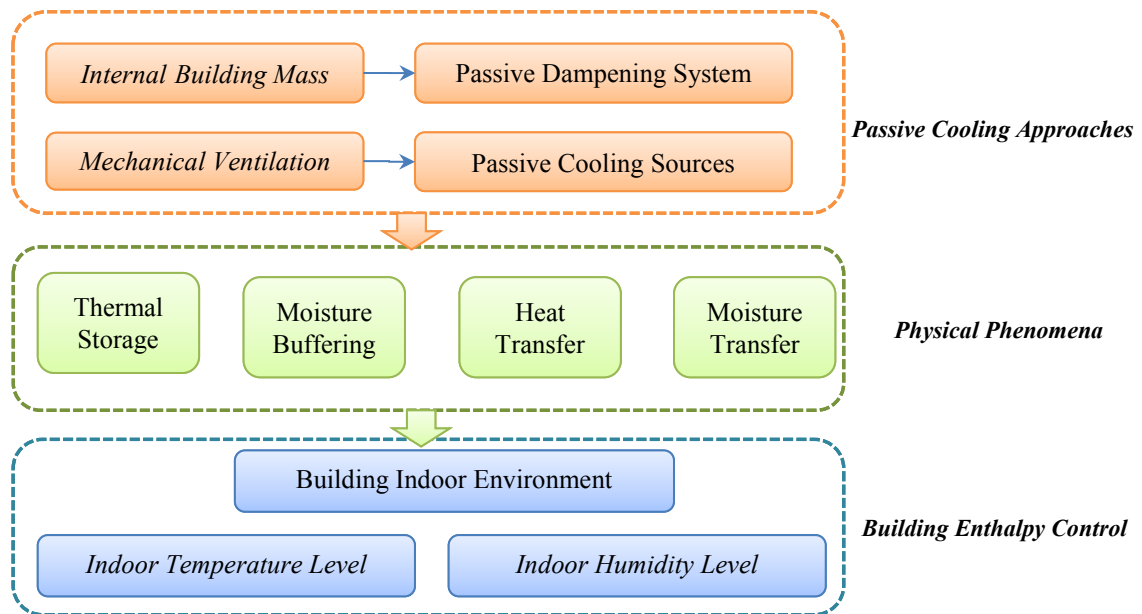


Fig. 1.2 Relationship between passive cooling approaches and building indoor environment

1.2.1 Internal building mass: a passive indoor environment dampening system

Internal building mass comprises the interior furnishing, furniture, walls, ceilings, and floors. It interacts with the indoor thermal environment and the building hygrothermal responses that will occur according to the intrinsic material properties, i.e., thermal storage effect and moisture buffering effect (Khudhair and Farid 2004).

The thermal storage effect describes the ability of internal mass to store heat and dampen/delay the transfer of heat. Combined with other energy saving techniques, such effect can moderate indoor temperature fluctuation under outdoor temperature swings (Brandemuehl, Lepore, and Kreider 1990). Several studies have showed that the potential for storing thermal energy within the internal mass is significant (Braun 1990) and can positively affect energy efficiency (Kosny et al. 1998; Snyder and Newell 1990).

The moisture buffering effect refers to the ability of internal mass to adsorb and desorb moisture from the adjacent indoor air environment (Zhang, Yoshino, and Hasegawa 2012). This effect contributes to moderate the indoor humidity variations and sudden change of indoor moisture level, without active system energy cost (Yang et al. 2012). According to the previous research, moisture buffering materials may account for one third of the indoor moisture load at certain periods, and thus introduce considerable influence on the building indoor environment (Hameury 2005; Tariku, Kumaran, and Fazio 2010).

Due to its thermal storage and moisture buffering effects (Fig. 1.3), internal building mass is considered as a passive system to dampen the indoor fluctuations of humidity and temperature (Hameury 2005; Bornehag, Sundell, and Hägerhed 2003). It can be positively used to stabilize the indoor air conditions and improve thermal comfort, and to reduce peak heating, cooling

and dehumidification load and subsequently building energy consumption (Yang et al. 2012; Hameury 2005).

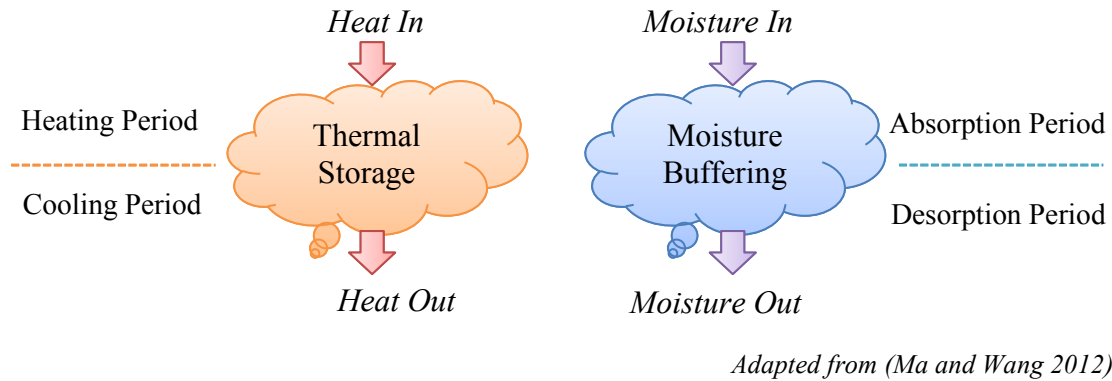


Fig. 1.3 Thermal storage and moisture buffering effects of internal building mass

1.2.2 Mechanical ventilation with passive cooling sources

As one form of passive sustainable building technique, ventilation with passive cooling sources (PCV) has proven effective and energy efficient to transfer heat from buildings to natural heat sinks. It makes use of building thermal mass to store the heat during a warm period and then release it at a later time during the cooler part of the day. In this process, mechanical fans may be used as the driving ventilation component. It can provide significant potential to reduce building cooling load and HVAC energy consumption and good indoor air quality and thermal comfort as an indirect positive outcome (Artmann, Manz, and Heiselberg 2008).

Note that PCV is a passive cooling approach in terms of cooling sources, because it does not operate refrigeration cycles to generate heat sinks. However, it still relies on the electricity driven mechanical fans for ventilation. Hence, it is not a completely passive approach of the term.

1.2.3 Literature review of passive cooling approaches

Researchers have conducted a wide range of investigations on the internal building mass. Some scholars investigated building mass at the material level, such as the characterization of the material hygrothermal property, and the development of experimental methods to evaluate the moisture buffering performance (Zhang, Yoshino, and Hasegawa 2012; Rode et al. 2007). Some scholars studied internal building mass at the room level. For instance, Hameury and Ogoli focused on the dynamical behavior of different types of internal building mass with indoor air environment (Hameury 2005; Ogoli 2003; Li, Fazio, and Rao 2012) ; Yoshino et al. studied the moisture buffering effect of hygrothermal materials in a single room under steady state exterior conditions (Yoshino, Mitamura, and Hasegawa 2009); Zhu, Hurt et al. performed detailed energy saving analyses on thermal mass walls demonstrated in a zero energy house (Zhu et al. 2009). Some scholars focused on the introduction of new construction forms (Corgnati and Kindinis 2007) or materials (Kuznik, Virgone, and Noel 2008) to enhance the hygrothermal performance of the internal building mass.

Researchers have also extensively investigated PCV, especially the night ventilation as one of the most important PCV strategies. Some scholars studied the performance of PCV from an energy conservation point of view. For instance, Blondeau et al. listed the key parameters related to the efficiency of night ventilation and classified them into different categories (Blondeau, Spérandio, and Allard 1997); Geros et al. investigated the influence of the urban environment on the efficiency of night ventilation (Geros et al. 2005). Some scholars studied the feasibility of PCV in different climate regions. For example, Artmann et al. showed that there was significant potential for passive cooling by night ventilation over the whole Europe (Artmann, Manz, and Heiselberg 2007). Some scholars investigated the influence of PCV on

thermal comfort (Breesch and Janssens 2010; Kolokotroni and Aronis 1999; Kolokotroni et al. 2001).

There are also some scholars who focused on the coupling between PCV and internal building mass. Yam et al. presented a theoretical study on the nonlinear coupling between thermal mass and indoor airflow rate using an ideal naturally ventilated building model. Several dimensionless numbers were developed to determine the phase shift and fluctuation of the indoor temperature corresponding to various constant ventilation rates (Yam, Li, and Zheng 2003). Yang et al. and Zhou et al. built the heat transfer model coupling thermal mass and night ventilation, and estimated the impact of external and internal thermal mass on the cooling load reduction respectively (Yang and Li 2008; Zhou et al. 2008). Zhou et al. developed a new virtual sphere method to estimate the impact of thermal mass in natural ventilated buildings (Zhou et al. 2011).

In the previous studies, however, the following three aspects are often not dealt with and need further development.

Firstly, the dynamic process of the buildings is not well considered to support the passive operation strategy design. In the previous studies on the coupling between PCV and internal building mass, fixed or simple index based operating strategies are usually pre-defined for PCV, without sufficiently considering the response properties of the building system. In reality, due to the thermal storage effect and moisture buffering effect of building materials, excitations from the surrounding environment and building equipment may take hours to affect changes to the indoor environment. The variations of the affecting parameters over the whole process (such as the outdoor air temperature and relative humidity) as well as the lag

and decay between various excitations and responses, should be taken into account to fully explore the energy saving potentials contributed by the passive cooling.

Secondly, the passive cooling approaches are usually investigated without considering its integration performance with active air conditioning systems, especially those with enhanced dehumidification features. But in fact, it may be necessary for the passive approaches to integrate with active systems when it is not able to continuously provide acceptable indoor thermal environment under certain weather circumstances. The integrated passive-active operation needs to concurrently address the performance of all the involved systems and their different response properties to offer more options for potential energy saving.

Thirdly, humidity is seldom considered as a parameter in the room-level studies on the performance of passive cooling approaches. Most researchers use outdoor air temperature as the only index to evaluate the climatic potential for PCV without considering the influence of outdoor humidity, and the humidity transfer process is not included in the ventilation model (Yang and Li 2008; Zhou et al. 2008; Artmann, Manz, and Heiselberg 2008; Zhou et al. 2011; Yam, Li, and Zheng 2003; Pfafferott, Herkel, and Jäschke 2003; Wang, Yi, and Gao 2009). However, maintaining the appropriate humidity level for thermal comfort, either by mechanical methods or by chemical methods, consumes significant amount of energy and hence affect the effectiveness of PCV (Mazzei, Minichiello, and Palma 2005; Zhai 2008; Angrisani et al. 2011; Capozzoli et al. 2006; Enshen 2005). According to the previous research, moisture has a much more profound effect on the performance of air conditioning systems when compared with its impact on the heating system performance (El Diasty, Fazio, and Budaiwi 1993; Kerestecioglu, Swami, and Kamel 1989; Wong and Wang 1990). Moreover, the heat and moisture transfer are coupled with each other in both the movement

and storage processes. This means that without considering the moisture conditioning of the building, the actual thermal performance of PCV may be misrepresented and some potential humidity problems may arise.

1.3 Active Air Conditioning Approaches with Dehumidification Features

Passive cooling approaches can provide significant building cooling load reduction and energy saving potential, but may not be sufficient to provide acceptable indoor thermal environment continuously. It may also cause potential humidity problems under certain weather conditions. Therefore, it is commonly necessary to integrate passive approaches with active air conditioning systems to achieve more stable and reliable building enthalpy control.

1.3.1 Building enthalpy control

With an increase in concerns about the building thermal comfort and indoor air quality (IAQ), indoor humidity conditions are gaining greater attentions in the HVAC system design and operation. Compared with the traditional air conditioning system that operates solely based on the indoor temperature conditions, many advanced air conditioning systems aim to implement various techniques to achieve higher building enthalpy control performance, that is, to better maintain both the indoor temperature and humidity levels (Lam et al. 2005; Lengsfeld, Holm, and Krus 2007; Vu et al. 2013).

The importance of maintaining indoor humidity at an appropriate level has been well known. Evidence has indicated that the problem of indoor humidity environment is highly related to many health problems (Sato, Fukayo, and Yano 2003; Fisk, Lei - Gomez, and Mendell 2007; Kishi et al. 2009). It is also believed that moisture is one of the primary causes for the

durability problem observed on building envelopes, since high indoor humidity and condensation can result in excess moisture accumulation in the building structures and deterioration of building components due to corrosion. (Tariku, Kumaran, and Fazio 2011; ASHRAE 2008; De Freitas, Abrantes, and Crausse 1996; Brown et al. 2002). In some cases, moisture would cause mold and mildew growth which affects both the building durability (Tariku, Kumaran, and Fazio 2011) and occupants' health (Cerolini et al. 2009; El Diasty, Fazio, and Budaiwi 1992). Besides, indoor humidity is an important parameter to determine the occupants' perception of indoor air quality (Fang, Clausen, and Fanger 2000) and thermal comfort (Tariku, Kumaran, and Fazio 2011; Fanger 1970).

Moreover, a large number of studies have proven the significance of indoor humidity control in improving the building energy performance. In many regions, ventilation moisture loads exceed sensible loads (Harriman et al. 1997). The level of indoor humidity affects both the thermal performance of building components and the energy efficiency of the HVAC systems (El Diasty, Fazio, and Budaiwi 1993; Harriman, Plager, and Kosar 1999). It has been pointed out that the ignorance of moisture may lead to an misunderstanding of the peak cooling load and overall energy consumption (El Diasty, Fazio, and Budaiwi 1992; Hameury 2005).

Indeed, an imbalance of thermal, moisture, and air quality may yield less energy efficiency and affect the overall building performance (Tariku, Kumaran, and Fazio 2010; Lengsfeld, Holm, and Krus 2007).

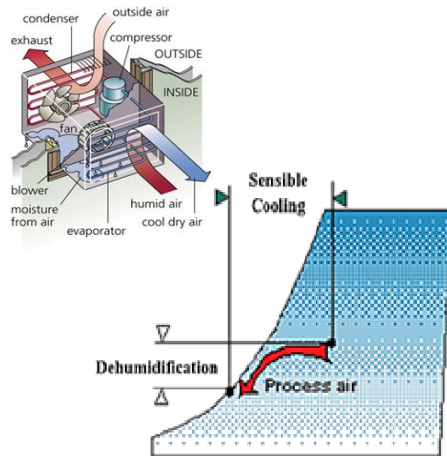
1.3.2 Mechanical dehumidification and chemical dehumidification

The air conditioning products with dehumidification featured in the current HVAC marketplace can be divided into two types: mechanical dehumidification and chemical

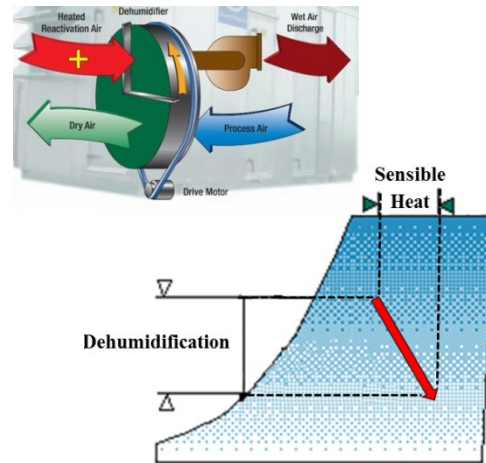
dehumidification. Some systems may implement a combination of both for the operating efficiency improvement or installation cost reduction purposes (ASHRAE 2008; Mazzei, Minichiello, and Palma 2005).

Mechanical dehumidification is the dominant cooling dehumidification approach implemented in the traditional air conditioning systems. In such systems, dehumidification is accomplished by passing the supply air over cooling coils with a surface temperature below the air's dew point. In this way, part of the moisture in the air is condensed onto the coil surfaces and thus a lower level of the absolute moisture content is achieved. One significant feature of this approach is that both the sensible and latent loads are concurrently handled by the coil (Fig. 1.4). However, in order to prevent overcooling the space and provide appropriate indoor temperature control, it is usually necessary to reheat the sub-cooled supply air before supplying it into the space, which leads to extra energy consumption. Meanwhile, the dehumidification performance of the cooling coil is usually limited and thus the indoor humidity control ability of the system may be unsatisfactory (Zhai et al. 2005; ASHRAE 2008; Angrisani et al. 2010).

Compared with mechanical dehumidification, **chemical dehumidification** is usually regarded as a more durable, effective and energy efficient approach to achieve enhanced indoor humidity control. It is typically accomplished via desiccant wheels, which contains high affinity materials to attract moisture. Given the energy, environment and cost benefits provided by the desiccant wheel, it has gained increasing attention from the HVAC engineers and building owners and become one of the most common types in commercial applications (Ge et al. 2008; ASHRAE 2008; Zhai et al. 2005; Angrisani et al. 2010).



Mechanical Dehumidification



Chemical Dehumidification

<http://www.everything-ice.com/>

Fig. 1.4 Psychrometric comparison of mechanical and chemical dehumidification

Differing from the traditional air conditioning system relying solely on mechanical dehumidification, the desiccant wheel system (including the enthalpy recovery wheel and active desiccant dehumidification wheel) removes the latent load from the coils by separating the dehumidification process with the cooling process (Fig. 1.4). It does not need the sub-cooling and reheating steps and thus avoids the extra energy consumption and the potential indoor air quality problems caused by condensation. It is also believed that the system can achieve better indoor humidity control due to the enhanced dehumidification performance of the desiccant wheels (Ge et al. 2008; ASHRAE 2008; Angrisani et al. 2010). Some other significant advantages of the desiccant wheel system can be summarized as: (1) adaptability in various climates or environmental conditions, (2) flexibility to cooperate with other air conditioning components, and (3) capability to utilize low-grade thermal energy sources such as solar energy, geothermic energy and waste heat (Daou, Wang, and Xia 2006; ASHRAE 2008; Hatami et al. 2012). Therefore, the desiccant cooling can be either an ideal supplement

to the traditional vapor compression air conditioning technology, or an alternative to it (Daou, Wang, and Xia 2006).

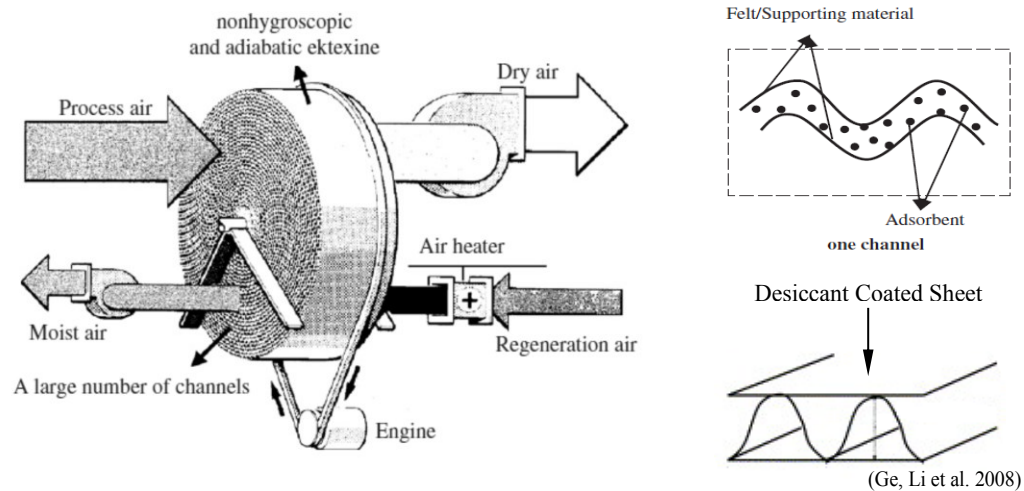


Fig. 1.5 Schematic figure of a typical desiccant wheel

Although desiccant wheels may have various configurations in different applications, the basic components and working principles remain the same. As shown in Fig. 1.5, a typical desiccant wheel is made up of several main components, including the matrix, clapboard, wheel case, and driving motor. There is an air heater in the active desiccant dehumidification wheel system, but not in the enthalpy recovery wheel system. The clapboard divides the cross section of the wheel into two parts: the process air side and the regeneration air side. The case of the wheel consists of a large quantity of channels whose walls are coated with desiccant material (such as silica gel, zeolites, activated alumina, and hygroscopic salts) which performs a key role in the moisture dehumidification of the process air. The motor is used to drive the rotation of the wheel at a specified velocity (Ge et al. 2008; ASHRAE 2008).

When the wheel operates, the humid process air passes through the wheel. The vapor pressure differential between the process air and the desiccant on the wheel drives the moisture content to transfer from the air onto the desiccant by the adsorption process. After becoming loaded with moisture, the desiccant is reactivated by the reactivation air. In this process, the vapor pressure of the material is increased to a level higher than that of the air. With the vapor pressure differential reversed, the moisture content moves from the desiccant to the reactivation air and is carried away from the equipment through the desorption process. During the adsorption process, sensible heat is released, coming from the latent heat of condensation of the removed moisture plus additional chemical heat from the desiccant material. Such heat is called the latent heat of wetting, and it increases the temperature of the process air (and thus the sensible load on the system) and decreases the sorption capacity of the wheel. Therefore, the heat and moisture transfer within the desiccant are coupled and should be simultaneously considered in evaluating the performance of the wheel (Ge et al. 2008; ASHRAE 2008).

1.3.3 Literature review of active dehumidification approaches

Researchers have investigated the evaluation and application of active dehumidification systems, especially the desiccant wheel systems, with a wide range of foci.

Some scholars paid attention to the mathematical modelling and solution methods associated with the fundamental heat and moisture transfer phenomena occurring within the chemical dehumidification, using either analytical approaches (MacLaine-Cross and Banks 1972; Banks 1985) or numerical approaches (Sphaier and Worek 2004; Nia, van Paassen, and Saidi 2006; Zhai 2008). Depending on the research purposes, these models focus on various levels of details with different assumptions.

Several studies focused on the overall performance and impact parameters of the desiccant wheels. For instance, Zhai and Liao investigated the energy consumption and humidity control performance of desiccant wheels in various system configurations, implementing a pre-defined operation schedule (Zhai et al. 2005). Zhang and Zhai et al. investigated the development of unified performance indicators for better evaluate the wheel performance (Zhang and Niu 2002; Zhai 2008). In these investigations, either one dimensional models (Zheng, Worek, and Novosel 1995; Simonson and Besant 1997; Majumdar and Worek 1989) or two dimensional models (Zhang and Niu 2002; Sphaier and Worek 2004) were implemented.

Some scholars conducted research on the improvement of the wheel performance by optimizing the wheel design parameters, such as desiccant and channel wall thicknesses (Majumdar and Worek 1989; Niu and Zhang 2002), airflow channels shapes (Slayzak and Ryan 2000) and regeneration area ratio (Chung, Lee, and Yoon 2009). Other scholars conducted thermodynamic analysis in order to optimize the wheel operation parameters, such as revolution speed (De Antonellis, Joppolo, and Molinaroli 2010) and regeneration temperature (Chung, Lee, and Yoon 2009). There are also some scholars who tried to improve the overall wheel efficiency by introducing new supporting components/systems and various low grade thermal energy sources (Hatami et al. 2012; Ahmed, Kattab, and Fouad 2005; La et al. 2010).

In the previous studies, however, dehumidification is often solely investigated under certain static conditions, without considering its dynamic properties and addressing its interaction with other air conditioning approaches, especially passive and mixed-mode approaches (Nia, van Paassen, and Saidi 2006; Zhai et al. 2005; De Antonellis, Joppolo, and Molinaroli 2010).

Some researchers studied the integration of desiccant wheels and other mechanical systems from system configuration optimization point of view, such as the cooperation with solar collector (Hatami et al. 2012; Ahmed, Kattab, and Fouad 2005) and evaporative cooling system (La et al. 2010), but the building response properties and potential operational conflicts of the involved systems are not fully explored which may lead to further energy saving potentials.

1.4 Research Motivations and Purposes

1.4.1 Research motivation

Table 1.1 Comparison between the proposed thesis work and related studies

Topic Label	A	B	C	D	E	F	G
<i>Yam et al., 2003</i>	●	●	○	●	●	○	○
<i>Enshen, 2005</i>	○	○	●	○	○	○	○
<i>Geros et al., 2005</i>	●	○	○	●	○	○	○
<i>Zhai and Liao, 2005</i>	○	○	●	●	○	●	○
<i>Yang and Li, 2008</i>	●	○	○	●	●	○	○
<i>Zhou et al., 2008</i>	○	●	○	●	●	○	○
<i>Zhai, 2008</i>	○	○	●	●	○	●	○
<i>Dong, 2010</i>	○	○	○	●	○	●	○
<i>Wang et al., 2009</i>	●	○	○	○	●	●	○
<i>Zavala et al. 2009</i>	●	○	○	●	●	○	●
<i>La, Dai et al. 2010</i>	○	○	●	○	○	●	○
<i>Zhou et al., 2011</i>	●	●	○	○	●	○	○
<i>Sheikhi et al. 2012</i>	○	○	○	●	●	●	●
<i>Zhang, 2014</i>	●	●	●	●	●	●	●

Topic Label Note:

A: External Thermal Mass Considered

B: Internal Thermal Mass Considered

C: Humidity Transfer Considered

D: Dynamic Boundary Conditions Explored

E: System response properties addressed

F: Integrated Operation Explored

G: Process Optimization Conducted

Based on the literature review, it is observed that there is a lack of investigation on the design and evaluation of the integrated operation of passive and active building enthalpy control approaches, making effective use of the information on (1) dynamic response properties of the building system, (2) cooling and dehumidification features of the active air conditioning system, and (3) the diverse variations of the building boundary conditions over the whole operation process, as well as properly addressing (1) the cooperation between the active-passive building enthalpy control strategies, and (2) the numerous parameter conflicts in the integrated operations. No mature approach or method is provided to improve the overall efficiency of the integrated system operation taking into account all these issues.

1.4.2 Research objectives

The objective of the thesis is to investigate the integration of passive and active building enthalpy control approaches making effective use of the information on the operational conditions and dynamic system behaviors, and to explore the magnitude of achieved energy efficiency improvement. For this purpose, the thesis aims to present a systematic approach to address the dynamic optimization of the integrated active-passive strategies for building enthalpy control, through:

- Developing differential-algebraic equation (DAE) based physical models describing the operational behavior of both the buildings and the air conditioning systems. For this purpose, a number of sub-models developed for specific building components/phenomena are introduced and integrated, and a reduced-order building model

development framework is established by coupling with the high-order building energy simulations.

- Presenting a dynamic optimization formulation of the integrated operation for the air conditioning systems with different dehumidification features. The simultaneous collocation method is employed in the solution algorithm, translating the dynamic optimization formulation into a nonlinear program, which is then implemented in the GAMS platform and handled by the IPOPT solver.
- Interpreting the optimization results from building physics perspectives to obtain in-depth understanding of the energy saving resulted from the optimization process and to provide more informative support on the design and evaluation of the integrated system.

1.5 Challenges of the Integrated Operation Optimization

To accomplish the proposed research objectives, however, several critical challenges have to be carefully addressed, which can be summarized into the following three categories:

1.5.1 Complexity of the dynamic operation process analysis

The building energy system investigated in the thesis is a dynamic system involving various responsive components and constantly changing building boundary conditions. The time-dependence property of the system presents considerable complexity to the description and analysis of its dynamic behavior.

1.5.1.1 The various response properties of building materials and mechanical plants

The response properties of building materials and mechanical plants are at the heart of the management of building energy systems (Levermore 2000). Because of the thermal storage effect and moisture buffering effect of building materials, excitations from the surrounding environment and building equipment may take hours to cause changes in the building energy system loads, and there may be significant decay between them. In other words, the space sensible and latent cooling load at a specific time is not only related to the system state at that time but also the operation conduction in the prior time period. Hence, the timing for the integrated operation can greatly change the building latent and sensible load curves during the operation process, and thus affect the efficiency of the integrated system and the total energy consumption.

1.5.1.2 The diverse variations of the building boundary conditions over the whole process

To obtain the optimal operation strategy, the variation of the outdoor temperature and humidity level should be thoroughly analyzed for the following reasons. First, high humidity may increase the building latent load and thus the energy consumption for dehumidification, which may consequently offset the energy saving in cooling. In addition, the temperature and humidity levels have a synergistic influence on the performance of desiccant wheels and can lead to different energy consumption. To further complicate the problem, the outdoor air temperature and humidity may have quite diverse combinatory variations as well.

1.5.2 Coupling effect and synergistic influence of the key parameters

In the integrated active-passive operations, there are a large number of physical and operational parameters which may be coupled with each other and generate a synergistic

influence on the component/system performance. Such effect and influence can significantly increase the difficulty of the physical model development and dynamic optimization formulation. More specifically:

1.5.2.1 The coupled heat and moisture transfer and storage in the building mass and desiccant material

The moisture condition of the building material generates considerable effect on its thermal performance by influencing its thermal properties such as thermal conductivity and heat storage capacity. Meanwhile, the temperature condition also affects the moisture properties of the material, such as vapor diffusion coefficient and moisture capacity, and thereby influences the moisture transfer within the hygrothermal material, including the building mass and the desiccant material within the wheels.

1.5.2.2 The synergistic influence of process air property and quantity on the performance of desiccant wheels

As mentioned previously, the latent heat of wetting is released during the adsorption process in the desiccant wheel. This phenomenon further complicates the evaluation of the desiccant wheel performance. On the one hand, the amount of the removed moisture determines the amount of heat release which then increases the temperature of the process air. On the other hand, the increase of the temperature decreases the sorption capacity of the wheel and thus its dehumidification performance. Furthermore, the process air amount determines the face velocity across the wheel which highly affects the heat and moisture transfer inside. Therefore, the property and quantity of the process air generates a synergistic influence on the performance of desiccant wheels and should be simultaneously considered.

1.5.2.3 The combined effect of temperature and relative humidity on creating a satisfactory level of indoor thermal comfort

According to the field tests and the theory of thermal comfort, both temperature and humidity play critical roles in creating desirable thermal environment (Fanger 1970; Hamdi, Lachiver, and Michaud 1999). There are numerous combinations of the temperature and relative humidity levels within the acceptable thermal comfort zone. For example, in the cooling season, occupants prefer warmer temperatures when the environment is kept dry, which in turn may provide energy saving potentials for cooling operations (Fischer and Bayer 2003).

1.5.3 Balancing of a large quantity of potential operational conflicts

In the integrated operation, increase number of the affecting parameters may introduce more potential operational conflicts and thus present more challenging decision-making trade-offs. These potential conflicts need to be carefully handled during the integrated operation.

1.5.3.1 The operational availability of PCV may need to be manipulated to balance the decrease of the sensible cooling load and the increase of the latent cooling load.

Under certain weather conditions with low air temperature and high humidity ratio, PCV mode may store moisture in the building material and thus increase the building latent load during office hours, while cooling the building thermal mass and thus leading to a reduction of the sensible cooling load. So, the operational availability of PCV needs to be well manipulated to balance these two aspects in order to obtain the maximum energy saving over the whole process.

1.5.3.2 The ventilation rates of PCV may need to be manipulated to balance the decrease of energy consumption for cooling and the increase of energy consumption by fans.

PCV may reduce the total cooling load of the coil and thereby reduce its energy consumption. However, the increase of the ventilation amount also requires more support from the ventilation fans and thereby increases the corresponding energy consumption. So, the ventilation rates of PCV need to be well manipulated to balance these two aspects.

1.5.3.3 The operational availability of the operation of desiccant wheels may need to be manipulated to balance the decrease of the energy consumption by the cooling coil and the increase of the energy consumption by the wheel operation

In the operation of desiccant wheels, the reduction of moisture in the process air is offset by the cost of the energy consumption to run the wheel motor and provide the regeneration air. This cost is constant during the operation of desiccant wheels, but the benefit corresponding to the latent cooling load reduction may vary at different times, because the performance of the desiccant wheel is considerably related to the fluctuations of the outdoor condition and variations of the building sensible and latent loads. So, the operational availability of the operation of desiccant wheels needs to be well manipulated to assure that more benefits can be produced than the operation costs.

1.5.3.4 The process air amount in the operation of desiccant wheels may need to be manipulated to balance sensible load increase and latent load decrease

In the desiccant wheels, the reduction of the latent load leads to an increase of the sensible load, because the heat of sorption of moisture removed from the air is converted to sensible heat. The process air amount in the operation of desiccant wheels determines: 1) the face

velocity across the wheel which affects the heat and moisture transfer inside, and 2) the ratio between the bypass air flow and the process air flow which affects the property of the supply air as a mixture of the two flows. The manipulation of the process air amount can change the degree of the sensible load increase and latent load decrease in the process.

1.5.3.5 The setpoints of the indoor air environment may need to be manipulated to balance the sensible cooling load and the latent cooling load.

The indoor temperature and relative humidity setpoints as well as the outdoor weather conditions significantly change the values of the synchronous sensible and latent cooling loads which are highly related to the system efficiency and energy consumption. Furthermore, the indoor setpoints at a specific time can influence the sensible and latent cooling loads at a later time. Therefore, the well-designed setpoints curves taking into account the variations of the building boundary conditions may improve the dynamic balance between the sensible cooling load and the latent cooling load resulting in reduced cooling energy consumption through the overall process.

1.5.4 Summary of the Challenges

Fig. 1.6 summarizes the complex relationship between various aspects involved in the integrated active-passive thermal conditioning system operation. It can be seen that it is a multifaceted process operation problem with a large number of coupling operation parameters and potential conflicts, and the design of the operation strategy is a sophisticated and challenging task that has to concurrently address the complex dynamic process characteristics and physical performance of the integrated system.

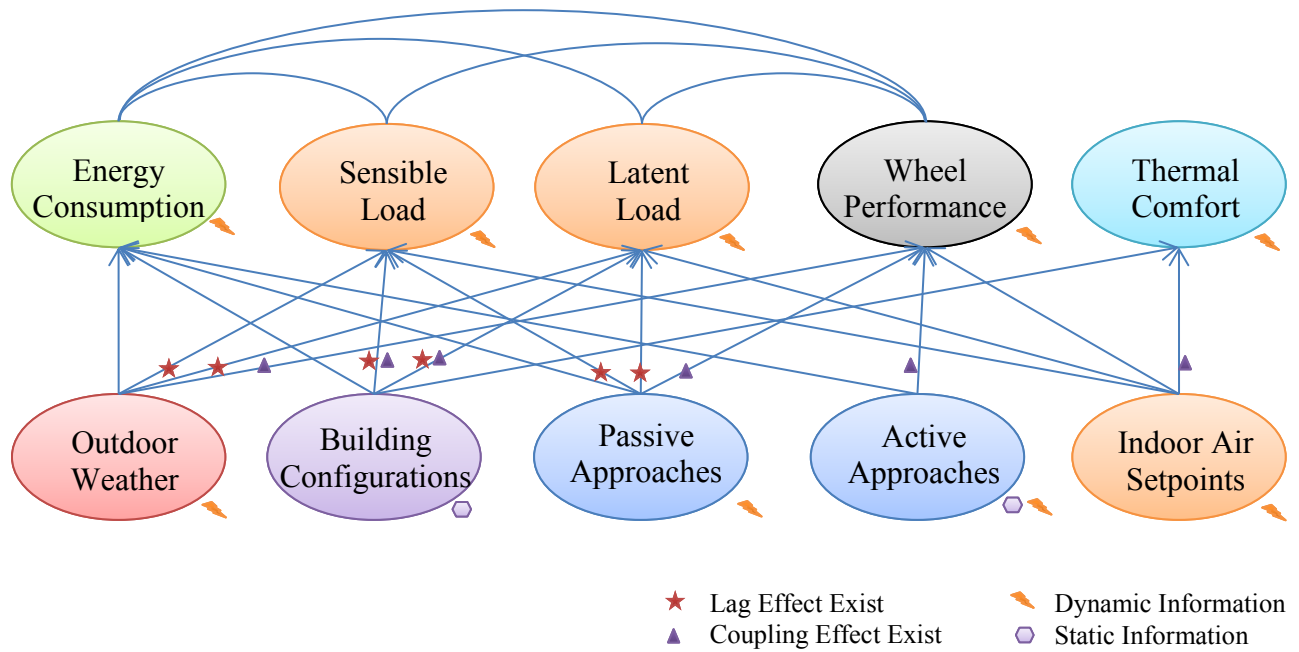


Fig. 1.6 Relationship between various aspects involved in the integrated active-passive thermal conditioning system operation

1.6 Proposed Methodology

In order to overcome the numerous challenges mentioned above, this thesis proposes to develop a systematic approach for the design and evaluation of the integrated active-passive operation, implementing advanced physical system models and process analysis methods. The proposed approach is carried out in two successive steps as described in the sections below.

1.6.1 Physical model development

In the first step, the integrated system is modelled dynamically using differential-algebraic equations.

The formulation consists of differential equations that describe the dynamic behavior of the system such as moisture and energy balances, and algebraic equations that represent the physical and thermodynamic relations. This first-principle based model is essential to conduct the following optimization task. The aim of the physical model is to describe the dynamic process of heat and moisture transfer in the building, as well as the operation behavior of the passive and active air conditioning systems. Instead of being treated as a black box, these physical models have to be specifically described by DAE-based mathematical equations in order to provide the dynamic information essential to perform the optimization. For this purpose, several well-recognized advanced building/system/component models are introduced and integrated, as illustrated in Fig. 1.7.

In order to obtain the reduced-order DAE descriptions of real buildings which may present complex operational and physical characteristics, a computational platform coupling with

high-order model based building energy simulations is developed. It runs EnergyPlus, a simulation engine that has been well tested and recognized, in order to pre-process the input information and support the reduced-order model calibration.

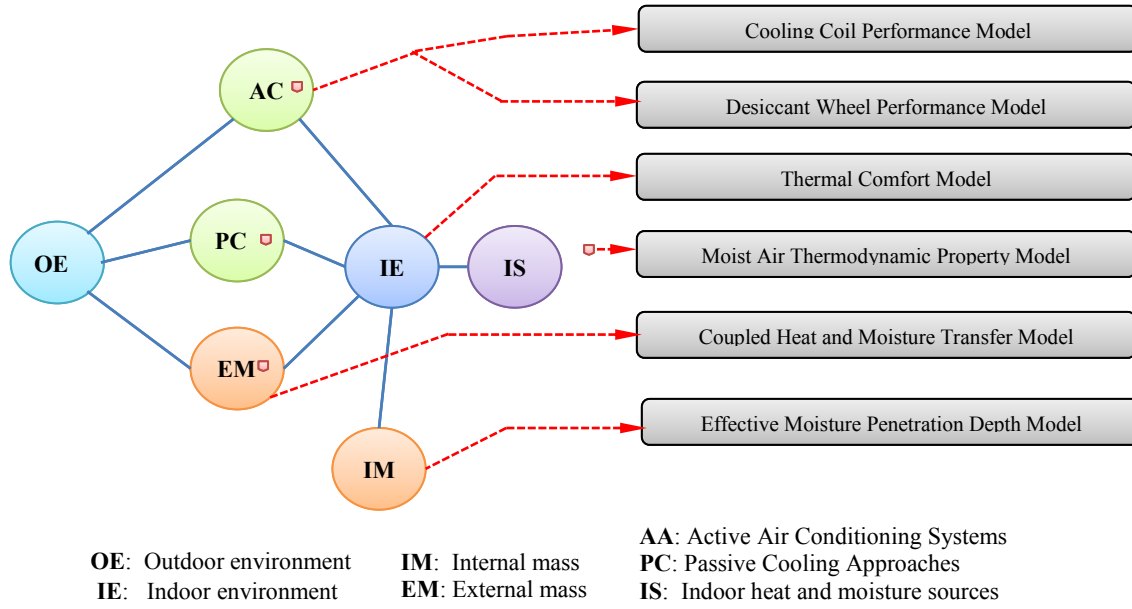


Fig. 1.7 Overview of the physical models implemented in the study

In the physical model, various time-dependent derivative terms are introduced to address the accumulation of heat and moisture in the indoor air environment and internal mass. This makes it a complex dynamic process simulation and optimization problem, which is much more challenging than the steady state simulations from the computational and mathematical perspectives (Schlegel et al. 2005; Rhodes 1996).

1.6.2 Dynamic optimization for process system operation

In the second step, a dynamic optimization formulation is introduced to determine the optimal integrated active-passive operation strategies for building enthalpy control.

The simultaneous collocation method is employed in the optimization algorithm to translate the dynamic optimization problem to a continuous nonlinear programming problem (NLP), which is further solved by the Interior Point Optimizer (IPOPT) that adopts the classic interior point algorithm. This method has been successfully applied to many real-world process optimization problems in various research areas such as Chemical Engineering (Nie, Biegler, and Wassick 2012; Grossmann 2005) and Economics (Gondzio and Grothey 2007; Esteban-Bravo 2008).

Some scholars also applied this method in building energy fields. For example, Zavala et al. established an on-line optimization framework to exploit disturbances of weather conditions for the operation design of a simplified building energy system, and found that more proactive and cost-effective operations can be obtained (Zavala et al. 2009). Sheikhi et al. proposed an optimization model to find the optimal size and operation for combined cooling, heat and power systems, in order to reduce power loss and enhance service reliability of the system (Sheikhi, Ranjbar, and Oraee 2012).

1.7 Thesis Organization

The organization of the thesis is as follows:

Chapter 1 introduces the research background, identifies the research gaps, describes the motivation of the thesis work, establishes the research objectives, and briefly introduces the research methods.

Chapter 2 presents a reduced-order model calibration framework to generate differential-algebraic equations based physical building models, by coupling with the high-order building energy simulations and implementing co-simulation programs. The reduced-order building model can describe the dynamic building thermal behaviors and address substantial time delay effects intrinsic in the building heat transfer and moisture migration.

Chapter 3 explains the development of the physical models for the active air conditioning systems, which are used to specify the dynamic hygrothermal behavior and energy performance of the system under various operating conditions. Two representative air conditioning systems are investigated as case studies: the VAV system implementing mechanical dehumidification, and the DW system implementing chemical dehumidification.

Chapter 4 reports on the dynamic optimization formulation and implementation. A dynamic optimization problem is first presented based the physical model developed in the previous two chapters, and then the simultaneous collocation method is implemented as the solution algorithm to translate the dynamic optimization formulation into an NLP problem, which is

solved by the IPOPT solver in the GAMS platform. The selection and application of the solution approaches, algorithms and solvers is described in this chapter.

Chapter 5 interprets the optimization results from building physics perspectives. The optimal strategies are analyzed in details from different aspects, to obtain in-depth understanding on the optimization results. The influences of the weather data types and the climate regions on the optimization are also explored to support the design and evaluation of the integrated system.

Finally, the conclusions and findings are summarized and the future work is briefly discussed in Chapter 6.

CHAPTER 2 REDUCED-ORDER PHYSICAL MODELS FOR BUILDING THERMAL PERFORMANCE EVALUATION

To conduct the optimization task, it is essential to develop a differential-algebraic equations based physical model describing the operational behavior of both the building and the air conditioning system. The DAE formulation consists of differential equations that describe the dynamic behavior of the building system such as moisture and energy balances, and algebraic equations that ensure physical and thermodynamic relations.

The physical model comprises two parts: (1) the building model for the building thermal performance evaluation as described in this chapter, and (2) the system model for the air conditioning system performance evaluation as described in Chapter 3. These two parts will be integrated together to form a complete physical model to be applied in the operation optimization.

2.1 Overview of the Building Thermal Performance Evaluation

This chapter presents a systematic approach to develop and calibrate the reduced-order building model by coupling with high-order whole building energy simulation model (i.e., EnergyPlus). It is assumed that the high-order building model is well developed and calibrated

via site measurements, and thus can be used as the benchmark of the reduced-order model development (Henninger and Witte 2013).

The reduced-order building model consists of several sub-models for various load components, which will be simulated simultaneously to determine the building transient sensible and latent cooling load.

2.1.1 Challenges for reduced-order building model development

The whole building energy system consists of several major elements that are related to the building thermal performance, including the HVAC system, internal heat/moisture sources, thermal masses and the outdoor and indoor environments. The hygrothermal responses of a building can be considered as the consequences of the dynamic interactions of these elements (Tariku, Kumaran, and Fazio 2010). As shown in Fig. 2.1, these elements are directly or indirectly related and interactive. For example, the changes of outdoor climate conditions can affect both the efficiency of the HVAC system and the hygrothermal properties of building enclosures, which further influence the indoor thermal conditions.

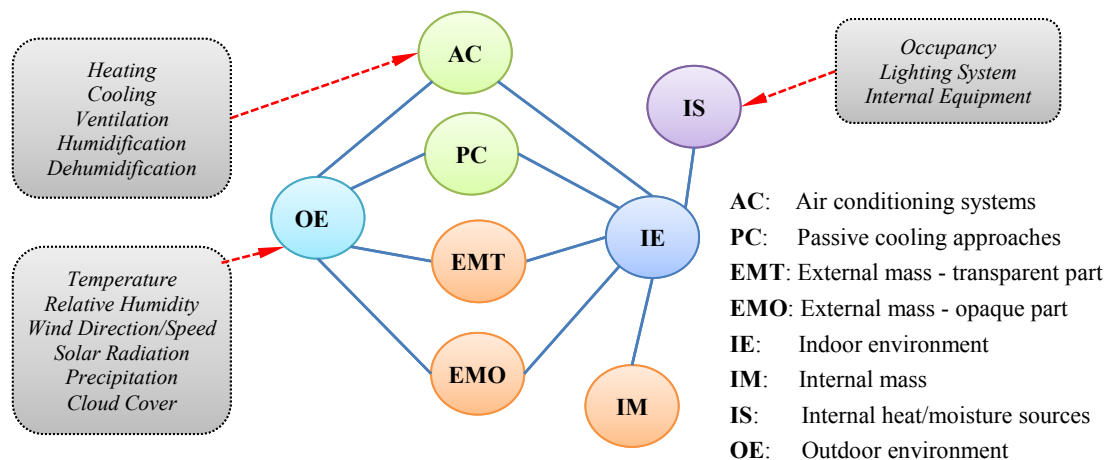


Fig. 2.1 Major elements related to building thermal performance

The underlying basic physical phenomena in the building energy system include the conductive, convective and radiative heat transfer as well as the dependent moisture migration and buffering, which follow the fundamental heat and mass transfer principles. Although the basic transport theory has been well developed, it is quite challenging to build a mathematical building energy system model completely based on the first principles, due to the complexity and diversity inherent in buildings.

Take the solar radiation through a particular window as an example. It involves the following complex processes to accurately estimate the corresponding cooling load. First, it is necessary to obtain the incident solar radiation, which is a date and time dependent variable influenced by the building location, weather conditions, surrounding shading objects, and window surface angle/tilt. Second, the energy transfer through the window has to be quantified, which is related with the size of window, glazing configuration, shading component configuration, and thermal properties of the glazing material. The detailed modeling of this single process may need a large amount of input information, as depicted in Fig. 2.2 (Karaguzel et al. 2013). After this process, the transferred energy consists of direct solar radiation, diffuse solar radiation and conductive heat gains. These three portions should be treated separately in calculating the corresponding cooling loads because they have different transfer mechanisms. More specifically, the radiative part must first be absorbed by the internal room surfaces, and then later transferred by convection from these surfaces to the room air as part of the cooling load. To perform a first-principle based modeling, a detailed surface-by-surface heat balance analysis has to be conducted, in which the calculation of nonlinear radiant heat exchange between surfaces is needed and the collection of extensive information (such as the view

angles between all the surfaces) is required. This is even more demanding when the geometry of the building space is complex and the number of internal surfaces is large.

In the previous research, many scholars developed first-principle based single-zone building models for different research purposes. It is reasonable and may be necessary to implement such lumped building models, especially when the study purpose is to deeply investigate selective building components/features (Yang and Li 2008; Tariku, Kumaran, and Fazio 2010; Lapinskiene and Martinaitis 2013; Qin et al. 2009; Li, Fazio, and Rao 2012; Yoshino, Mitamura, and Hasegawa 2009; Hameury 2005) or to investigate the application of new control/optimization methods for various building energy systems (Wang, Zmeureanu, and Rivard 2005; Calvino et al. 2010; Evins et al. 2012; Li et al. 2013; Smolka 2013; Lee 2007). However, it usually requires tremendous amount of manual work to apply such models for other building spaces with different geometrical characteristics and thermal response properties, and therefore, it may not be widely applied in real building analysis.

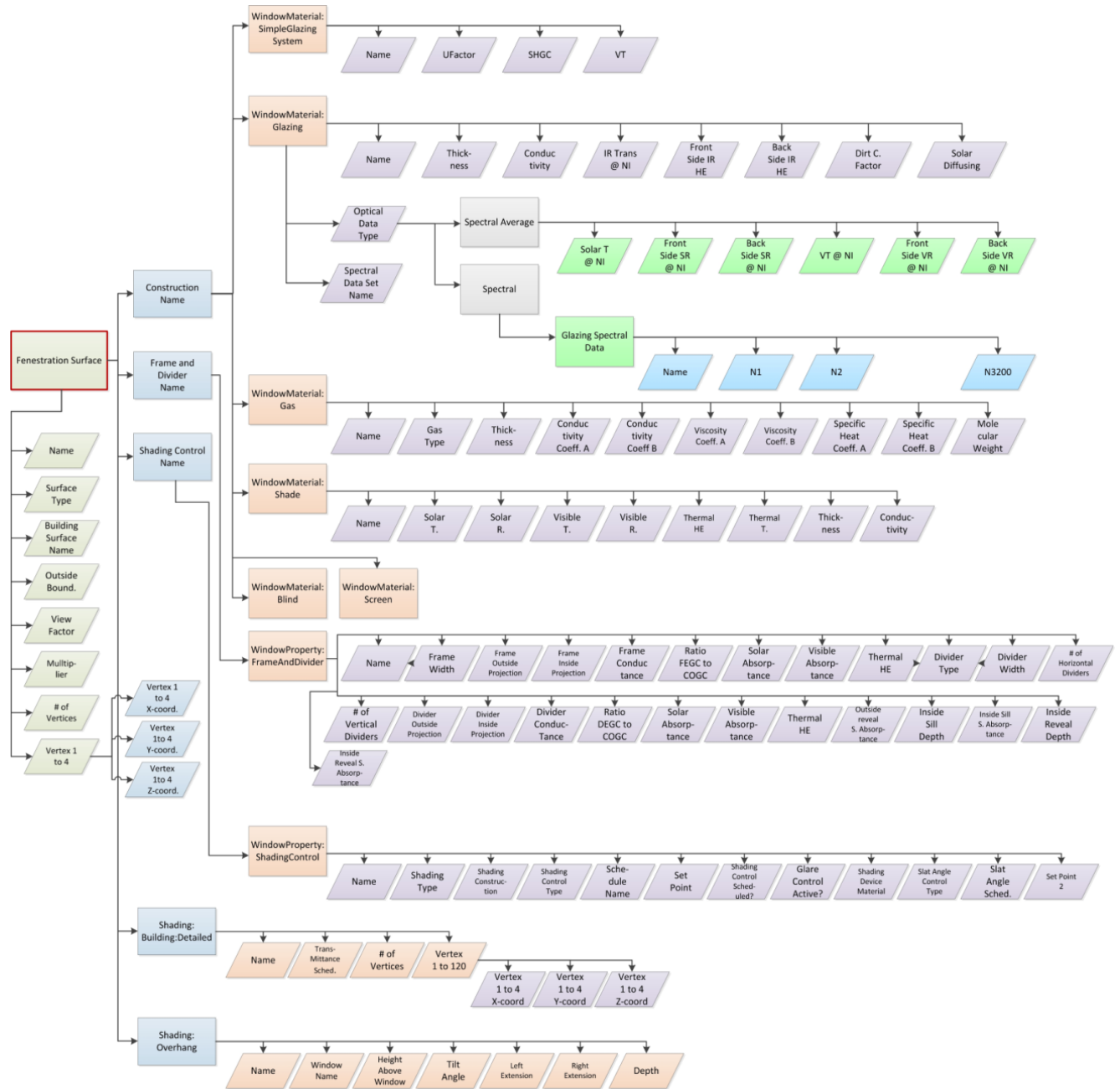


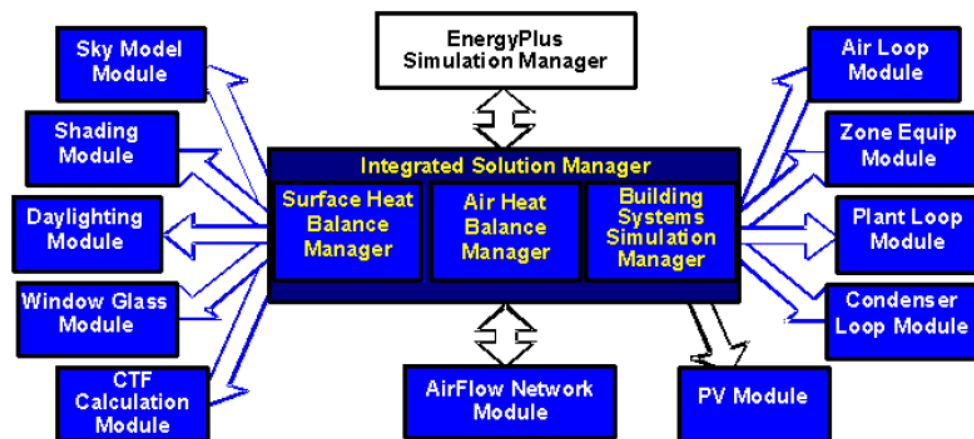
Fig. 2.2 Schematic description of EnergyPlus modeling structure for transparent fenestration definitions

2.1.2 Introduction to high-order building energy simulation

The techniques of whole building energy simulation and building information modeling have gained significant progress in the past two decades, with the help of great advances in the computational power and algorithms. These techniques have a much stronger capability in handling the building energy modeling challenges mentioned above. Although there is still a fair amount of skepticism as to the predictive accuracy of high-order building simulations in the industry, the problem may not be attributed so much to the underlying scientific algorithm of the tools but rather in their proper use and careful checking of the accuracy and reliability of the input. In the thesis, it is assumed that the high-order building models are properly developed and well calibrated, and thus can be used as the benchmark of the reduced-order model development (Henninger and Witte 2013).

Several mature advanced building simulation engines have been developed by different institutions in the past two decades, such as DOE-2 (Winkelmann et al. 1993), BLAST (BSL 1999), EnergyPlus (Crawley et al. 2001; DOE 2013), TRNSYS (Duffy et al. 2009) and DeST (Yan et al. 2008). They have been widely used throughout the world to support the building physics research and the actual new/retrofitting building design, operation and management. Although these engines may implement different modeling methods and/or program structures and thus have different advantages and features, they all share the following common capabilities: 1) to handle the high-order building energy models containing the detailed information about the functional and physical characteristics of the buildings, and 2) to perform co-simulation of a large number of subroutines to obtain more accurate estimations on the heat and mass energy flows throughout the whole building (Crawley et al. 2001).

Among these simulation engines, EnergyPlus, developed by LBNL Simulation Research Group and U.S. DOE, is considered to be a state-of-art and the most widely recognized simulation engine in the building energy efficiency field (DOE 2013; Henninger and Witte 2013; LBNL 2012). As shown in Fig. 2.3, EnergyPlus is a collection of many program modules that can work simultaneously, allowing the real-time interaction among different model components (DOE 2013; Crawley et al. 2001). It has been well tested and validated via a number of research projects (Henninger and Witte 2013).



(Crawley et al. 2001)

Fig. 2.3 EnergyPlus integrated simulation manager: correlation between program modules

As a simulation engine designed for research purposes, EnergyPlus does not have a user-friendly interface, but a fair number of third-party “front-end” programs have been developed to link with EnergyPlus engines for particular tasks (Fig. 2.4). These programs highly facilitate the application of EnergyPlus in the current architecture, engineering and construction (AEC) industry. Moreover, the development of building information modeling

(BIM) further facilitates the process of building energy simulation in the industry, by providing an organized approach to handle the tremendous building information already existing in the traditional building design phase and bridge the gap between the building modeling and simulation platforms (NIBS 2007).

The high-order building energy engine has many great features in terms of simulation capacity and accuracy. However, it can only be treated as a black-box when coupling with other control or optimization programs due to its high level of complexity (Wetter 2011; Karaguzel, Zhang, and Lam 2012). It cannot easily and directly work with the algorithms and methods that require a complete DAE based mathematical description of the physical model. An approach to effectively implement such computational coupling and interoperability has to be developed.

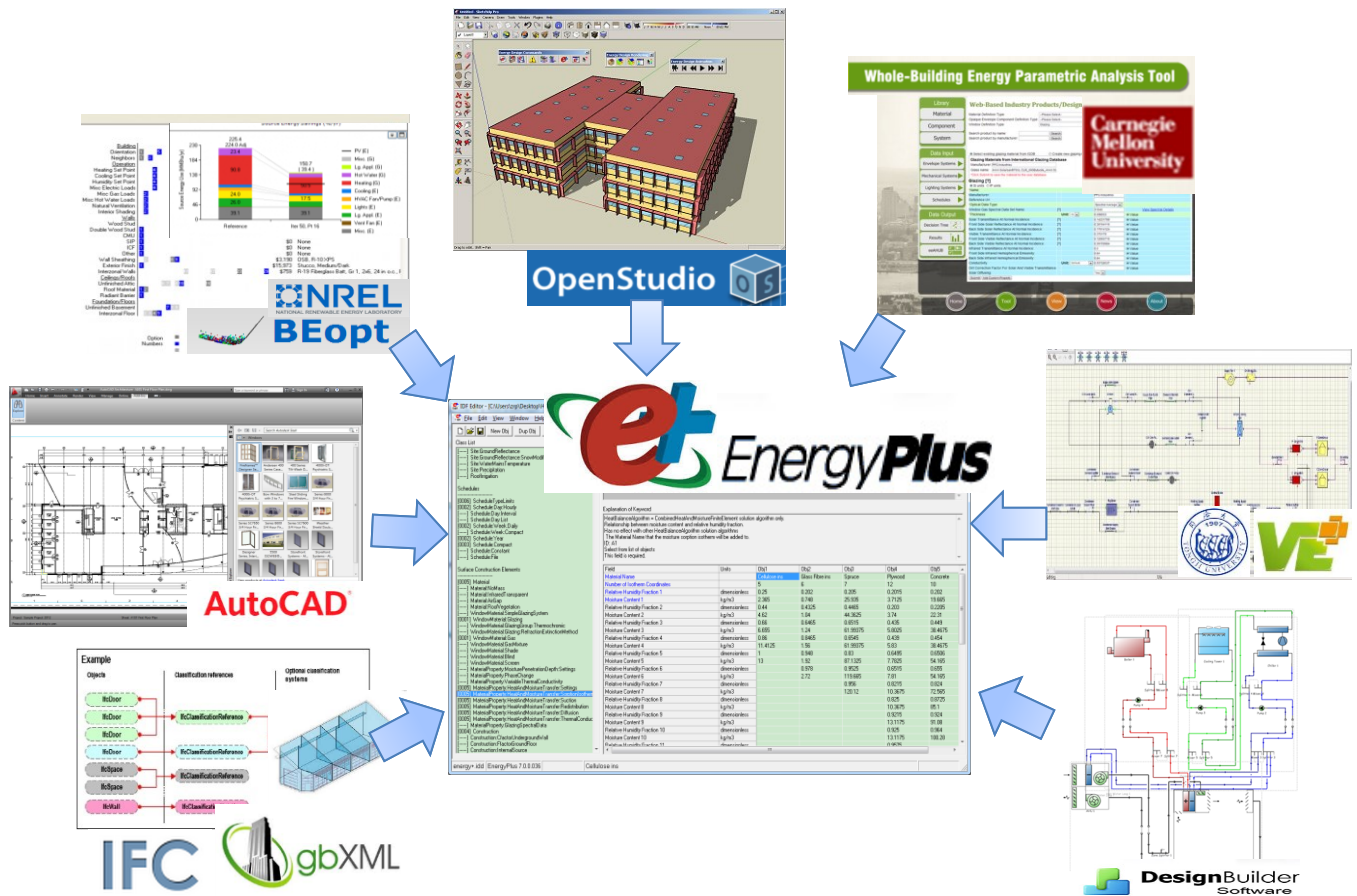


Fig. 2.4 EnergyPlus interoperability: building modeling information from various supporting tools

2.2 Framework of the Reduced-Order Model Development

An approach to develop reduced-order building energy models by coupling with the high-order building energy simulations conducted within EnergyPlus is proposed. It aims to generate DAE descriptions of the building models to support the optimization task, making full use of the high-order building simulation features and capabilities.

The general idea is to extract from EnergyPlus the modules that are directly related with the optimization tasks, and transfer them into corresponding reduced-order models as described in the following sections. The other modules will remain be operated within EnergyPlus engine to calculate the parameters that are not directly correlated with the control variables in the optimization, e.g., the solar incident radiation and zone infiltration airflow rate. Such parameters are treated as the inputs to the reduced-order models.

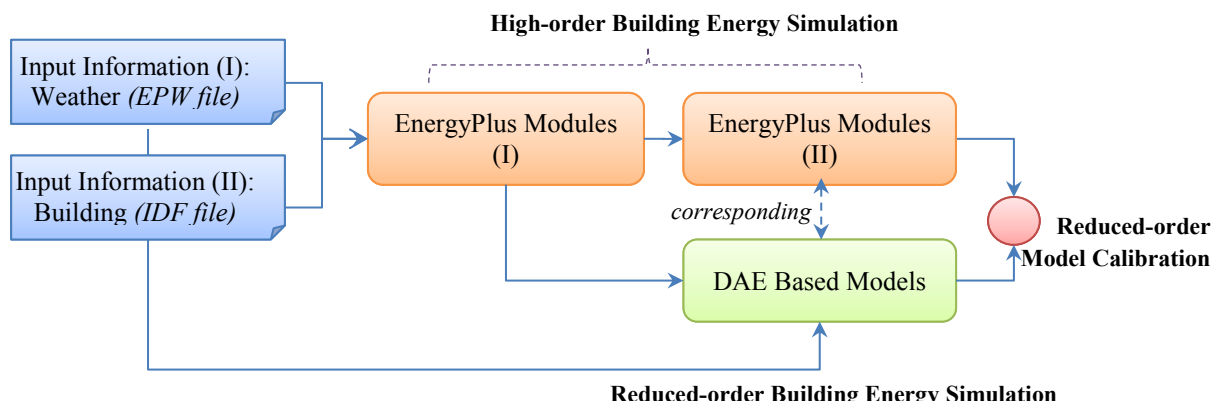


Fig. 2.5 Flow diagram of reduced-order model development

The framework of the reduced-order model development procedure is depicted in Fig. 2.5. As can be seen in the diagram, the high-order building energy simulation performs two roles in the framework:

- EnergyPlus Modules (I): pre-process the input information for the reduced-order model, including the IDF file containing a complete building description and the EPW file containing the typical meteorological weather data for a specific location;
- EnergyPlus Modules (II): support the calibration of the DAE-based reduced-order models.

The proposed procedure provides several significant advantages for the reduced-order model development:

- A big portion of simulation task is shared by well-tested high-order building models, for example, the analysis of the shading effect between different buildings. Compared with the method incorporating all the modules in the reduced-order model, this will increase the simulation reliability and accuracy.
- After the high-order model pre-processing of the weather and building information, the reduced-order model only need to deal with a considerably reduced-order amount of input information. This makes it much less challenging and time consuming to develop the reduced-order building model.
- The procedure has the capability to analyze realistic buildings with many thermal zones and complex geometry configurations. Moreover, the reduced-order model can be modified to apply to other buildings with different physical and functional characteristics..
- Having the high-order simulation as a bridge, the proposed reduced-order building model has the potential to couple with a large variety of commercial building modeling software existing in the current AEC industry.

The reduced-order building model is built in the Matlab computing environment which is well recognized for its powerful programming and visualization functions (MathWorks 2013). The interconnection between the EnergyPlus and Matlab simulations is achieved via MLE+, an open-source co-simulation platform developed by University of Pennsylvania (Bernal et al. 2012). It makes use of the advanced Energy Management System (EMS) feature within EnergyPlus to allow the coupling of different simulation programs for distributed simulation or real-time simulation related to the building energy system (LBNL 2012).

2.3 Model Reduction for the Cooling Load Components

Three substantial time delay effects inherent in the building heat and moisture transfer have to be well represented in the reduced-order building model development, including:

- Radiant time delay effect: delay of radiative heat gain conversion to building cooling loads
- Conduction time delay effect: delay of conductive heat gain through external building envelopes
- Internal mass time delay effect: due to the thermal storage and moisture buffering of the internal mass

In the high-order building simulations, the sub-models addressing the first two effects are too complex to be described by DAEs, and therefore, the corresponding reduced-order models are derived as described in section 2.3.1 and 2.3.2 and then calibrated as described in section 2.4. The third delay effect can be addressed by DAE based model as shown in section 2.3.3.

2.3.1 Radiative heat gain conversion to building cooling loads

The reduced-order model handling the radiation cooling load calculations is derived from the Radiant Time Series Method (RTSM) which is originally developed in the late 1990s (Spitler, Fisher, and Pedersen 1997; Spitler and Fisher 2000; ASHRAE 2005). Compared with the heat balanced method implemented in the high-order building simulations, RTSM is a transformation-based procedure that can be described by DAEs in a simpler form, requiring a less amount of input information. Such characteristics make it well-suited for the reduced-order model development in the study.

2.3.1.1 Radiative cooling load estimation in the high-order simulation

The radiative heat gains must first be absorbed by the interior room surfaces, and then be converted to the cooling load when it is later transferred by convection from those surfaces to the room air. Thus, a surface by surface heat balance analysis is necessary to perform the first-principle based radiative cooling load estimation. Fig. 2.6 shows the radiation components in the surface heat balance analysis. Both the short-wave and long-wave radiations should be taken into consideration: the former includes the incident solar radiation and the emittance of internal lighting sources, and the latter includes the absorption and emittance of zone surfaces, equipment and occupants (DOE 2013).

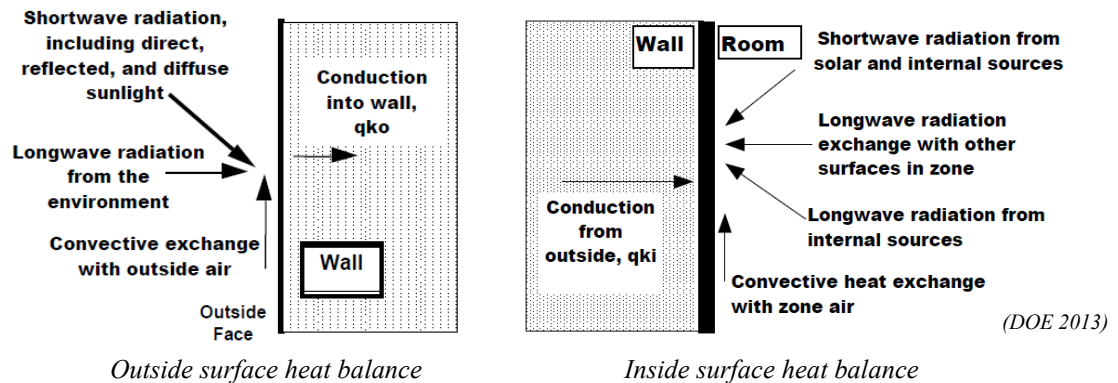


Fig. 2.6 Radiation components in the surface heat balance analysis

To perform the surface-by-surface analysis, however, it is necessary to calculate the radiation exchange between all the surfaces and other surroundings radiative sources such as the sky, the ground and the internal radiative sources. This requires a large amount of information, including: building geometry, sun path, shading design and operation, surface temperatures, surface material properties, and spatial relationships between surfaces and surroundings (direct view factors). The material properties of the surface, such as emissivity and

absorptivity, are complex functions of angle, temperature, and wavelength for each participating surface.

Moreover, the exact calculation of the direct view factors is usually computationally intensive, especially when the building configuration is complex. Even in the high-order simulations such as EnergyPlus, some simplification procedures are implemented to lower the computational time (DOE 2013).

Therefore, it may be too challenging and time-consuming to include the first-principle based radiative cooling load estimation in a DAE based model.

2.3.1.2 RTS based reduced-order model for radiation cooling load evaluation

RTSM was first developed to perform peak design cooling load calculations for the purpose of HVAC system sizing. Instead of solving the instantaneous convective and radiative heat transfer from surface by surface analysis, it provides a simplified transformation-based approach to quantify the radiative heat gain conversion to cooling loads.

The key concept of the method is radiant time series (RTS), which are used to address the time-dependent response of the zone to the radiant energy pulses. RTS contains a group of radiant time factors specifying the portion of the radiant pulse that is convected to zone air in the current and the following hours. In other words, these factors represent the distribution of radiant heat gains over time. When estimating the cooling load for a specific hour, radiant time factors are multiplied with the corresponding radiant heat gains occurred in both the current and past hours (Spitler, Fisher, and Pedersen 1997; ASHRAE 2005).

Most heat sources within buildings (such as lights, people, walls, roofs, windows, appliances) transfer energy by both convection and radiation. RTSM applies an estimated coefficient to split each of the heat sources into convective and radiation portions. The convective portion is treated as instantaneous cooling load, and the radiation portion is treated using radiant time factors corresponding to the heat sources. Thus, the cooling load contributed by a single load source for a specific hour is the sum of the instantaneous convection portion from that source and the time-delayed portion of radiant heat gains.

The radiant cooling load for a specific hour can be obtained using the following equation:

$$Q_{r,\theta} = r_0 q_{r,\theta} + r_1 q_{r,\theta-1} + \cdots + r_N q_{r,\theta-N} \quad (2.1)$$

where

r_0, \dots, r_N radiant time factors for the heat source [--]

N number of hours that the effect of a radiant energy pulse last [h]

$Q_{r,\theta}$ radiant cooling load for the current hour (θ) [W]

$q_{r,\theta-n}$ radiant heat gain n hour ago [W].

In the reduced-order model development for radiation cooling load evaluation, the concept of RTS is implemented while the specific procedures are further improved. With the support of EnergyPlus simulations, several features of traditional RTSM are expanded as summarized below:

- Traditional RTSM computes building loads for a 24-hour design day based on the assumption of steady-periodic conditions, that is, the weather conditions and the building operations of the design day are identical to those of previous days. In the proposed procedure, however, this assumption is not necessary because EnergyPlus can be used to provide the necessary information of previous

days. Therefore, it is able to perform cooling load calculations for a much longer period, rather than peak load estimation for only the design day.

- Theoretically, a separate series of radiant time factors is needed for each unique zone, since different massing and arrangement of zone construction surfaces may lead to diverse thermal response characteristics. In the traditional RTSM, this cannot be achieved because the users are only allowed to determine a specific set of RTS from pre-tabulated factors. During this process, designers need to use their experience to select the zone types that most closely match the actual situation, but this may not be clear in all cases (Spitler and Nigusse 2010). In the proposed procedure, however, the RTS for each zone can be derived separately by the optimization algorithms during the calibration process. This tends to create a higher degree of accuracy than the traditional RTSM.

Fig. 2.7 shows the detailed steps for developing the RTS based reduced-order models for radiation cooling load evaluation. Firstly, EnergyPlus is activated to perform the pre-processing of the input building and weather information and perform calculations of the heat gains for each radiation-related load source, such as the transmitted solar heat gains for each window and the internal lighting heat gains. Secondly, the calculated heat gains are imported to the reduced-order model for further analysis. In the reduced-order model, the convective/radiative split coefficient is applied to separate the radiation and convection portion for the heat gains, and the radiant time factors are applied to process the radiative heat gains of different types. Thirdly, the instantaneous convective heat gains and the processed radiative heat gains are added together to obtain the cooling load profiles for these radiation-related load sources.

In the study, three series of radiant time factors are implemented for different radiation types:

- Direct solar RTS: for analyzing the directly transmitted solar radiation
- Diffuse solar RTS: for analyzing diffuse solar radiation
- Internal radiation RTS: for analyzing the radiant heat gains from internal heat sources, including occupants, lights and equipment.

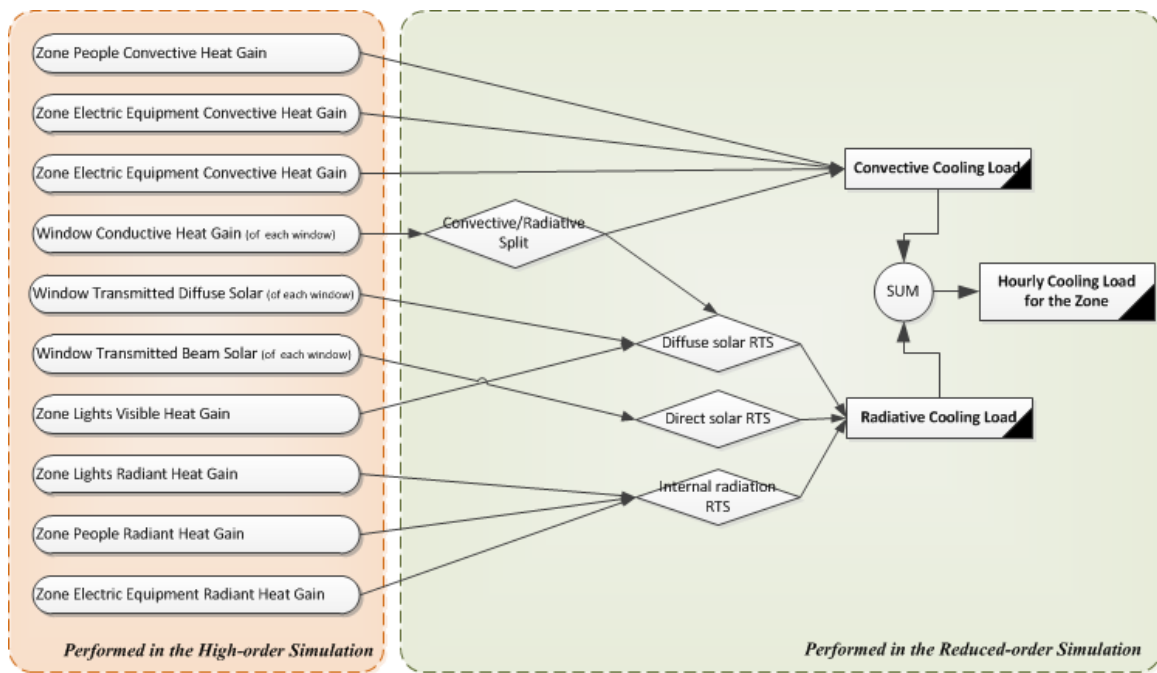


Fig. 2.7 Overview of the procedure for RTS based reduced-order model for radiation cooling load evaluation

Fig. 2.8 illustrates the RTS values for a group of representative constructions (ASHRAE 2005). These typical RTS values set up a range which will be used as the feasible region in determining the RTS during the calibration process as described in section 2.4. Take the first radiant time factor r_0 (solar radiation) for example, it typically varies between 21%

(corresponding to heavy constructions with no carpet) and 53% (corresponding to light constructions with 90% carpet), and therefore, the bounds for r_0 in the calibration process is set as [21%, 53%].

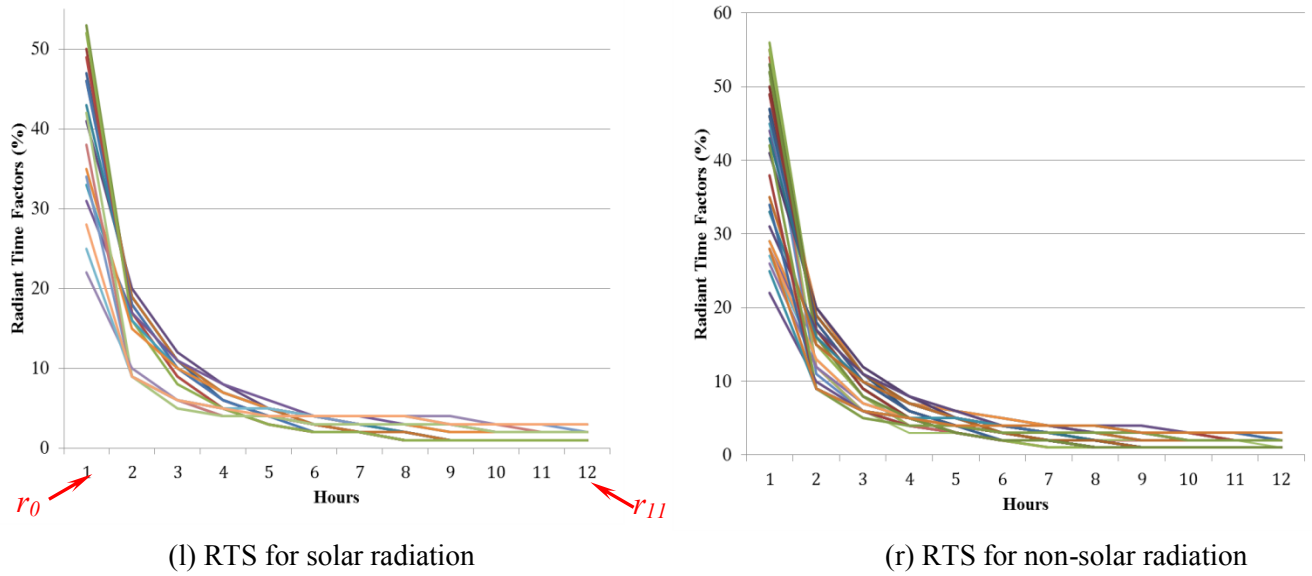


Fig. 2.8 RTS values corresponding to a group of representative constructions

2.3.2 Heat and moisture migration through external envelopes

Compared with the convective moisture transfer via infiltration and ventilation, the amount of moisture transfer through external envelopes is usually of a much smaller magnitude and the corresponding latent heat gain is not significant. Therefore, the moisture diffusion via external envelop is often neglected in the indoor air humidity balance analysis (El Diasty, Fazio, and Budaiwi 1992; Harriman, Plager, and Kosar 1999). However, it is critical to take the moisture into account to study the sensible load through envelopes, since the moisture content within

the envelope may have a considerable impact on the material thermal properties and thus change the heat transfer behaviors of the envelope (Mendes et al. 2003).

In the study, the Combined Heat and Moisture Transfer (HAMT) model implemented in the EnergyPlus simulations is used to address the coupled moisture and heat migrations in the envelope, and then the high-order simulation results are used to calibrate the conduction time series (CTS) based reduced-order model which only involves the heat transfer.

2.3.2.1 Hygrothermal models for building envelope elements

Many building envelope elements are made from capillary porous materials, within which the moisture can be transported in two forms: liquid or vapor. As illustrated in Fig. 2.9, the following transfer phenomena following different transfer mechanisms may occur simultaneously in the materials (Mendes et al. 2003; Kerestecioglu, Swami, and Kamel 1989):

- Liquid transfer driven by the relative humidity difference
- Vapor transfer driven by the partial vapor pressure difference
- Heat transfer driven by the temperature difference

These three types of transfer are usually coupled with each other and are highly dependent on the hygrothermal properties of the material (Wu, Fazio, and Kumaran 2008; Abahri, Belarbi, and Trabelsi 2011).

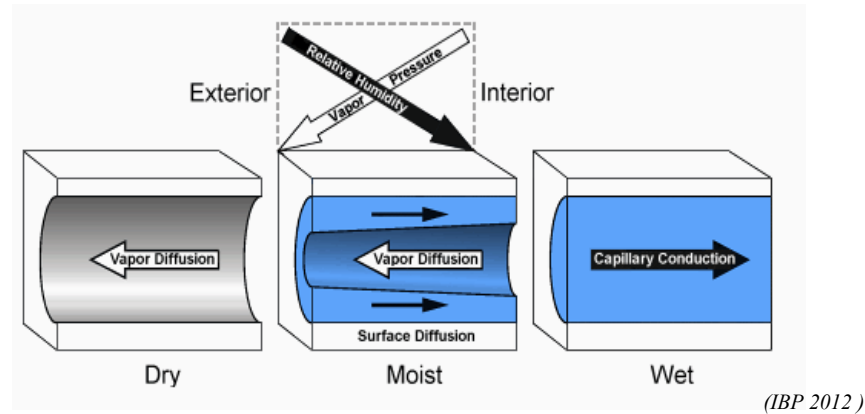


Fig. 2.9 Moisture transfer phenomena in the pores of capillary porous materials

A number of advanced hygrothermal analysis models have been developed to deal with the complex interrelated and coupled effects during the transfer process (Liesen 1994; El Diasty, Fazio, and Budaiwi 1993; Cunningham 1988; De Freitas, Abrantes, and Crausse 1996; Majumdar and Worek 1989; Häupl et al. 1997). These models are different in terms of modeling assumptions, hygroscopic property characterization approaches, or research scopes (material level, component level, or room level), but they are all able to predict the coupled temperature and moisture behavior through multi-layered porous media (Li, Fazio, and Rao 2012).

In general, the modeling process demands a large number of hygrothermal properties of the material. Most of these properties are time-variant and depend on the conditions of the material (such as material temperature and moisture content), the outdoor environment (such as rainfall, solar radiation, and wind pressure), and the indoor environment (such as ventilation conditions and the indoor moisture generation) (Wu, Fazio, and Kumaran 2008; Abahri, Belarbi, and Trabelsi 2011; Li, Fazio, and Rao 2012). Moreover, some of these properties are usually very difficult to obtain and may only be determined experimentally, which further add to the complexity of modeling. The dynamic interactions between building

envelopes and mechanical systems may also need to be considered (Tariku, Kumaran, and Fazio 2011) and the airflow simulations such as CFD may be integrated (Steeman et al. 2009; Woloszyn et al. 2009) to achieve a higher level of simulation accuracy.

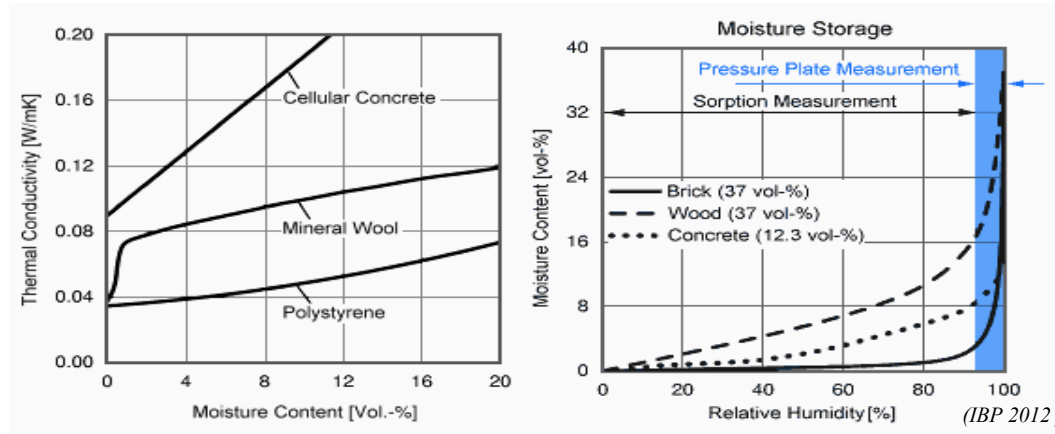


Fig. 2.10 Illustration of the relationship between various hygrothermal properties

2.3.2.2 HAMT model in the high-order building simulation

Among these models, HAMT model has been widely accepted in the building hygrothermal research and is adopted by several simulation engines such as WUFI and EnergyPlus (IBP 2012 ; DOE 2013). It is a completely coupled model simulating the movement and storage of heat and moisture simultaneously. It can provide the total heat and moisture flow amount as well as the temperature and moisture profiles through composite building walls (Künzel et al. 2005; DOE 2013).

The governing partial differential equations to model the one-dimension heat and moisture transfer through a specific porous material are derived from first-principle heat and mass balances, as stated in Eqs. (2.2) and (2.3).

Energy Conservation:

$$C_h \cdot \frac{\partial T}{\partial \tau} = \nabla \cdot (k^w \cdot \nabla T) + h_v \cdot \nabla \cdot \left(\frac{\delta}{\mu} \cdot \nabla p \right) \quad (2.2)$$

Moisture Conservation:

$$C_w \cdot \frac{\partial \varphi}{\partial \tau} = \nabla \cdot \left(D_w \cdot \frac{dw}{d\varphi} \cdot \nabla \varphi \right) + \nabla \cdot \left(\frac{\delta}{\mu} \cdot \nabla p \right) \quad (2.3)$$

where

C_h	moisture dependent heat storage capacity of the control volume [J/m ³ ·K]
C_w	moisture dependent moisture capacitance of the control volume [kg/m ³]
D_w	liquid diffusivity [m ² /s]
h_v	evaporation enthalpy [J/kg]
k^w	thermal conductivity [W/(m·K)]
T	temperature [C]
p	partial vapor pressure [Pa]
w	moisture content [kg/m ³]
φ	relative humidity [–]
τ	time [s]
δ	vapor permeability [kg/(m·s·Pa)]
μ	vapor diffusion resistance factor [–].

In Eq. (2.2), the three terms represent the storage, transport and generation of heat respectively.

In Eq. (2.3), the three terms represent the storage of moisture, the transport of liquid moisture and the transport of vapor respectively.

Note that some parameters shown in the above equations may need to be further described by other hygrothermal parameters of the material. For example, heat storage capacity C_h is dependent on the specific heat capacity of dry material, specific heat capacity of moisture, moisture content of the material and the density of dry material. Most of these parameters are interrelated and present a complex nonlinear relationship. Fig. 2.11 depicts a general overview of the key parameters/items in HAMT. For a more detailed description, refer to (DOE 2013; Künzle et al. 2005; Künzle 1995).

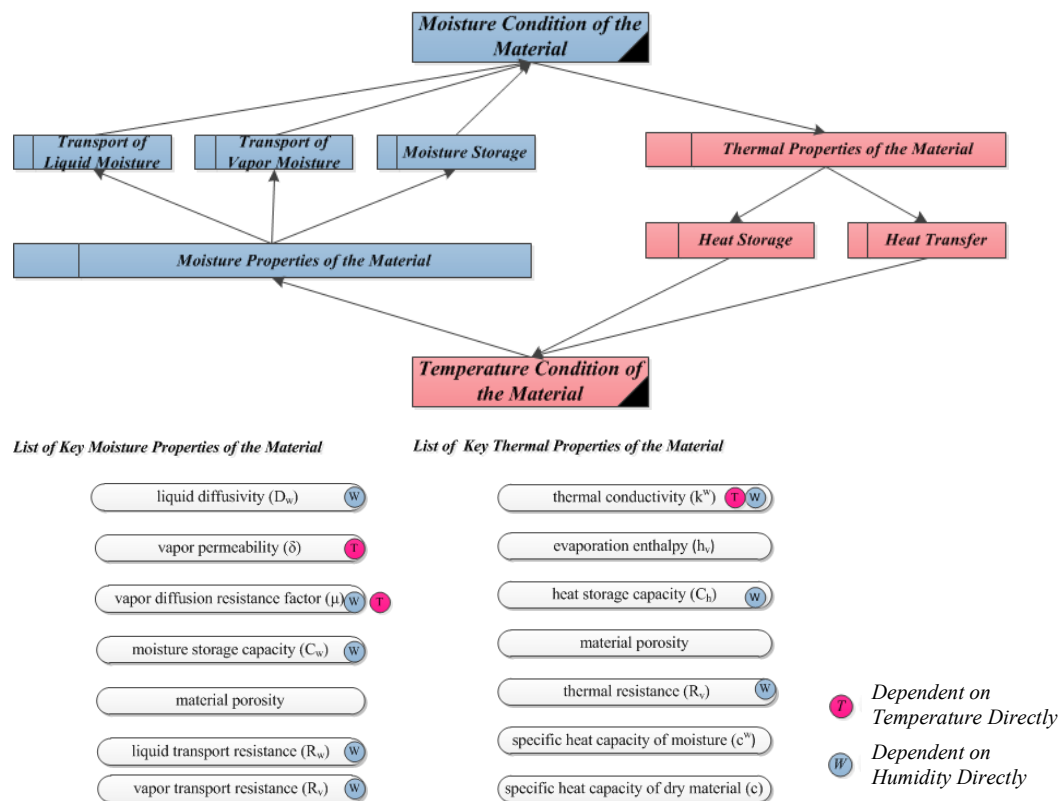


Fig. 2.11 Schematic chart of combined heat and moisture transfer in capillary porous materials

In EnergyPlus, the HAMT model can be activated by setting the heat balance algorithm as *CombinedHeatAndMoistureFiniteElement*. A finite element based solution algorithm is then applied to solve the governing differential equations simultaneously.

2.3.2.3 CTS based reduced-order model for conductive cooling load evaluation

Conduction time series (CTS) are used here to develop the reduced-order model to address the time delay effect of conductive heat gain through external building envelopes. Similar to the RTS described above, CTS uses a group of conduction time factors to specify the portion of the conductive heat input at the exterior envelope that is converted to the zone conductive heat gains in the current and the following hours.

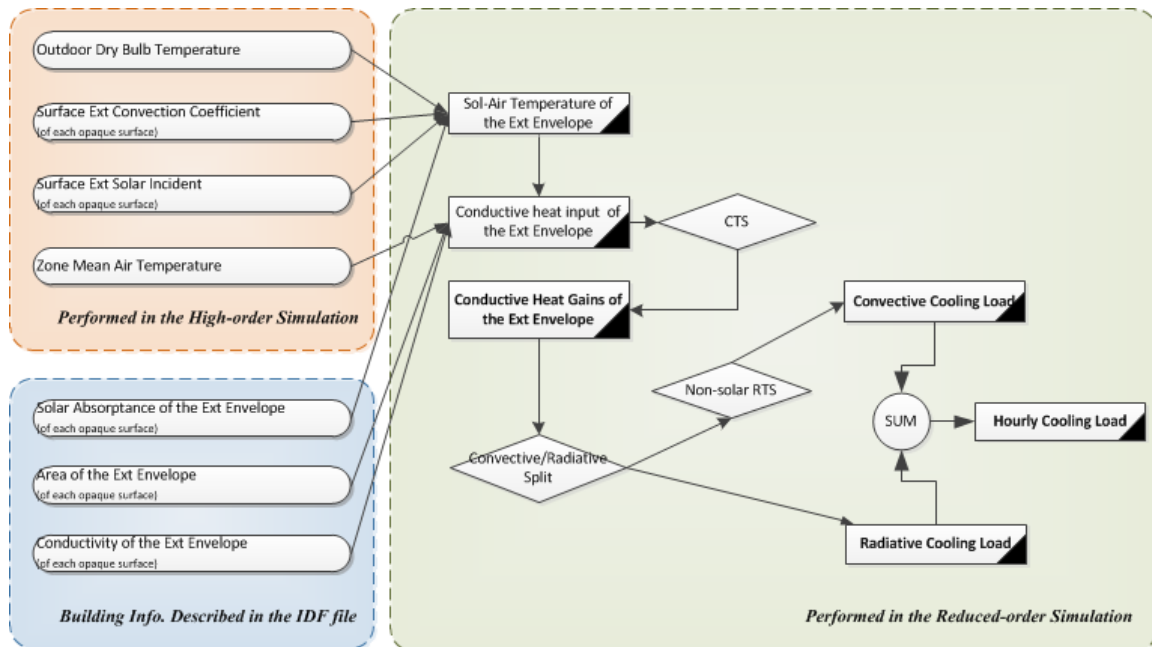


Fig. 2.12 Overview of the procedure for developing the CTS based reduced-order model for conductive cooling load evaluation through external envelopes

Fig. 2.12 shows the detailed steps to perform CTS based conductive cooling load evaluations.

Firstly, the sol-air temperatures for each external surface are calculated as (ASHRAE 2005) :

$$T_{sol-air} = T_0 + \frac{\alpha E_t}{h_0} - \frac{\varepsilon \Delta R}{h_0} \quad (2.4)$$

where

- E_t total solar radiation incident on the external surface [$\text{W/m}^2 \cdot \text{K}$]
- h_0 convection heat transfer coefficient at the external surface [$\text{W/m}^2 \cdot \text{K}$]
- T_0 outdoor air temperature [K]
- α solar absorptance of the external surface [--]
- ε hemispherical emittance of the external surface [--]
- ΔR difference between long-wave radiation incident from sky/surroundings on the surface and the radiation emitted by blackbody at outdoor air temperature; can be ignored for most vertical surfaces [W/m^2].

Secondly, the conductive heat input for each surface is calculated using the sol-air temperatures calculated above:

$$q_c = U_o A (T_{sol-air} - T_i) \quad (2.5)$$

where

- A area of the surface [m^2]
- T_i indoor air temperature [K]
- $T_{sol-air}$ sol-air temperature for the external surface [K]
- q_c conductive heat input of the external surface [W]
- U_o overall heat transfer coefficient for the surface [$\text{W/m}^2 \cdot \text{K}$].

After that, the conductive heat gains of the surface for a specific hour can be obtained by multiplying the conduction time factors with the corresponding conductive heat inputs occurring in both the current and past hours (ASHRAE 2005) :

$$Q_{c,\theta} = c_0 q_{c,\theta} + c_1 q_{c,\theta-1} + \cdots + c_N q_{c,\theta-N} \quad (2.6)$$

where

$c_0 \dots c_N$ conduction time factors for the surface [--]

N number of hours that the effect of a conductive heat input can last [h]

$Q_{c,\theta}$ conductive heat gain of the zone for the current hour (θ) [W]

$q_{c,\theta-n}$ conductive heat input of the external surface n hour ago [W].

Finally, the calculated conductive heat gains are split into convective and radiation portions and further addressed with non-solar RTS as described in section above.

Fig. 2.13 illustrates CTS values for a group of representative constructions (ASHRAE 2005). During the calibration process, the CTS values for each wall are selected within the range formed by these typical CTS values. Take the first conduction time factor c_0 for example. It typically varies between 0% (corresponding to brick walls, insulation board, sheathing, gyp board) and 25% (corresponding to Metal wall panel, insulation board, gyp board), and therefore, the bounds for c_0 in the calibration process is set as [0%, 25%].

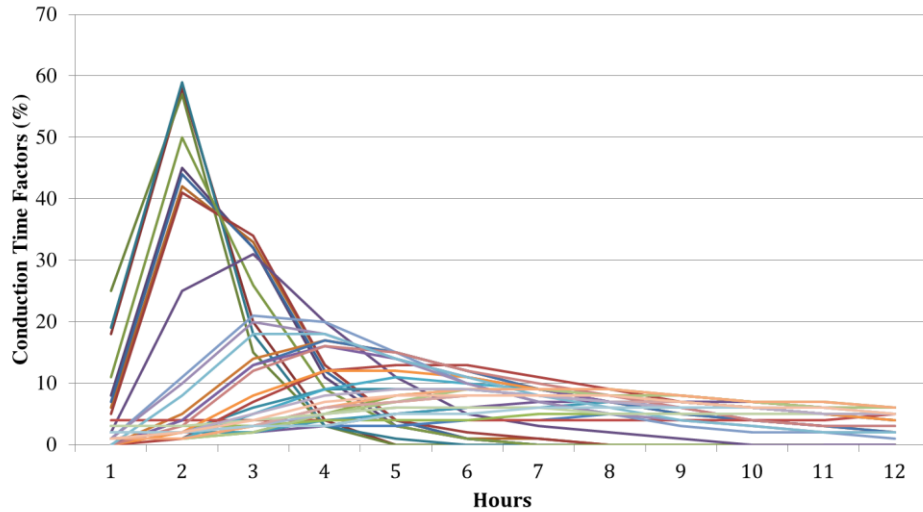


Fig. 2.13 CTS values corresponding to a group of representative constructions

2.3.3 Thermal storage and moisture buffering in the internal building mass

Interior building materials may present a considerable time delay effect which tends to dampen the fluctuations of the indoor temperature and humidity fluctuations. Depending on the interior material characteristics, moisture absorption/desorption processes of interior building materials can remove/add different amounts of moisture to the indoor air environment. According to Diasty, indoor room surfaces can absorb as high as one third of the moisture generated in the room space (El Diasty, Fazio, and Budaiwi 1992).

The Effective Moisture Penetration Depth (EMPD) Model is implemented in the study to simulate the thermal storage and moisture buffering effect of the building materials. It is a lumped approach developed on the transient heat and mass transfer analogy. The model can simulate the heat storage and moisture buffering response for most building materials, especially when the material surface resistance is large compared to the internal resistance for moisture flow (Tariku, Kumaran, and Fazio 2011). Note that the EMPD model is described by

DAE equations with an acceptable level of complexity, and thus can be directly implemented in the reduced-order building model without the calibration procedure.

As shown in Fig. 2.14, the model assumes that the moisture exchange between the material and the indoor air is limited to a few millimeters depth of the material and with no moisture gradient across the material (Kerestecioglu et al. 1988; Kerestecioglu, Swami, and Kamel 1989; Cunningham 1992).

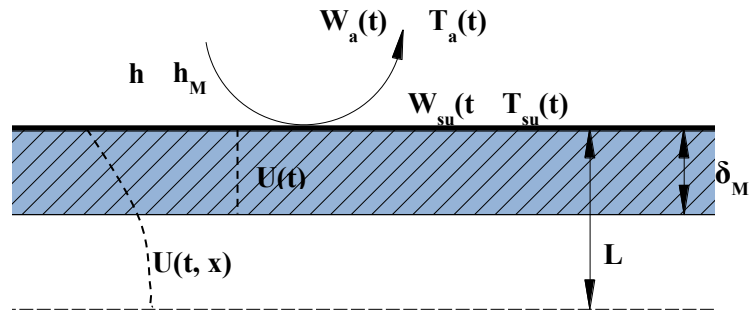


Fig. 2.14 Schematic chart of the Effective Moisture Penetration Depth Model

In EMPD, a uniform moisture content (U) is applied in the model to represent the moisture content in the material. This can be stated as:

$$\int U(x)dx = U\delta_M \quad (2.7)$$

where

U moisture content of the material [$\text{kg}_w/\text{kg}_{\text{material}}$]

δ_M effective moisture penetration depth of the material[m].

The moisture content U can be defined in a general form, which is applicable for most building materials (Kerestecioglu et al. 1988) :

$$U = a\varphi^b + c\varphi^d \quad (2.8)$$

where

$a \sim d$ parameters describing the hygrothermal properties of the material [–]

φ relative humidity [–].

The parameters $a \sim d$ describe the hygrothermal properties of a specific material. The parameter values of common building material can be found in the EnergyPlus hygrothermal material database (DOE 2013).

The relative humidity used in Eq. (2.9) can be calculated via moist air properties equations expressed as:

$$\varphi = \frac{W_{su}}{W_{s,sat}} \quad (2.9)$$

$$W_{su,sat} = \frac{1}{R_v \rho_a T_{su}} \exp\left(23.7093 - \frac{4111}{T_{su} - 35.45}\right) \quad (2.10)$$

where

R_v ideal gas constant [461.52 J/kg·K]

T_{su} temperature of the air at the material surface [K]

W_{su} humidity ratio of the air at the material surface [kg_w/kg_{air}]

$W_{su,sat}$ saturated humidity ratio of the air at the material surface [kg_w/kg_{air}]

τ time [s]

ρ_a air density [kg/m³].

Given that $U = f(W_s, T_s)$, the differentiation of U with respect to time can be stated as:

$$\frac{dU}{d\tau} = \frac{\partial U}{\partial W_{su}} \frac{dW_{su}}{d\tau} - \frac{\partial U}{\partial T_{su}} \frac{dT_{su}}{d\tau} = A_T \frac{dW_{su}}{d\tau} - B_p \frac{dT_{su}}{d\tau} \quad (2.11)$$

$$A_T = \frac{ab\varphi^b + cd\varphi^d}{W_s} \quad (2.12)$$

$$B_p = - \left[\frac{1}{T_{su}} - \frac{4111}{(T_{su} - 35.45)^2} \right] \times (ab\varphi^b + cd\varphi^d) \quad (2.13)$$

where

A_T isothermal moisture capacity [m^3/kg]

B_p thermal gradient coefficient [K^{-1}].

The moisture balance equation for a specific internal surface can be presented as

$$(\rho\delta_M) \frac{dU}{d\tau} = h_M (W_a - W_{su}) \quad (2.14)$$

where

h_M convective moisture transfer coefficient [$\text{kg} / \text{m}^2 \cdot \text{s}$]

W_a humidity ratio of the surrounding air [$\text{kg}_w/\text{kg}_{\text{air}}$]

ρ material density [kg / m^3].

The differentiation of W_s with respect to time can be obtained by combining Eqs. (2.11)~(2.14):

$$(\rho\delta_M A_T) \frac{dW_{su}}{d\tau} = h_M (W_a - W_{su}) + (\rho\delta_M B_p) \frac{dT_{su}}{d\tau} \quad (2.15)$$

The heat balance equation for a specific internal surface can be presented as

$$M c_p \frac{dT_{su}}{d\tau} = h_T A (T_a - T_{su}) + h_v h_M A (W_a - W_{su}) \quad (2.16)$$

where

A	surface area of the internal mass [m^2]
c_p	specific heat of air [$\text{J/kg}\cdot\text{K}$]
h_T	convective heat transfer coefficient [$\text{W/m}^2\cdot\text{K}$]
h_v	evaporation enthalpy [J/kg]
T_a	temperature of the surrounding air [K]
M	mass of the internal mass [kg].

Eqs. (2.15) and (2.16) are the final equations for estimating the moisture and heat behaviors of a specific hygrothermal surface.

2.3.4 Energy and moisture balances for the building zone air

The zone air model is developed to predict the indoor temperature and humidity conditions, taking into account the dynamic interaction between indoor environment and other cooling load components such as building enclosure and occupants. The zone air model introduced in this section and the other sub-models developed in the previous sections form a whole building hygrothermal model for further optimization analysis.

The temperature condition for a specific zone is the consequence of the balance between heat gains and losses from the zone space. The heat fluxes incorporated in the zone air model include (ASHRAE 2005; DOE 2013):

- (1) conductive heat transfer through opaque external envelopes,
- (2) radiant heat transfer of the zone through windows,
- (3) convective heat transfer with interior building materials,
- (4) heat transfer by ventilation,
- (5) heat transfer by mechanical air conditioning system,
- (6) heat transfer by infiltration,
- (7) heat transfer due to internal operational activities.

The transient air heat balance equation can be expressed by:

$$\begin{aligned} \rho_a V_z c_p \frac{dT_i}{d\tau} = & \dot{Q}_c + \dot{Q}_r + \sum_j h_T A_j (T_m - T_i) + \dot{m}_{vent} c_p (T_o - T_i) \\ & + \dot{m}_{sys} c_p (T_s - T_i) + \dot{m}_{inf} c_p (T_o - T_i) + \dot{Q}_i \end{aligned} \quad (2.17)$$

where

A_j	surface area of the internal mass [m^2]
c_p	specific heat of air [$\text{J/kg}\cdot\text{K}$]
h_T	convective heat transfer coefficient [$\text{W/m}^2\cdot\text{K}$]
\dot{m}_{inf}	mass flow rate of infiltration [kg/s]
\dot{m}_{vent}	mass flow rate of ventilation [kg/s]
\dot{m}_{sys}	mass flow rate of supply air from air conditioning [kg/s]
\dot{Q}_c	conductive cooling load of the zone [W]
\dot{Q}_i	zone internal cooling load [W]
\dot{Q}_r	radiant cooling load of the zone [W]
T_i	temperature of the indoor environment [K]
T_m	temperature of the internal mass [K]
T_o	temperature of the outdoor environment [K]
T_s	temperature of the supply air from air conditioning [K]
V_z	zone space volume [m^3]
ρ_a	air density [kg/m^3].

Similarly, the humidity conditions for a specific zone is the consequence of a number of moisture fluxes (Künzel et al. 2005; DOE 2013; Li, Fazio, and Rao 2012), including:

- (1) moisture absorption/desorption of interior hygrothermal building materials,
- (2) moisture addition and removal by ventilation,
- (3) moisture addition and removal by mechanical system,
- (4) moisture addition and removal by infiltration,
- (5) moisture addition into zone due to internal operational activities.

The transient air moisture balance equation can be expressed by:

$$\rho_a V_z \frac{dW_i}{d\tau} = \sum_j h_M A_j (W_m - W_i) + m_{vent} \dot{m} (W_o - W_i) + m_{sys} \dot{m} (W_s - W_i) + m_{inf} \dot{m} (W_o - W_i) + \dot{w}_l \quad (2.18)$$

where

- h_M convective moisture transfer coefficient [kg / m²·s]
- W_i humidity ratio of the indoor environment [kg_w/kg_{air}]
- W_m humidity ratio of the internal mass [kg_w/kg_{air}]
- W_o humidity ratio of the outdoor environment [kg_w/kg_{air}]
- W_s humidity ratio of the supply air from air conditioning [kg_w/kg_{air}]
- \dot{w}_l moisture addition into zone due to internal operational activities [kg/s].

2.4 Reduced-order Building Model Calibration by Integrated Simulation

In this section, the reduced-order model is calibrated using the EnergyPlus simulation results for a representative office building. A single-objective multivariable optimization problem is formulated in order to capture the proper settings of the reduced-order model. The calibrated building model will be directly implemented in the dynamic optimization to perform the operational analysis in the following chapters.

2.4.1 Configurations of the case building

The case is a medium-sized commercial office reference building provided by the U.S. Department of Energy Building Technologies Program (DOE 2013). It is a three story office building with the same plan layout for each floor, as depicted in Fig. 2.15. The building definition is given in the form of whole-building energy simulation model compatible with EnergyPlus program (Deru, Griffith, and Torcellini 2006). It includes both perimeter and core zones and meets the minimum energy performance requirements for commercial buildings given by ASHRAE Standard 90.1 (ASHRAE 2010)

The model is using Chicago, IL, U.S. (41 °N, 87°W) as the assumed site, which is classified as ASHRAE Climate Zone 5A and has a heating dominated, cool and humid weather conditions with annual 3430 heating and 506 cooling degree days (18 °C baseline). Ideal loads air system is implemented in the model, which at all times maintains the desired temperature setpoint of 25°C by varying the air flow rate.

The four perimeter zones in the middle floor are selected in the study. These zones have external walls facing to four orientations and thus represent four types of cooling load profiles. A summary of the building/zone configurations is listed in Table 2.1 ~ Table 2.3, and the internal occupancy, electrical equipment and lighting schedules are depicted in Fig. 2.16 ~ Fig. 2.18, respectively (Thornton et al. 2011).

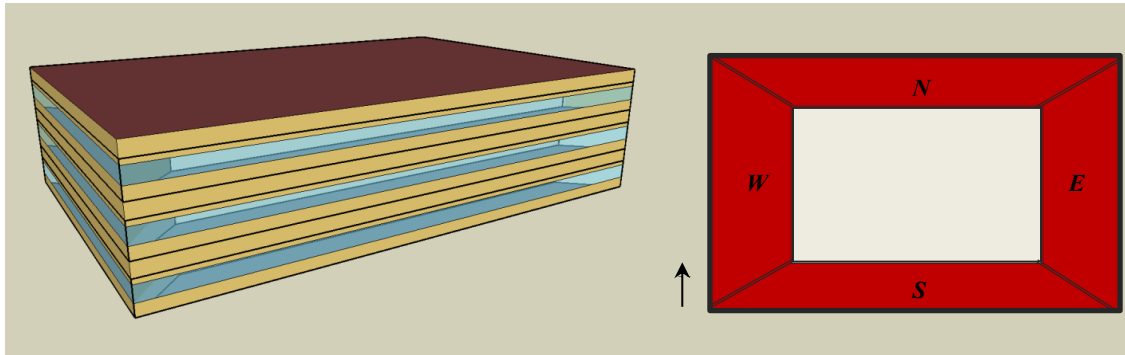


Fig. 2.15 Exterior view (l) and plan layout (r) of the case building

Table 2.1 Summary of the physical and operational configurations of the building case

	SOUTH ZONE	EAST ZONE	NORTH ZONE	WEST ZONE
Space Volume [m ³]	239.25	103.31	239.25	103.31
Space Height [m]	2.4	2.4	2.4	2.4
External Wall Area [m ²]	51.39	27.36	51.39	27.36
Fenestration Area [m ²]	21.81	9.12	21.81	9.12
Number of occupants [--]	11	5	11	5
Internal Lighting Level [W]	1584	684	1584	684
Internal Equipment Level [W]	1056	456	1056	456

Table 2.2 Summary of the external wall configurations of the building case

	Layer 1	Layer 2	Layer 3	Layer 4
	Spruce	Concrete	Cellulose Insulation	Spruce
Roughness	Rough	Rough	Rough	Rough
Thickness [m]	0.012	0.1	0.066	0.012
Conductivity [W/m-K]	0.09	1.6	0.04	0.09
Density [kg/m ³]	455	2300	55	455
Specific Heat [J/kg-K]	1500	850	1880	1500
Thermal Absorptance [--]	0.9	0.9	0.9	0.9
Solar Absorptance [--]	0.7	0.7	0.7	0.7
Visible Absorptance [--]	0.7	0.7	0.7	0.7
(Total U-Factor with Film 0.470W/m ² -K)				

Table 2.3 Summary of the fenestration configurations of the building case

	Window (Dbl Clr 3mm/13mm Air)			Glass Door (sgl grey 3mm)
	Layer 1 clear 3mm	Layer 2 air 13mm	Layer 3 clear 3mm	grey 3mm
Thickness [m]	0.003	0.013	0.003	0.003
Solar Transmittance at Normal Incidence [--]	0.837	/	0.837	0.626
Front Side Solar Reflectance at Normal Incidence [--]	0.075	/	0.075	0.061
Back Side Solar Reflectance at Normal Incidence [--]	0.075	/	0.075	0.061
Visible Transmittance at Normal Incidence [--]	0.898	/	0.898	0.611
Front Side Visible Reflectance at Normal Incidence [--]	0.081	/	0.081	0.061
Back Side Visible Reflectance at Normal Incidence [--]	0.081	/	0.081	0.061
Infrared Transmittance at Normal Incidence [--]	0.000	/	0.000	0.000
Front Side Infrared Hemispherical Emissivity [--]	0.840	/	0.840	0.840
Back Side Infrared Hemispherical Emissivity [--]	0.840	/	0.840	0.840
Conductivity [W/m-K]	0.900	/	0.900	0.900

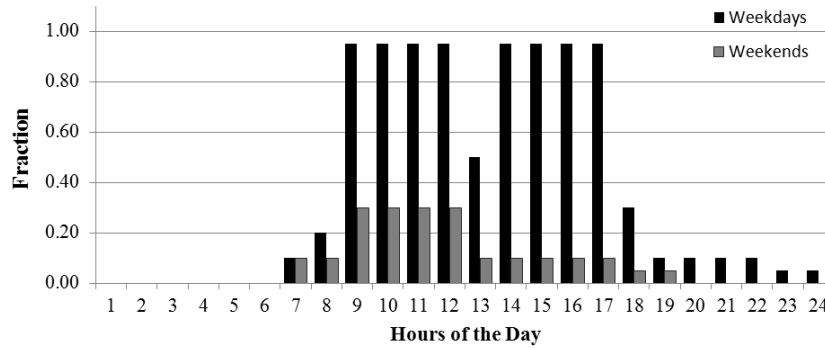


Fig. 2.16 Hourly internal occupancy schedule for the building case

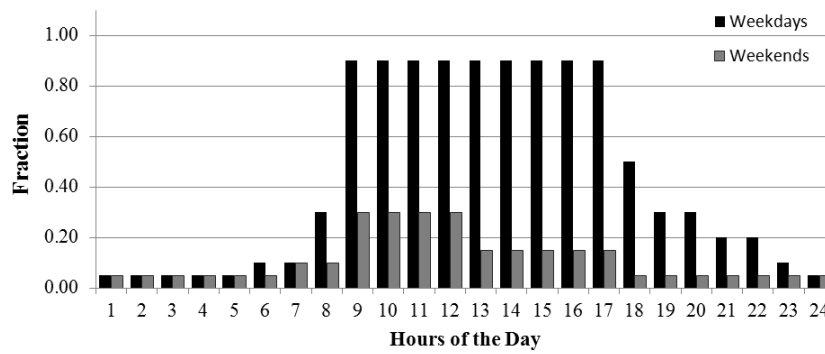


Fig. 2.17 Hourly internal lighting schedule for the building case

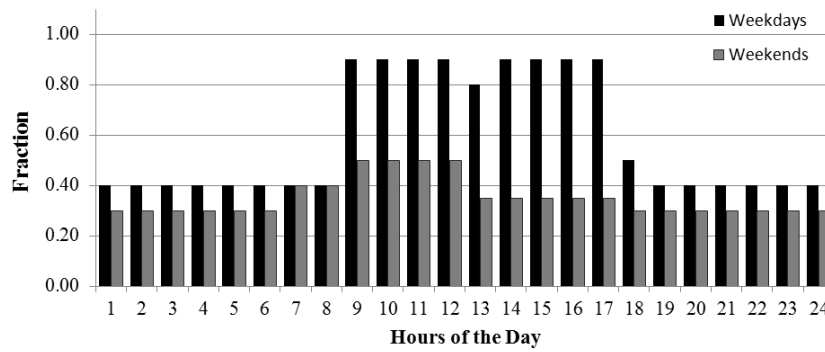


Fig. 2.18 Hourly internal equipment schedule for the building case

2.4.2 Procedure for the reduced-order model calibration and simulation

Fig. 2.19 shows the specific calibration and simulation workflows for the reduced-order model development. It is carried out in the following two successive steps:

- (1) The calibration is performed for an M-day period to recover the reduced-order model, by comparing the reduced-order model simulations with the EnergyPlus simulations;
- (2) The recovered reduced-order model performs the simulation for the following one day, and the calculated building cooling loads are compared with the EnergyPlus simulation results to evaluate the performance of the reduced-order model.

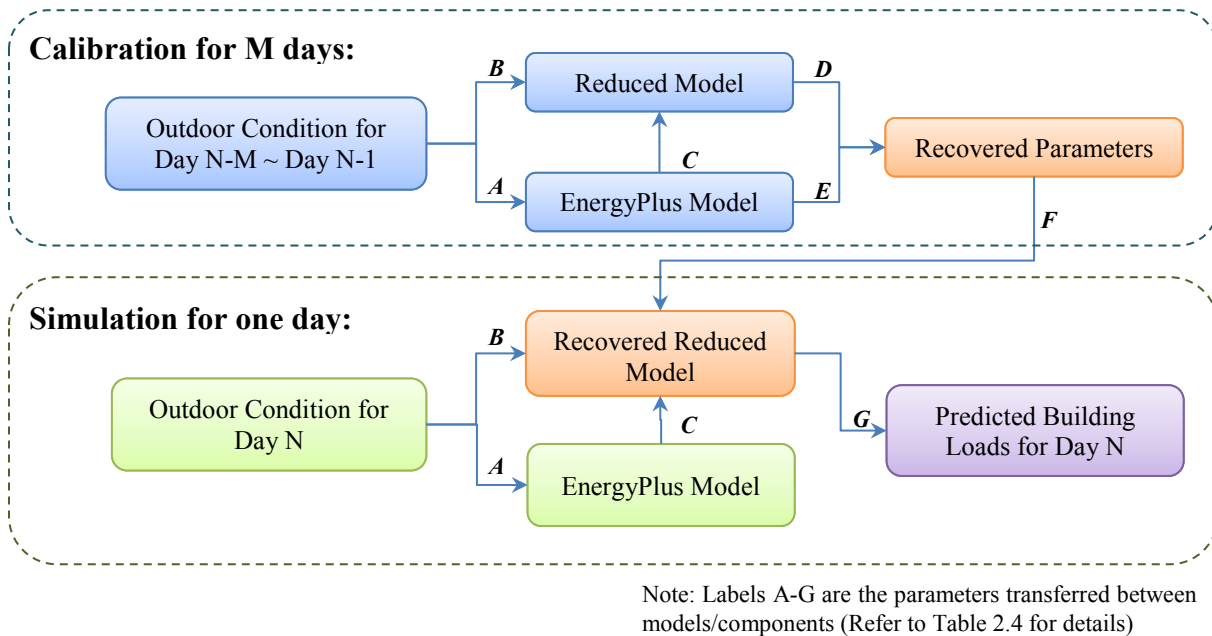


Fig. 2.19 Calibration and simulation procedure for the reduced-order model development

A big number of parameters with various modeling levels (site>building>zone>surface) are transferred between different models/components during the model calibration and simulation, as shown in Fig. 2.19. These parameters are listed and categorized in Table 2.4.

Table 2.4 List of parameters transferred between models/components during the model calibration and simulation

Step Label	Parameter Name	Modeling Level	Resolution
A	<i>Solar-related data</i>		
	Solar declination angle	site	daily
	Time of sunrise and sunset	site	daily
	Sun's altitude and azimuth angles	site	time-step
	Direct normal radiation	site	time-step
	Diffuse horizontal radiation	site	time-step
	Direct normal radiation	site	time-step
	Diffuse horizontal radiation	site	time-step
	<i>Sky data</i>		
	Atmospheric extinction coefficient	site	daily
	Cloud cover	site	time-step
	<i>Outdoor air data</i>		
	Dry-bulb temperature	site	time-step
	Dew-point temperature	site	time-step
	Relative humidity	site	time-step
	Barometric pressure	site	time-step
	Wind speed	site	time-step
	Wind direction	site	

<i>Other weather data</i>			
	Ground temperature	site	time-step
	Precipitation	site	time-step
B	Dry-bulb temperature	site	time-step
	Dew-point temperature	site	time-step
	Relative humidity	site	time-step
C	Zone mean air temperature	zone	time-step
	Zone air humidity ratio	zone	time-step
	Surface external convection coefficient	surface	time-step
	Surface external solar incident	surface	time-step
	Window heat gain	surface	time-step
	Window transmitted solar radiation	surface	time-step
	Zone people radiant heat gain	zone	time-step
	Zone people convective heat gain	zone	time-step
	Zone lights radiant heat gain	zone	time-step
	Zone lights visible heat gain	zone	time-step
	Zone lights convective heat gain	zone	time-step
	Zone electric equipment radiant heat gain	zone	time-step
	Zone electric equipment convective heat gain	zone	time-step
	Zone infiltration mass	zone	time-step
D	Zone conductive cooling load	zone	time-step
	Zone internal cooling load	zone	time-step
	Zone radiant cooling load	zone	time-step
	Zone infiltration cooling load	zone	time-step
	Zone total sensible cooling load	zone	time-step

E	Zone total sensible cooling load	zone	time-step
F	Direct solar RTS	surface	daily
	Diffuse solar RTS	surface	daily
	Internal radiation RTS	zone	daily
	CTS values	surface	daily
	Convective/radiation split coefficient	surface	daily
G	Zone conductive cooling load	zone	time-step
	Zone internal cooling load	zone	time-step
	Zone radiant cooling load	zone	time-step
	Zone infiltration cooling load	zone	time-step
	Zone total sensible cooling load	zone	time-step

Note: time-step is 15min.

2.4.3 Optimization formulation for the calibration

The reduced-order model is comprised of the sub-models described in section 2.3.1~2.3.4, which have many parameters to be configured for specific buildings. The purpose of the calibration is to configure the reduced-order model such that it can perform building thermal performance evaluations as similarly to the high-order models as possible. More specifically, the difference between the building cooling load predictions by the reduced-order and high-order simulations should be minimized.

This can be taken as a single-objective multivariable optimization problem with the objective function defined by:

$$\min \sum_{i=1}^{N_s} \sum_{j=1}^{N_z} (Q_{h,i,j} - Q_{r,i,j})^2 \quad (2.19)$$

where

N_s number of time steps in the calibration period [--]

N_z number of building thermal zones [--]

$Q_{h,i,j}$ cooling load at time step i for zone j by the EnergyPlus simulations [W]

$Q_{r,i,j}$ cooling load at time step i for zone j by the reduced-order simulations [W]

In the study, the calibration is performed for a 3-day period with a 15-minute time interval, and thus the value of N_s is 288 (i.e., the division of the calibration period and the time interval).

The minimization is achieved by manipulating the variables describing the reduced-order model, including:

- Direct solar RTS (surface level)
- Diffuse solar RTS (surface level)
- Internal radiation RTS (zone level)
- CTS values (surface level)
- Convective/radiation split coefficient (surface level)

As mentioned in section 2.3, a group of CTS and RTS values corresponding to a number of typical constructions are used to set the constraints for the optimization problem. The mean of these typical values is chosen as the initial value in the optimization.

The solution of the minimization is achieved in the MATLAB environment, using constrained nonlinear multivariable optimization method, namely *fmincon* (MathWorks 2013). In the study, it can solve the optimization for a single 3-day calibration with computation times of several minutes on an 8-core 64-bit desktop.

2.4.4 Calibration results and discussions

The reduced-order model calibration and simulation is performed for the four study zones of the building case for July (4× 24 time steps per day).

To quantitatively evaluate the performance of the recovered reduced-order model, the relative error (RE) for each time step is defined as:

$$RE_{i,j} = \frac{\dot{Q}_{h,i,j} - \dot{Q}_{r,i,j}}{\dot{Q}_j} \times 100\% \quad (2.20)$$

where

$\dot{Q}_{h,i,j}$ cooling load predictions at time i for zone j by EnergyPlus simulations [W]

$\dot{Q}_{r,i,j}$ cooling load predictions at time i for zone j by reduced-order simulations [W]

$\overline{\dot{Q}}_j$ average cooling load during the office hours of the day for zone j [W].

The RE distributions for each zone are depicted in Fig. 2.20. Although the RE for different zones have slightly different distributions, they can generally be kept at low levels, mostly within $\pm 10\%$. The fitted normal distributions have the mean value between $-0.15\% \sim 3.22\%$ and the standard deviation between $3.14\% \sim 4.72\%$. This means that the recovered reduced-order model can generate an acceptable level of simulation accuracy.

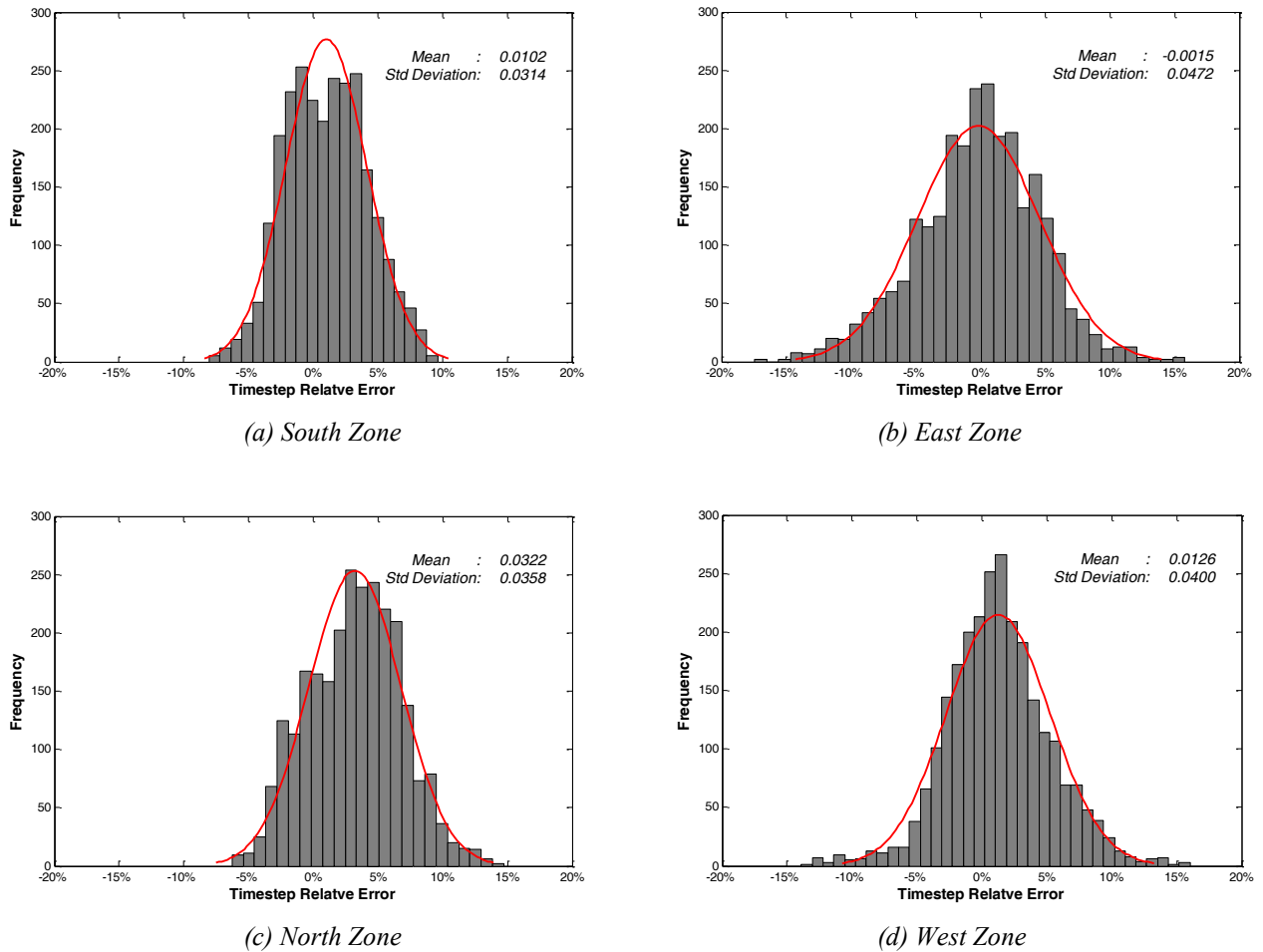
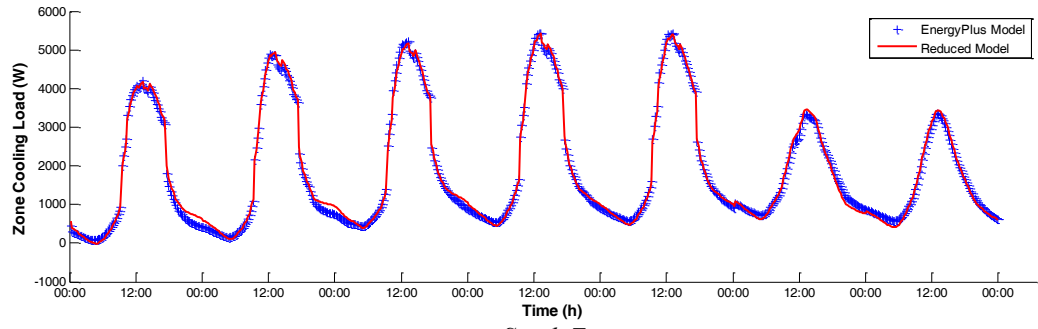
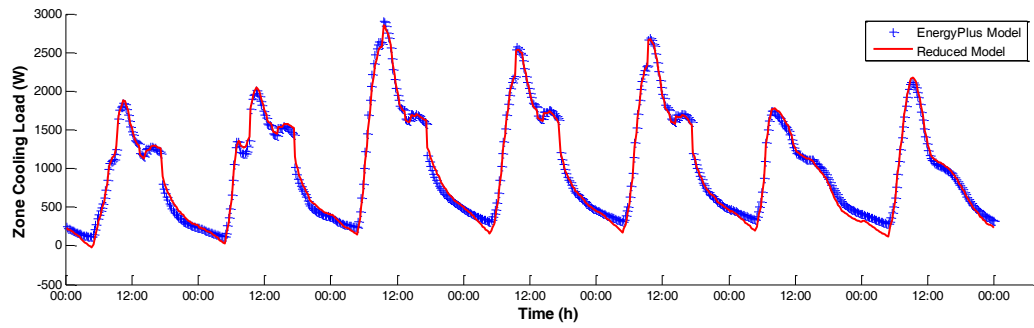


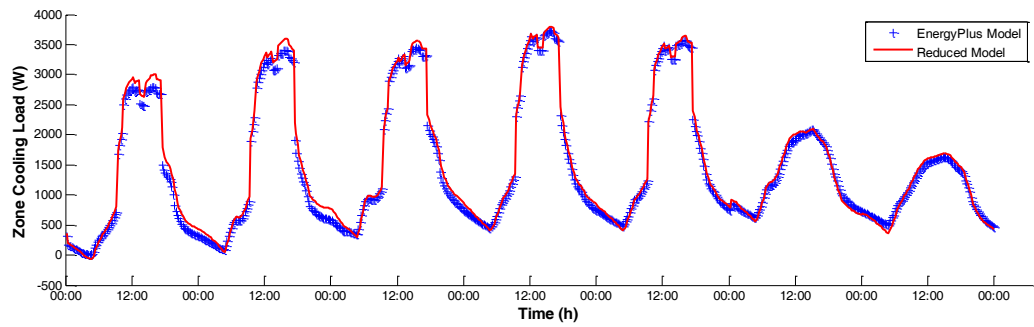
Fig. 2.20 Relative error distribution of the reduced-order model simulations for one month (July)



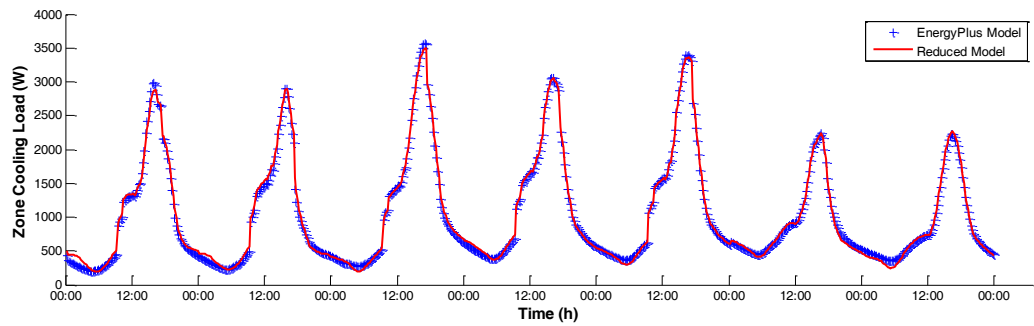
(a) South Zone



(b) East Zone



(c) North Zone



(d) West Zone

(One typical week: Jul. 14-20)

Fig. 2.21 Comparison of the cooling load predictions by the EnergyPlus and reduced-order model simulation

The cooling load predictions by the the EnergyPlus and the reduced-order model for a typical week (Jul. 14-20) is displayed in Fig. 2.21. It shows good agreement between the reduced-order model and high-order model simulations. It can be seen that both the weekdays (Jul. 14-18) and the weekends (Jul. 19-20) can be well handled by the reduced-order model, although they have quite different operational schedules.

Note that the four zones present daily cooling load profiles with diverse patterns, as shown in Fig. 2.22. More specifically, the cooling load of the east zone achieves its peak at around 10:00am in the morning, while that of the west zone has a peak at around 4:00pm in the afternoon. The north and south zones present symmetric load profiles with the peaks at around 2:00pm.

The results reflect the relationship between the solar radiation schedule and zone orientation, and can inform the operational strategy design for the air conditioning systems.

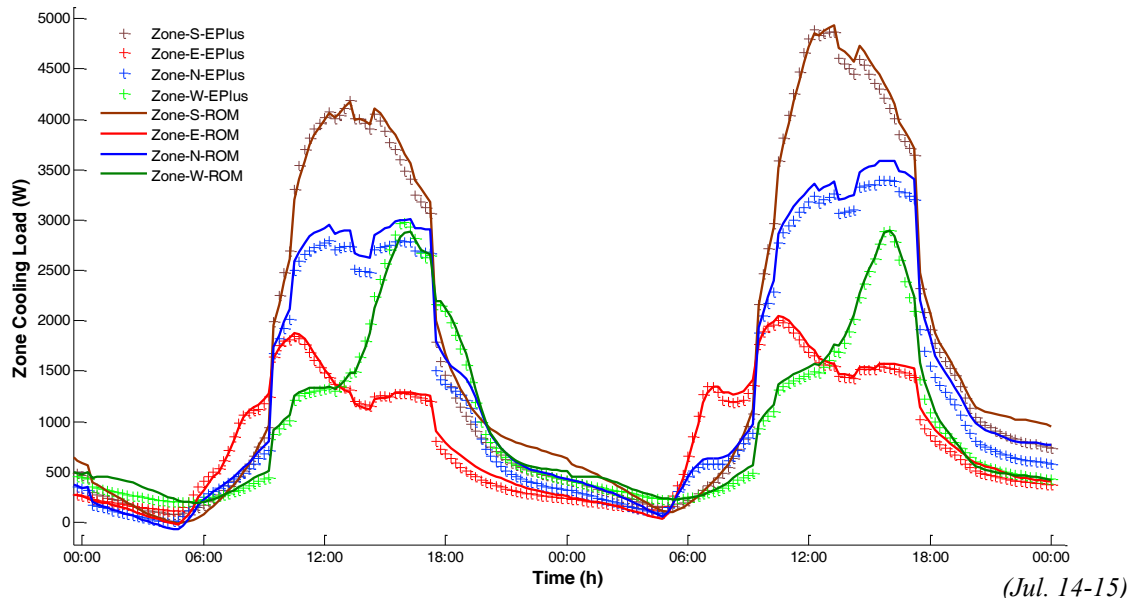


Fig. 2.22 Comparison of the daily cooling load profiles for four zones

A set of CTS and RTS values is obtained for each 3-day calibration for each zone, so 120 sets (the number of zones \times the number of simulation days) are obtained in the monthly study of the four zones discussed above. It is found that the four zones have similar RTS and CTS profiles, which is largely due to the similar shapes and surface configurations of the different zones. Fig. 2.23 shows the distribution of the recovered CTS and RTS sets as well as the corresponding upper and lower bounds in the optimization. It can be seen that the recovered values tightly gather together with a small deviation.

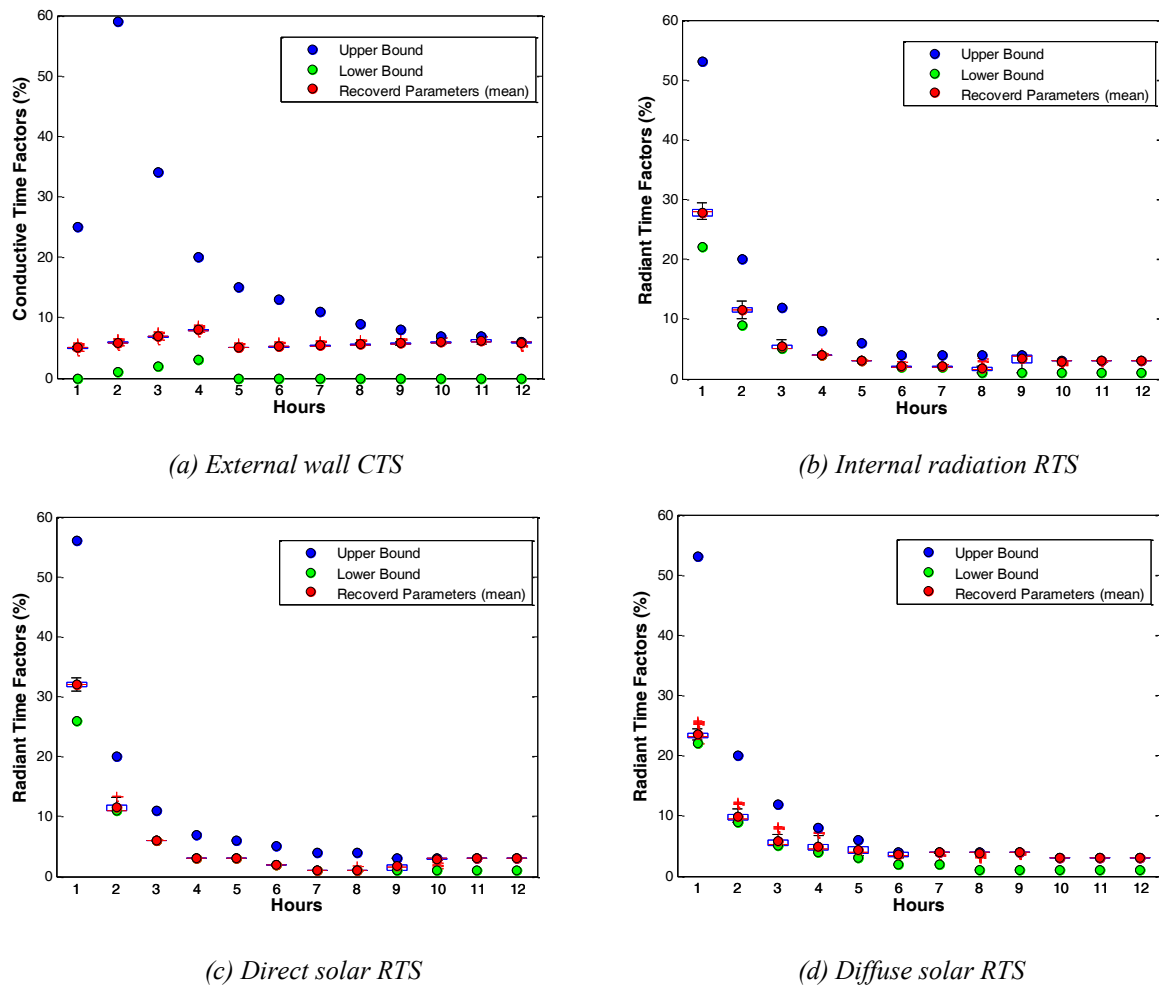


Fig. 2.23 Recovered CTS and RTS values in the calibration for one month (July)

In summary, the reduced-order building model can be well calibrated with the support of high-order EnergyPlus simulations following the proposed procedures. In the one month study for the building case, the calibrated model can yield satisfactory cooling load predictions for all the study zones for both the weekdays and weekends. The recovered reduced-order model will be directly implemented in the dynamic optimization to support the operational analysis in the following chapters.

2.4.5 Parameter Sensitivity Analysis and Ranking

As introduced above, there are 12 time factors in each of the RTS/CTS sets. In order to understand the importance of these time factors in the calibration process, the QR factorizations with a column permutation (QRcp) method is applied in the reduced-order building model to perform parameter sensitivity analysis and ranking (Lund and Foss 2008; Lin 2011).

QRcp method is an effective approach for parameter selection and estimation through successive orthogonalization of the sensitivity matrix derivative for parameter ranking. Based on orthogonal factorization, the method is easy to implement and the results are easily interpreted.

The scaled sensitivity coefficient matrix used in the QRcp algorithm can be expressed as (Yao et al. 2003; Lin 2011):

$$X = \begin{bmatrix} \left. \frac{\theta_1^*}{y^*} \frac{\partial y}{\partial \theta_1} \right|_{t_1} & \left. \frac{\theta_2^*}{y^*} \frac{\partial y}{\partial \theta_2} \right|_{t_1} & \dots & \left. \frac{\theta_{P-1}^*}{y^*} \frac{\partial y}{\partial \theta_{P-1}} \right|_{t_1} & \left. \frac{\theta_P^*}{y^*} \frac{\partial y}{\partial \theta_P} \right|_{t_1} \\ \left. \frac{\theta_1^*}{y^*} \frac{\partial y}{\partial \theta_1} \right|_{t_2} & \left. \frac{\theta_2^*}{y^*} \frac{\partial y}{\partial \theta_2} \right|_{t_2} & & \left. \frac{\theta_{P-1}^*}{y^*} \frac{\partial y}{\partial \theta_{P-1}} \right|_{t_2} & \left. \frac{\theta_P^*}{y^*} \frac{\partial y}{\partial \theta_P} \right|_{t_2} \\ & \vdots & \ddots & \vdots & \\ \left. \frac{\theta_1^*}{y^*} \frac{\partial y}{\partial \theta_1} \right|_{t_{N-1}} & \left. \frac{\theta_2^*}{y^*} \frac{\partial y}{\partial \theta_2} \right|_{t_{N-1}} & \dots & \left. \frac{\theta_{P-1}^*}{y^*} \frac{\partial y}{\partial \theta_{P-1}} \right|_{t_{N-1}} & \left. \frac{\theta_P^*}{y^*} \frac{\partial y}{\partial \theta_P} \right|_{t_{N-1}} \\ \left. \frac{\theta_1^*}{y^*} \frac{\partial y}{\partial \theta_1} \right|_{t_N} & \left. \frac{\theta_2^*}{y^*} \frac{\partial y}{\partial \theta_2} \right|_{t_N} & & \left. \frac{\theta_{P-1}^*}{y^*} \frac{\partial y}{\partial \theta_{P-1}} \right|_{t_N} & \left. \frac{\theta_P^*}{y^*} \frac{\partial y}{\partial \theta_P} \right|_{t_N} \end{bmatrix} \quad (2.21)$$

where

t_1, \dots, t_N the time-step points [--]

y responses, i.e., time-step cooling load [W]

y^* the cooling loads corresponding to the recovered RTS and CTS values [W]

$\theta_1, \dots, \theta_P$ parameters to be estimated, i.e., RTS and CTS values [--]

θ_i^* the recovered RTS and CTS values in the calibration [--].

The individual parametric sensitivity coefficients as elements of the matrix are numerically determined, as described in (Lin 2011).

Then the matrix singular value decomposition is carried out for X, as:

$$X = U D V^T \quad (2.22)$$

where D is a diagonal matrix of the same dimension as X, with non-negative diagonal elements in decreasing order, and U and V are unitary matrices.

It is assumed that the estimated parameters are affected by noise following a Gaussian distribution with zero mean and covariance matrix Σ_θ , which follows:

$$\Delta_{\theta}^T \Sigma_{\theta}^{-1} \Delta_{\theta} = \gamma \quad (2.23)$$

Σ_{θ} and X can be expressed by:

$$\begin{aligned} \Sigma_{\theta} &= (X^T \Sigma_y^{-1} X)^{-1} = (V D^T U^T \Sigma_y^{-1} U D V^T)^{-1} \\ &= \left(V D^T U^T \frac{I}{\sigma_y} U D V^T \right)^{-1} = \sigma_y (V D^T U^T U D V^T)^{-1} \\ &= \sigma_y (V D^T D V^T)^{-1} = \sigma_y (V \Lambda V^T)^{-1} \end{aligned} \quad (2.24)$$

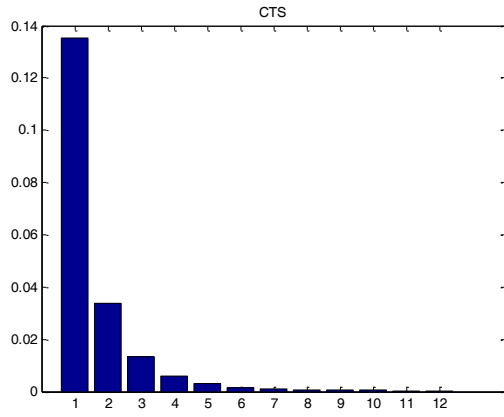
where

Σ_{θ} covariance matrix of the estimated parameters [--]

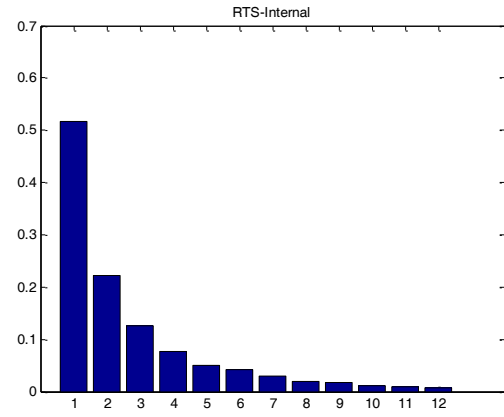
Σ_y, σ_y covariance matrix of the responses [--].

The triangular matrix Λ gives an easy form of the variance contribution of individual parameters, and is used as the criteria to assess the influence of the estimated parameters on the responses. The results for all the RTS/CTS sets are compared in Fig. 2.24.

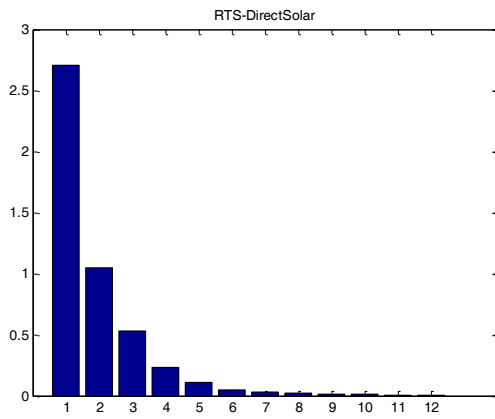
It can be observed that in all the RTS/CTS sets, the first several time factors present more influence on the cooling load outputs of the reduced-order model. In other words, the first ones are more prominent in the calibration than the later ones. Therefore, it is reasonable to choose only the first time factors in the RTS/CTS sets in the calibration, such as the first 6, in order to balance the calibration accuracy and the computational complexity. This may be very critical in analyzing buildings with complex configurations, which usually present a large parameter set.



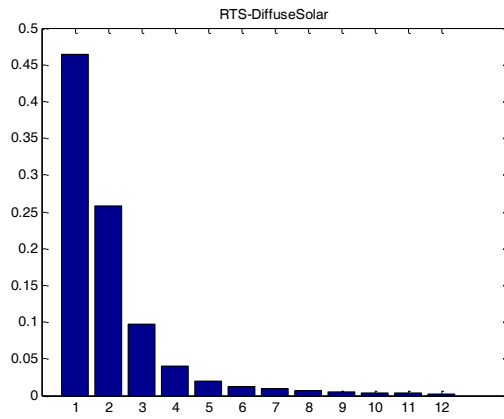
(a) External wall CTS



(b) Internal radiation RTS



(c) Direct solar RTS



(d) Diffuse solar RTS

Fig. 2.24 Variance contribution of CTS and RTS values for parameter sensitivity analysis and ranking

CHAPTER 3 PHYSICAL MODELS FOR AIR CONDITIONING SYSTEMS WITH DEHUMIDIFICATION FEATURES

This chapter develops the physical model for the active air conditioning systems, which is the other critical part of the physical model development for the dynamic optimization. The purpose of the model is to specify the dynamic hygrothermal behavior and energy performance of the system under various operating conditions. Two representative air conditioning systems are investigated as the study cases: variable air volume systems (VAV) with mechanical dehumidification, and the desiccant wheel system (DW) with chemical dehumidification.

3.1 Modeling of Variable Air Volume System: Mechanical Dehumidification

3.1.1 Introduction to the VAV system operation

Variable air volume systems (VAV) are the most widely used air conditioning systems with mechanical dehumidification features. It is an all-air space conditioning system which is capable of varying the volumetric flow of supply air to the space.

Fig. 3.1 shows the configurations of a typical VAV system. During cooling seasons, the outdoor air (OA) is first mixed with an appropriate amount of return air (RA), and then cooled and dehumidified by the cooling coil. After that, the low-temperature and low-humidity air (SA) is supplied into the building space. The temperature and moisture content of the supplied air should be properly manipulated to stay sufficiently low to absorb the extra heat and moisture of the space (McQuiston, Parker, and Spitler 2005).

To ensure acceptable indoor air quality for the occupants, sufficient outdoor air needs to be supplied. In the optimization formulation, the sum of ventilation and OA airflow rates is manipulated to satisfy the minimum ventilation rate requirement (2.5L/s/person) by ASHRAE (ASHRAE 2004).

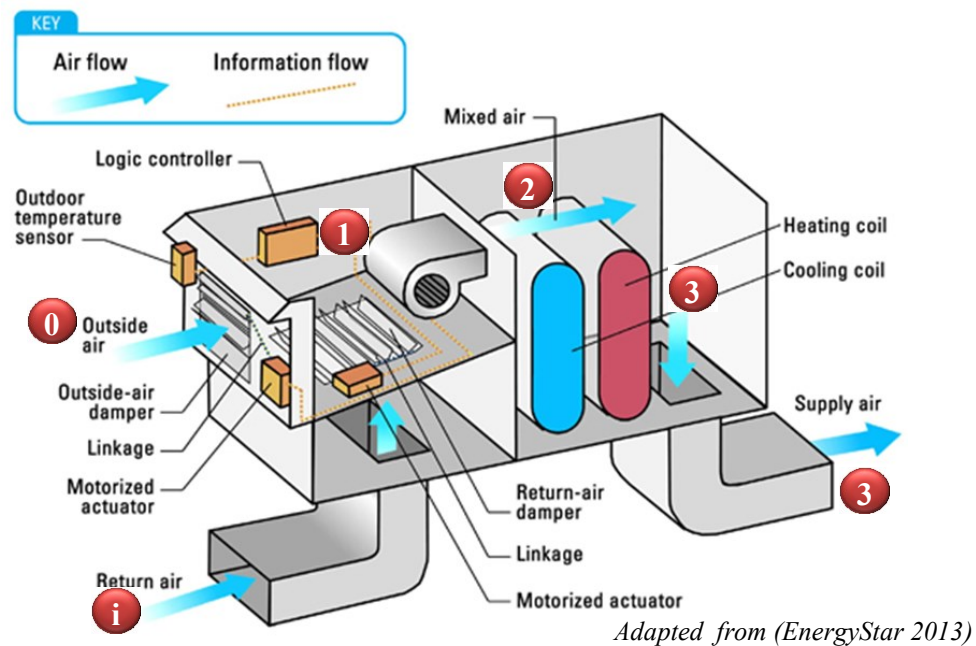


Fig. 3.1 Schematic figure of a typical VAV system

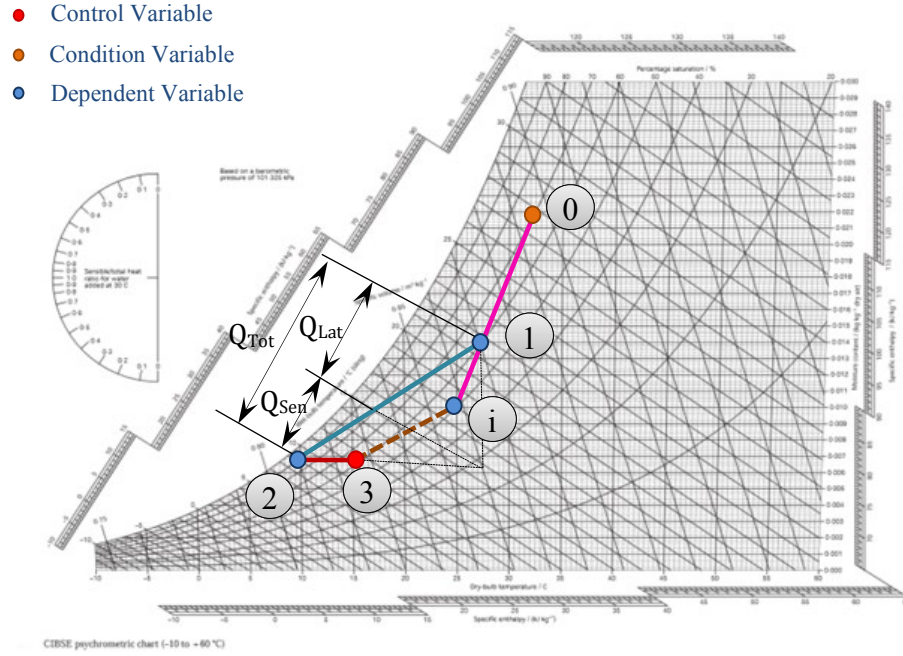


Fig. 3.2 Psychrometric representations of the VAV system operation

3.1.2 Performance modeling of the VAV system

As represented in the psychrometric chart in Fig. 3.2, the operation of VAV system can be divided into several moist air processes, including:

- **Air mixing process** (state point i & 0 > point1)

The mixing of RA and OA is assumed to be an adiabatic process. Heat losses and gains to the ducts are neglected in the study, so the moist air state of RA is same as that of the indoor air.

The mass balance on the dry air is given by

$$m_o + m_r = m_s \quad (3.1)$$

The mass balance on the moisture is given by

$$m_o W_o + m_r W_i = m_s W_1 \quad (3.2)$$

An energy balance gives

$$m_o h_o + m_r h_i = m_s h_1 \quad (3.3)$$

where

- \dot{m}_o mass flow rate of OA [kg/s]
- \dot{m}_r mass flow rate of RA [kg/s]
- \dot{m}_s mass flow rate of SA [kg/s]
- W humidity ratio of the air [kg_w/kg_{air}]
- h enthalpy of the air [kJ/kg]
- $o, i, l \dots$ labels of moist air state points [--].

It is assumed standard atmosphere pressure in the study, so the humidity ratio and enthalpy of the air can be obtained at given temperature and relative humidity levels, via the moist air property equations.

- **Cooling and dehumidification process** (state point 1 > point 2)

This process happens when the mixed air passes through the cooling coil. Air enters the coil at state point 1 (Fig. 3.2). The surface temperature of the coil is lower than the air's dew point, which leads to the condensation of the moisture in the air. In this way, the coil removes sensible heat as well as latent heat from the air stream. The dehumidified, cooled air leaves the coil at its saturation temperature at point 2 (ASHRAE 2008).

The Coil Refrigeration Load (CRL), which is the total rate of heat transfer from the moist air to the cooling coil, can be calculated by

$$q_{coil} = m_s [(h_1 - h_2) - (W_1 - W_2)h_v] \quad (3.4)$$

where

q_{coil} Coil Refrigeration Load [kW]

h_v evaporation enthalpy [kJ/kg].

On the right hand of Eq. (3.4), the first term is the change of enthalpy of the moist air, and the second one is the enthalpy of the condensation. The second term is usually neglected due to its small amount compared to the first one.

The energy consumption by cooling coil can be obtained by dividing CRL with the overall COP of the chiller system. In this study, COP is set as 3.5 which is a representative value for the medium size office building systems (Chong et al. 2014).

- **Reheating process** (state point 2 > point 3)

This process happens during the reheat of the cooled and dehumidified air. During this process, the dry bulb temperature of the air is increased while its humidity ratio remains the same. In the study, electric reheating is used which has a COP of 1.0.

The reheating load can be calculated by

$$q_h = m_s (h_3 - h_2) \quad (3.5)$$

- **Heating and humidification process** (state point 3 > point i)

After the reheating process, the temperature and humidity ratio of the supply air achieve the deserved levels, which enables the absorption of the heat of moisture within the indoor environment.

In the above processes, the analysis of the thermodynamic properties of moist air is essential for the calculation of the energy consumption. For this purpose, the moist air property equations given by ASHRAE are used (ASHRAE 2005).

In addition to the energy consumption by the cooling and reheating coils, the energy consumed by fans should also be considered. A polynomial-based fan model is implemented here to describe the relation between the volumetric flow rate and the fan electric power. This model is the one used in EnergyPlus for analyzing variable speed fan performance.

The model can be represented by the following equations:

$$F = \dot{m} / \rho_0 \quad (3.6)$$

$$F_{pl} = FC1 + FC2 * F + FC3 * F^2 + FC4 * F^3 + FC5 * F^4 \quad (3.7)$$

$$Q_{tot} = F_{pl} * \rho_0 * \frac{\Delta P}{e_{tol} * \rho_{air}} \quad (3.8)$$

$$Q_{shaft} = e_{motor} * Q_{tot} \quad (3.9)$$

where

FC_i empirical coefficients [--]

e_{tol} fan total efficiency [--]

e_{motor} motor efficiency [--]

\dot{m} air mass flow rate [kg/s]

\dot{m}_o design air mass flow rate [kg/s]

Q_{shaft} fan shaft power [W]

Q_{tot} is the fan power [W]

ΔP design pressure increase [Pa].

3.1.3 Control variables in the dynamic optimization for VAV

In the dynamic optimization of the integrated operation of the VAV system, the following five parameters are considered as control variables: (1) OA air flow rate (\dot{m}_o), (2) RA air flow rate (\dot{m}_r), (3) ventilation air flow rate (\dot{m}_{vent}), (4) SA temperature (T_3), (5) SA humidity ratio (W_3). The profiles of these parameters are well manipulated in the dynamic optimization to minimize the set objectives while satisfying the constraints during the whole operation process.

The general relationships between the control variables and other key parameters can be summarized as follows:

- OA and RA air flow rate: determines the thermodynamic properties of mixed air (point 1), and thus further affects the CRL (Eq. (3.4)).
- Ventilation air flow rate: changes the sensible and latent cooling loads of the building, and thus changes the requirements of the SA amount.
- SA temperature and humidity ratio: determines the thermodynamic properties of the air at the outlet of the cooling coil (point 2), and thus affects the CRL (Eq. (3.4)); determines the thermodynamic properties of the supply air (point 3), and thus affects the reheating load (Eq. (3.5)).

3.1.4 Summary of the key parameters in the VAV system operation

Table 3.1 lists the key parameters in the integrate VAV system operation, and summarizes their variable type and calculation methods.

Table 3.1 List of the key parameters in the VAV system operation

Name	Related Points	Variable Type	Sources
Outdoor air temperature (T_o)	0	Condition variable	Input information
Outdoor air humidity ratio (W_o)	0	Condition variable	Input information
Outdoor air enthalpy (h_o)	0	Dependent variable	Calculated from T_o, W_o
Mixed air temperature (T_l)	1	Dependent variable	Calculated from T_o, T_b, m_r, m_0
Mixed air humidity ratio (W_l)	1	Dependent variable	Calculated by Eq. (3.2)
Mixed air enthalpy (h_l)	1	Dependent variable	Calculated by Eq. (3.3)
Cooled air temperature (T_2)	2	Dependent variable	Calculated from $W_2, RH_2 (90\%)$
Cooled air humidity ratio (W_2)	2	Dependent variable	Calculated from $W_3 (equal)$
Cooled air enthalpy (h_2)	2	Dependent variable	Calculated from T_2, W_2
Supply air temperature (T_3)	3	Control variable	Manipulated by optimization
Supply air humidity ratio (W_3)	3	Control variable	Manipulated by optimization
Supply air enthalpy (h_3)	3	Dependent variable	Calculated from T_3, W_3
Indoor air temperature (T_i)	i	Dependent variable	Calculated by building model
Indoor air humidity ratio (W_i)	i	Dependent variable	Calculated by building model
Indoor air enthalpy (h_i)	i	Dependent variable	Calculated from T_i, W_i
Mass flow rate of OA (\dot{m}_0)	0, 1	Control variable	Manipulated by optimization
Mass flow rate of RA (\dot{m}_r)	i, 1	Control variable	Manipulated by optimization
Mass flow rate of SA (\dot{m}_s)	3	Dependent variable	Calculated by Eq. (3.1)
Coil refrigeration load (q_c)	1, 2	Dependent variable	Calculated by Eq. (3.4)
Reheating load (q_h)	2, 3	Dependent variable	Calculated by Eq. (3.5)

3.2 Modeling of Desiccant Wheel System: Chemical Dehumidification

Different from the typical VAV system, the desiccant wheel system (DW) rely on the chemical dehumidification modules for the humidity control purposes. The modules may include the enthalpy recovery wheel (ERW), or the active desiccant wheel (ADW), or both of them.

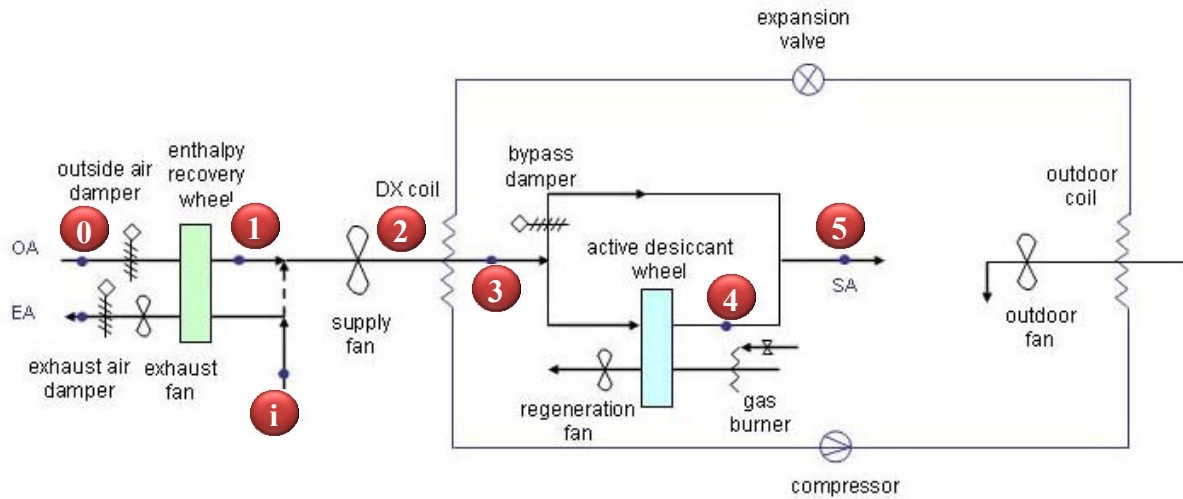
DW system may have various configurations in terms of component selection and arrangement. In this study, the SEMCO FVR 2000 and REV 2250 system installed in the Intelligent Workplace (IW) of Carnegie Mellon University is chosen as the specific case study. It includes both the enthalpy recovery and active desiccant wheels as part of the IW Energy Supply System (IWESS), as shown in Fig. 3.3 and Fig. 3.4. Extensive studies have been conducted under various static operation conditions, including its dehumidification effectiveness, energy saving and cost performance, and the cooperation performance with other systems such as bio diesel engine generators (Zhai, Archer, and Fischer 2008; Zhai 2008; Zhai, Archer, and Fischer 2008; Zhai et al. 2005).

3.2.1 Introduction to the DW system operation

As shown in Fig. 3.3 and Fig. 3.4, the DW system integrates three major components, namely the enthalpy recovery wheel module, the direct expansion (DX) cooling coil, and the active desiccant wheel module. The enthalpy removal task, which includes both the sensible and latent cooling, is accomplished by the combined functions of the three components at typical summer operating conditions.

The moist air conditioning processes in the above configured system are depicted in the psychrometric chart shown in Fig. 3.5. The outdoor air (OA) is first drawn through the enthalpy recovery wheel, where it is pre-conditioned by the exhaust air (EA) from the indoor environment (state point 0 > point 1). The preconditioned OA is then mixed with return air (RA) (state point 1 > point 2), and goes through the cooling coil where it is cooled and dehumidified (state point 2 > point 3). After that, the mixed air is split into two portions: one portion is brought into the active desiccant wheel where it is further dehumidified but heated (state point 3 > point 4); the other portion bypasses around the wheel through a modulating damper. The warm dry air from the desiccant wheel is then mixed with the cold moist bypass air (state point 3,4 > point 5), and then ducted into the building space to condition the space by absorbing heat and moisture (state point 5 > point i). In the DW system operations, the dampers, heat pump compressor and the desiccant regeneration air temperature can be adjusted to obtain the specified conditions of various moist points (Zhai, Archer, and Fischer 2008; Zhai 2008).

Compared with the VAV system operations introduced in Section 3.1.2, the DW system presents two more moist air processes, that is, the pre-conditioning process within the enthalpy recovery wheel, and the heating and dehumidification process within the active desiccant wheel. These two processes can be evaluated via the wheel performance models introduced in the following sections. All the other processes can be handled in the same way as the VAV system.

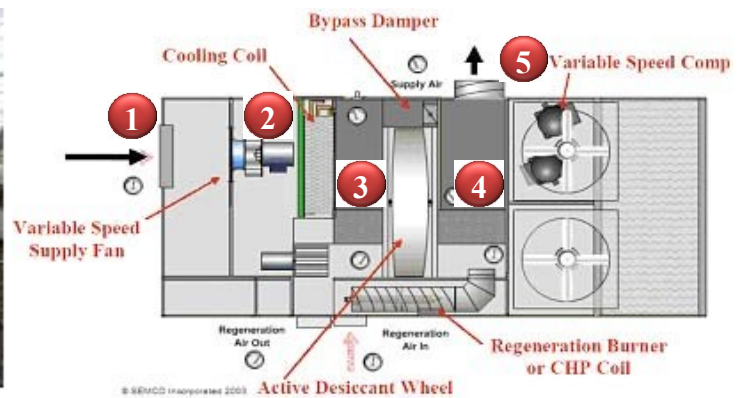


Adapted from (Zhai 2008)

Fig. 3.3 Flow diagram of the SEMCO FVR 2000 and REV 2250 desiccant wheel system installed in the IW at Carnegie Mellon



(l) Enthalpy recovery wheel



Adapted from (Zhai 2008)

(r) Active desiccant wheel

Fig. 3.4 Schematic charts of the FVR 2000 and REV 2250 desiccant wheel system

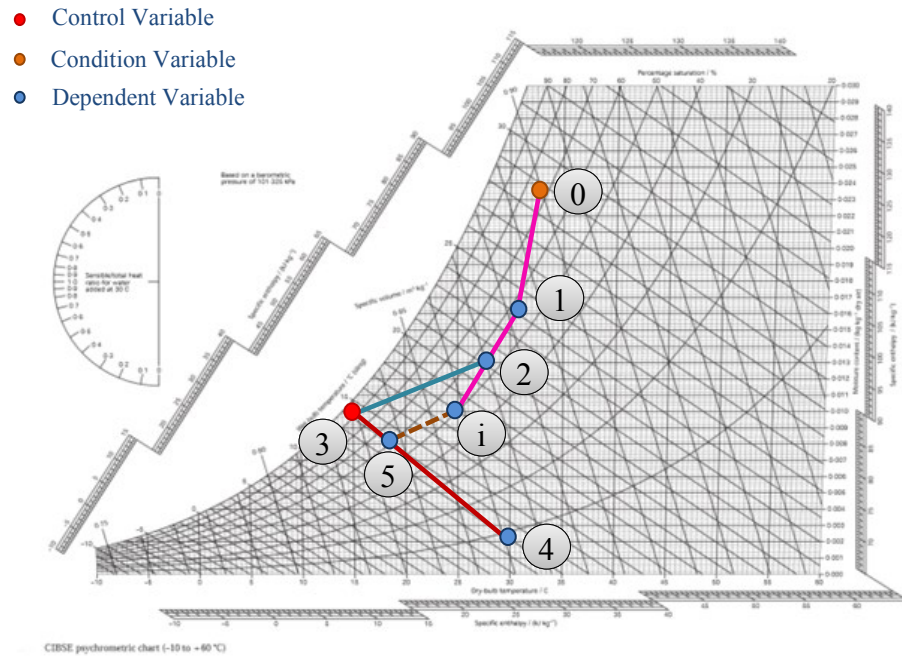


Fig. 3.5 Psychrometric representations of the DW system operation

3.2.2 Desiccant wheel performance modeling

Desiccant wheel, either the active desiccant wheel or the enthalpy recovery wheel, is widely acknowledged as the most critical component in the desiccant cooling system, in terms of system capacity, energy performance and operating cost (Ge et al. 2008; Zhai et al. 2005).

The performance of the desiccant wheel is affected by more than 20 parameters, including the design and operation parameters. The former are usually fixed by equipment manufacturers to provide predictable performance in common applications, while the latter usually vary due to the change of weather, moisture load, and reactivation energy levels (ASHRAE 2008).

A number of models have been developed to describe the desiccant performance. Some scholars formulated the model with complex mathematical details based on the heat and mass conservation principles. Such models need to address complicated thermodynamic properties of the porous coating material, as well as the interrelated and coupled effects during the transfer process (San 1993; Ge et al. 2008). Moreover, it needs to take into account both the gas-side resistances (GSRs) coming from the diffusion and heat conduction between air and desiccant, as well as the solid-side resistances (SSRs) coming from the heat conduction and mass diffusion within solid desiccant felt (Majumdar and Worek 1989; Charoensupaya and Worek 1988).

Some scholars believe that the mathematical models based on the detailed transfer phenomena may be too complicated and time-consuming for many applications, and therefore they develop empirical models by using large amounts of experimental results. Such models can usually be represented in a simpler form and thus is preferred in the numerical simulation based researches (Beccali et al. 2003; Jeong and Mumma 2005).

3.2.3 Performance modeling of the active desiccant wheel

The default performance model implemented in EnergyPlus is used in the study. It describes the typical performance of a generic solid desiccant wheel by a set of empirical curve equations representing the conservation of energy and mass and the adsorption equilibrium. The model relates the active desiccant wheel's energy performance with its design parameters and operating conditions (DOE 2013; Kosar 2006).

The input information for the model includes:

- Process air inlet dry-bulb temperature (1.7°C~48.9°C)
- Process air inlet humidity ratio (0.002857 kg_w/kg_{air} ~0.02857 kg_w/kg_{air})
- Process air velocity

The results from the model predictions are:

- Process air outlet dry-bulb temperature
- Process air outlet humidity ratio
- Regeneration energy consumption rate
- Regeneration air velocity

The process air outlet dry-bulb temperature is given by:

$$\begin{aligned}
 T_{po} = & TC0 + TC1 * T_{pi} + TC2 * W_{pi} + TC3 * V_p + TC4 * T_{pi} * W_{pi} + TC5 * T_{pi} * \\
 & V_p + TC6 * W_{pi} * V_p + TC7 * T_{pi} * T_{pi} + TC8 * W_{pi} * W_{pi} + TC9 * V_p * V_p + \\
 & TC10 * T_{pi} * T_{pi} * W_{pi} * W_{pi} + TC11 * T_{pi} * T_{pi} * V_p * V_p + TC12 * W_{pi} * W_{pi} * \\
 & V_p * V_p + TC13 * \log(T_{pi}) + TC14 * \log(W_{pi}) + TC15 * \log(V_p);
 \end{aligned} \tag{3.10}$$

where

TC_i empirical coefficients [--]

T_{pi} process air inlet dry-bulb temperature [°C]

T_{po} process air outlet dry-bulb temperature [°C]

V_p process air velocity [m/s]

W_{pi} process air inlet humidity ratio [kg_w/kg_{air}].

The process air humidity ratio is given by:

$$\begin{aligned}
 W_{po} = & WC0 + WC1 * T_{pi} + WC2 * W_{pi} + WC3 * V_p + WC4 * T_{pi} * W_{pi} + WC5 * \\
 & T_{pi} * V_p + WC6 * W_{pi} * V_p + WC7 * T_{pi} * T_{pi} + WC8 * W_{pi} * W_{pi} + WC9 * V_p * \\
 & V_p + WC10 * T_{pi} * T_{pi} * W_{pi} * W_{pi} + WC11 * T_{pi} * T_{pi} * V_p * V_p + WC12 * W_{pi} * \\
 & W_{pi} * V_p * V_p + WC13 * \log(T_{pi}) + WC14 * \log(W_{pi}) + WC15 * \log(V_p)
 \end{aligned} \tag{3.11}$$

where

WC_i empirical coefficients [--]

W_{po} process air outlet humidity ratio [kg_w/kg_{air}].

The regeneration air velocity is given by:

$$\begin{aligned}
 V_r = & RC0 + RC1 * T_{pi} + RC2 * W_{pi} + RC3 * V_p + RC4 * T_{pi} * W_{pi} + RC5 * T_{pi} * \\
 & V_p + RC6 * W_{pi} * V_p + RC7 * T_{pi} * T_{pi} + RC8 * W_{pi} * W_{pi} + RC9 * V_p * V_p + \\
 & RC10 * T_{pi} * T_{pi} * W_{pi} * W_{pi} + RC11 * T_{pi} * T_{pi} * V_p * V_p + RC12 * W_{pi} * \\
 & W_{pi} * V_p * V_p + RC13 * \log(T_{pi}) + RC14 * \log(W_{pi}) + RC15 * \log(V_p)
 \end{aligned} \tag{3.12}$$

where

RC_i empirical coefficients [--]

V_r regeneration air velocity [m/s].

The regeneration energy consumption rate is given by:

$$\begin{aligned}
 q_r = & QC0 + QC1 * T_{pi} + QC2 * W_{pi} + QC3 * V_p + QC4 * T_{pi} * W_{pi} + QC5 * T_{pi} * \\
 & V_p + QC6 * W_{pi} * V_p + QC7 * T_{pi} * T_{pi} + QC8 * W_{pi} * W_{pi} + QC9 * V_p * V_p + \\
 & QC10 * T_{pi} * T_{pi} * W_{pi} * W_{pi} + QC11 * T_{pi} * T_{pi} * V_p * V_p + QC12 * W_{pi} * W_{pi} * \\
 & V_p * V_p + QC13 * \log(T_{pi}) + QC14 * \log(W_{pi}) + QC15 * \log(V_p);
 \end{aligned} \tag{3.13}$$

$$Q_r = q_r * V_{nom} * \rho_a * (W_{pi} - W_{po}) \quad (3.14)$$

where

- w_r moisture removal rate [kg/s]
- q_r specific regeneration energy consumption rate [J/kg]
- Q_r energy consumption rate by regeneration [W]
- V_{nom} nominal volumetric flow rate of process air [m³/s]
- ρ_a nominal air density [kg/m³].

The empirical model performance coefficients describing the specific solid desiccant wheel assumed in the study are shown in Appendix 1.

3.2.4 Performance modeling of the enthalpy recovery wheel

The performance model used in this study for the enthalpy recovery wheel is also the one implemented in EnergyPlus (DOE 2013). It describes the performance of a balanced flow desiccant recovery wheel, by relating enthalpy exchange efficiency with the design parameters and operating conditions.

The input information for the model includes:

- Process air inlet dry-bulb temperature (4.58 °C~ 21.83 °C)
- Process air inlet humidity ratio (0.005000 kg_w/kg_{air} ~ 0.017514 kg_w/kg_{air})
- Exhaust air inlet dry-bulb temperature (17.83 °C ~ 48.89 °C)
- Exhaust air inlet humidity ratio (0.005143 kg_w/kg_{air} ~ 0.024286 kg_w/kg_{air})

- Nominal face velocity (2.286m/s ~ 4.826m/s)
- Electric power consumption of the motor

The results from the model predictions are:

- Process air outlet dry-bulb temperature
- Process air outlet humidity ratio
- Exhaust air outlet dry-bulb temperature
- Exhaust air outlet humidity ratio
- Electric energy consumption

The exhaust air outlet dry-bulb temperature and humidity ratio can be obtained by :

$$V_p = \dot{m}_p / A_{face} \quad (3.15)$$

$$T_{eo} = BE1 + BE2*W_{ei} + BE3*T_{ei} + BE4*(W_{ei}/T_{ei}) + BE5*W_{pi} + BE6*T_{pi} + BE7*(W_{pi}/T_{pi}) + BE8*V_p ; \quad (3.16)$$

$$W_{eo} = CE1 + CE2*W_{ei} + CE3*T_{ei} + CE4*(W_{ei}/T_{ei}) + CE5*W_{pi} + CE6*T_{pi} + CE7*(W_{pi}/T_{pi}) + CE8*V_p \quad (3.17)$$

where

A_{face} heat exchanger face area [m²]

BE_i empirical coefficients [--]

CE_i empirical coefficients [--]

\dot{m}_p volumetric flow rate of the regeneration air stream [m³/s]

T_{ei} exhaust air inlet dry-bulb temperature [°C]

T_{pi}	process air inlet dry-bulb temperature [°C]
V_p	face velocity of the regeneration (and process) air stream [m/s]
W_{ei}	exhaust air inlet humidity ratio [kg _w /kg _{air}]
W_{pi}	process air inlet humidity ratio [kg _w /kg _{air}].

The process air outlet dry-bulb temperature and humidity ratio can be obtained by:

$$T_{po} = (T_{ei} - T_{eo}) + T_{pi} \quad (3.18)$$

$$W_{po} = (W_{ei} - W_{eo}) + W_{pi} \quad (3.19)$$

where

T_{po}	process air outlet dry-bulb temperature [°C]
W_{po}	process air outlet humidity ratio [kg _w /kg _{air}].

The energy consumption by the motor of the wheel is given by:

$$Q_{elec} = Q_{nom} * m_p / (V_{nom} * \rho_a) \quad (3.20)$$

where

Q_{elec}	electric power corresponding to a certain amount of process air [W]
Q_{nom}	nominal electric power [W]
V_{nom}	nominal volumetric flow rate of process air [m ³ /s]
ρ_a	nominal air density [kg/m ³].

The empirical model performance coefficients describing the specific enthalpy recovery wheel assumed in the study are shown in Appendix 2.

3.2.5 Control variables in the dynamic optimization for DW

In the dynamic optimization of the integrated operation of the DW system, the following six parameters are considered as control variables: (1) OA air flow rate (\dot{m}_o), (2) RA air flow rate (\dot{m}_r), (3) flow rate of the air passing through the active desiccant wheel (\dot{m}_{adw}), (4) ventilation air flow rate (\dot{m}_{vent}), (5) temperature of the air after DX cooling coil (T_3), (6) humidity ratio of the air after DX cooling coil (W_3). The profiles of these parameters are well manipulated in the optimization to minimize the set objectives while satisfying the constraints during the whole operation process (described in Section 4.1.1).

The general relationships between the control variables and other key parameters can be summarized as follows:

- OA air flow rate: determines the thermodynamic properties of the air leaving the enthalpy recovery wheel (point 1), and affects the properties of the mixed air (point 2).
- RA air flow rate: determines the thermodynamic properties of the mixed air (point 2), and thus affects the cooling coil load (Eq. (3.4)).
- Flow rate of the air passing through the active desiccant wheel: determines the thermodynamic properties of the air leaving the active desiccant wheel (point 4), and further affects the properties of the supply air (point 5).
- Ventilation air flow rate: changes the sensible and latent cooling loads of the building, and thus changes the requirements of the SA amount.
- Temperature and humidity ratio of the air leaving the DX cooling coil: determines the thermodynamic properties of the air at the outlet of the cooling coil (point 3), and thus

affects the cooling coil load (Eq. (3.4)); affects the thermodynamic properties of the air leaving the active desiccant wheel (point 4) as well as the supply air (point 5).

3.2.6 Summary of the key parameters in the DW system operation

Table 3.2 lists the key parameters in the integrate DW system operation, and summaries their variable type and calculation methods.

Table 3.2 List of the key parameters in the DW system operation

Name	Related Points	Variable Type	Sources
Outdoor air temperature (T_o)	0	Condition variable	Input information
Outdoor air humidity ratio (W_o)	0	Condition variable	Input information
Temperature of the air leaving ERW (T_l)	1	Dependent variable	Calculated by ERW model
Humidity ratio of the air leaving ERW (W_l)	1	Dependent variable	Calculated by ERW model
Enthalpy of the air leaving ERW (h_l)	1	Dependent variable	Calculated from T_l , W_l
Energy consumption of ERW (Q_{erw})	0,1,i	Dependent variable	Calculated by ERW model
Mixed air temperature (T_2)	1	Dependent variable	Calculated from T_l , T_i
Mixed air humidity ratio (W_2)	1	Dependent variable	Calculated by Eq. (3.2)
Mixed air enthalpy (h_2)	1	Dependent variable	Calculated by Eq. (3.3)
Temperature of the air leaving DX (T_3)	3	Control variable	Manipulated by optimization
Humidity ratio of the air leaving	3	Control variable	Manipulated by optimization

DX (W_3)			
Enthalpy of the air leaving DX (h_3)	3	Dependent variable	Calculated from T_3 , W_3
Temperature of the air leaving ADW (T_4)	4	Dependent variable	Calculated by ADW model
Humidity ratio of the air leaving ADW (W_4)	4	Dependent variable	Calculated by ADW model
Enthalpy of the air leaving ADW (h_4)	4	Dependent variable	Calculated from T_4 , W_4
Energy consumption of ADW (Q_{adw})	3,4	Dependent variable	Calculated by ADW model
Supply air temperature (T_5)	5	Dependent variable	Calculated from T_3 , T_4
Supply air humidity ratio (W_5)	5	Dependent variable	Calculated from W_3 , W_4
Supply air enthalpy (h_5)	5	Dependent variable	Calculated from T_5 , W_5
Indoor air temperature (T_i)	i	Dependent variable	Calculated by building model
Indoor air humidity ratio (W_i)	i	Dependent variable	Calculated by building model
Indoor air enthalpy (h_i)	i	Dependent variable	Calculated from T_i , W_i
Mass flow rate of OA (\dot{m}_0)	0,1,2	Control variable	Manipulated by optimization
Mass flow rate of RA (\dot{m}_r)	i,2	Control variable	Manipulated by optimization
Mass flow rate of the air passing through ADW (\dot{m}_{adw})	3,4,5	Control variable	Manipulated by optimization
Coil refrigeration load (q_c)	1, 2	Dependent variable	Calculated by Eq. (3.4)

CHAPTER 4 DYNAMIC OPTIMIZATION FORMULATION AND IMPLEMENTATION

This chapter sets out the optimization problem based on the physical model developed in Chapter 2 and Chapter 3. A dynamic optimization formulation is first presented, which consists of ordinary differential and algebraic equations that satisfy the twice-differentiable condition. The simultaneous collocation method is then used in the solution algorithm, translating the dynamic optimization formulation into an NLP that is solved by IPOPT in the GAMS platform.

4.1 Dynamic Optimization Formulation

4.1.1 Objectives of the process optimization

The task of the dynamic optimization is to determine the corresponding optimal operating profiles of the associated system inputs (also termed as control variables) as summarized in sections 3.1.3 and 3.2.5, in order to minimize the total energy consumption of the building systems through the whole operation process while satisfying indoor thermal comfort criteria.

In the integrated operation of the VAV system, the energy consumption of the system comes from: (1) operation of the cooling coil for cooling and dehumidification, (2) operation of the

heating coil for reheating, and (3) operation of the fans for ventilation. Therefore, the objective function representing the energy load and can be written as:

$$\min \quad \Phi = \int_{t_0}^{t_f} (Q_{cooling} + Q_{reheating} + Q_{fan}) dt \quad (4.1)$$

where

$Q_{cooling}$ energy consumption rate in the cooling coil [W]

$Q_{reheating}$ energy consumption rate in the reheating coil [W]

Q_{fan} energy consumption rate by fans [W].

In the integrated operation of the DW system, the energy consumption of the system comes from: (1) operation of the cooling coil for cooling and dehumidification, (2) operation of the desiccant wheels, and (3) operation of the fans. Therefore, the objective function can be stated as:

$$\min \quad \Phi = \int_{t_0}^{t_f} (Q_{cooling} + Q_{dw} + Q_{fan}) dt \quad (4.2)$$

where

$Q_{cooling}$ energy consumption rate in the cooling coil [W]

Q_{dw} energy consumption rate in the desiccant wheels [W]

Q_{fan} energy consumption rate by fans [W].

4.1.2 Constraints for the integrated system operation

The quantities mentioned in the above objective functions can be determined from the intrinsic properties in the physical model developed in the previous chapters. These models,

including both the building model and system model, define the equations that have to be satisfied by the variables and thus are considered as equality constraints in the optimization. After careful check, it is found that the DAE model is a semi-explicit system of index 1 and thus can be suitably handled by the simultaneous collocation method introduced in section 4.2 (Biegler 2010).

Meanwhile, additional inequality constraints are introduced to represent the requirements on the following indices:

- **Indoor thermal comfort**

Ensuring the thermal comfort of building occupants during office hours is the primary purpose of building HVAC systems. Therefore, the indoor thermal comfort requirement is considered as a critical constraint for optimization. Although a large number of thermal comfort indices have been developed in many previous research studies (Gagge A.P. 1994; Fanger 1970; Hamdi, Lachiver, and Michaud 1999), the most widely used is the one developed by Fanger in which predicted mean vote (PMV) and predicted percentage dissatisfied (PPD) are defined as indices to evaluate the thermal comfort levels inside a building space (Fanger 1970). The value of the PMV index has a range between -3 and +3, corresponding to human sensations from cold to hot respectively.

The thermal comfort level is affected by the metabolic rate, the clothing label and ambient air environmental (ASHRAE 2005; ISO 2005). For a common summer office working condition (metabolic energy production 1.2 Met; rate of mechanical work 0 W; mean radiant temperature 22°C; basic clothing insulation 1 clo; relative air velocity 0.2 m/s), PMV and

PPD are determined given the indoor air temperature and relative humidity levels, as expressed in Eq. (4.3) and (4.4):

$$PMV = -3.435 - 0.342 \times \varphi + (0.1282 + 0.04233 \times \varphi) \times T_i \quad (4.3)$$

$$PPD = 100 - 95 \times \exp(-0.2179 \times PMV^2 - 0.03353 \times PMV^4) \quad (4.4)$$

where

PMV predicted mean vote [--]

PPD predicted percentage dissatisfied [%]

T_i indoor air temperature [°C]

φ relative humidity [--].

In the integrated operation, the control strategy is set to ensure that the PPD does not exceed the limit of 10%, which corresponds to the PMV range of ± 0.5 .

- **Indoor air quality**

Sufficient outdoor air needs to be supplied to assure the good indoor air quality, which is related to the health and productivity of the occupants. In the optimization formulation, the sum of ventilation and OA airflow rates is specified to satisfy the minimum ventilation rate requirement (2.5L/s/person) by ASHRAE (ASHRAE 2004) to ensure acceptable indoor air quality.

- **Indoor moisture condensation**

Indoor air temperature should be higher than the dew point temperature in order to prevent moisture condensation. The calculation of the dew point temperature of indoor air can be carried out in the moist air thermodynamic property model stated earlier in section 3.1.2.

- **System operation characteristics**

The thermodynamic properties of the moist air at various system locations need to fall into the normal ranges representing the equipment operational characteristics, as described in chapter 3. Key constraints include: (1) in the mechanical dehumidification, the air leaving the cooling coils is close to the saturation point, so the RH level should be greater than 90%, (2) in the chemical dehumidification, the air leaving the cooling coils is at a temperature level between 10°C~16°C, (3) the supply air temperature should be greater than 16°C to avoid local discomfort, (4) the supply air should have lower temperature and humidity levels than the indoor air, in order to be stable to absorb the indoor heat and moisture.

4.1.3 General form of the dynamic optimization

After proper reformulations, the dynamic optimization problem can be stated in a general form:

$$\begin{aligned}
 & \min \quad \Phi(z(t_f)) \\
 & s. t. \quad \frac{dz(t)}{dt} = f(z(t), y(t), u(t), p), z(t_0) = z_0 \\
 & \quad \quad \quad g(z(t), y(t), u(t), p) = 0 \\
 & \quad \quad \quad h(z(t), y(t), u(t), p) \leq 0
 \end{aligned} \tag{4.5}$$

where, z and y are the differential and algebraic state variables, respectively; u represents the vector of the control variables. Variables z , y and u are all functions of the scalar time parameter $t \in [t_0, t_f]$, while p represents time-independent parameters. The first-principle based

physical model is represented by the DAEs in f and g , while the inequality constraints are represented in h .

4.2 Solution Approaches for Dynamic Optimization

4.2.1 Comparison of methods for dynamic optimization

To apply the DAE formulation to dynamic optimization, a number of methods can be taken, as summarized in Fig. 4.1. In particular, these methods can be divided into two categories: analytical solution and numerical solution.

Analytical solution of the dynamic optimization problem shown in Eq. (4.5) requires solving corresponding Hamilton–Jacobi–Bellman equations, which remains quite difficult and they cannot handle inequality constraints. On the other hand, **numerical solution** techniques have been significantly advanced over the past few decades. These methods can be generally separated into two types: the sequential (Feehery and Barton 1998; Schlegel et al. 2005) and simultaneous approaches (Biegler 2010).

In the **sequential approach**, also known as control vector parametrization or single shooting, optimization is carried out only in the input space. Standard integration algorithms are employed to integrate the DAEs and piecewise-polynomial approximates are used to represent the control variables. In order to update controls via various search methods, the sensitivity information may be derived (Schlegel et al. 2005). However, this approach requires repeated numerical integration of the DAE model that may lead to significant computational power demands. It also dramatically slows down with the increase of the time horizon length and

degrees of freedom in control which causes fast growth of the problem size. Moreover, the approach converges only along feasible paths that may fail for a system with unstable modes.

The **simultaneous approaches** include the multiple shooting (Bock and Plitt 1984) and simultaneous collocation method (Biegler and Kameswaran 2006). In **multiple shooting**, the time horizon of interest is divided into several segments, and the sequential approach is applied to each time slot. This method unleashes the potential of handling unstable systems while increasing the size of resultant problems.

Comparing with the above competing approaches, the **simultaneous collocation** method has a number of advantages for dynamic optimizations (Biegler 2007; Kameswaran and Biegler 2008) and is selected as the solution approach for the problem formulated in the thesis. The concepts, properties and characteristics of this approach are summarized in detail in the following section.

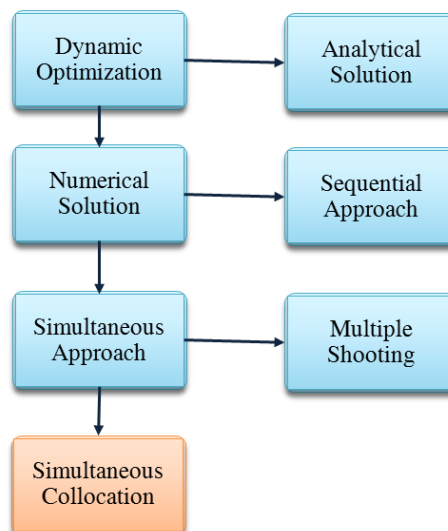


Fig. 4.1 Summary of solution approaches for dynamic optimization

4.2.2 Problem transformation using simultaneous collocation method

The simultaneous collocation method (also called direct transcription) is motivated by avoiding explicit integration for state profiles that is required by the aforementioned approaches. With this method, a DAE system is fully discretized for both the states and controls. In particular, the time domain is first divided into a proper number of finite elements, and several collocation points are then placed in each element. A comprehensive review of the simultaneous collocation method is given in (Biegler 2007).

The choice of collocation points has an influence on the accuracy of the approximation. In this study, **Radau collocation points** are used because of their high accuracy and stability properties. Table 4.1 lists the interpolation locations of Radau roots as collocation points for various degree values, which allow the further construction of the collocation equations. The detailed determination and proof process of Radau collocation points can be found in (Biegler 2010).

Table 4.1 Interpolation locations of Radau roots as collocation points for various degrees

Degree K		Radau Roots			
1	1.000000				
2	0.333333	1.000000			
3	0.155051	0.644949	1.000000		
4	0.088588	0.409467	0.787659	1.000000	
5	0.057104	0.276843	0.583590	0.860240	1.000000

After discretization, the states and controls are approximated via **orthogonal polynomial representations** at collocation points, as shown in Fig. 4.2. More specifically, for the differential states, a Runge-Kutta basis representation is introduced:

$$z(t) = z_{i-1} + h_i \sum_{j=1}^K \Omega_j(\tau) \frac{dz}{dt_{i,j}} \quad (4.6)$$

Here, i is the index of finite elements and j corresponds to collocation points; t is the time from t_i to $t_i + h_i$; $\tau = \frac{t-t_i}{h_i}$ is the normalized time from 0 to 1; z_{i-1} is the value of the variable at the beginning of i ; h_i is the element length; $\dot{z}_{i,j}$ is the first-order derivative value in element i at point j ; and $\Omega_j(\tau)$ is a polynomial of order K , defined as:

$$\Omega_j(\tau) = \int_0^\tau l_j(\tau') d\tau' \quad (4.7)$$

where, l_j is a Lagrange interpolation polynomial shown as follows:

$$l_j(\tau) = \prod_{j'=0, \neq j}^K \frac{\tau - \tau_{j'}}{\tau_j - \tau_{j'}} \quad (4.8)$$

To this end, the differential variables have been discretized. In addition, to ensure the **continuity condition** across element boundaries, the following equation is introduced:

$$z_i = z_{i-1} + h_i \sum_{j=1}^K \Omega_j(1) \frac{dz}{dt_{i,j}} \quad (4.9)$$

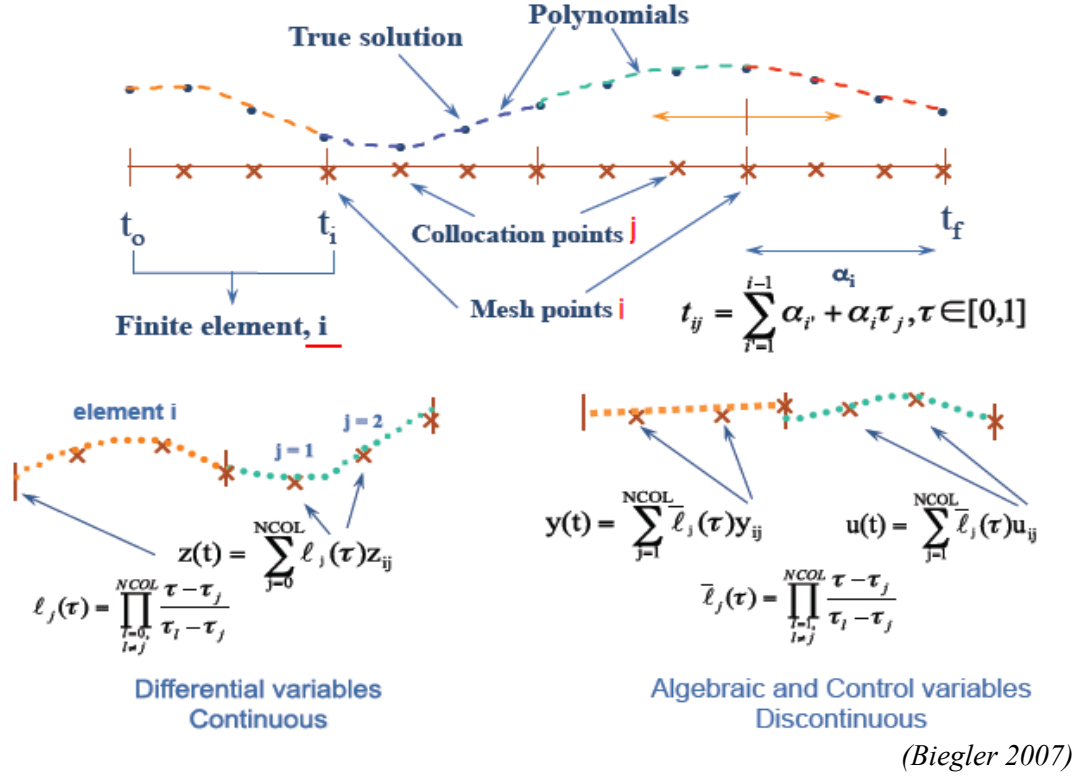


Fig. 4.2 Orthogonal polynomial representations at collocation points on finite elements

Similarly, for the **algebraic states**, the profiles can be represented with **Lagrange polynomials**:

$$y(t) = \sum_{j=1}^K l'_j(\tau) y_{i,j} \quad (4.10)$$

The weight l'_j is similarly defined as in Eq. (4.8) with degree K . It is worth noting that discontinuity is allowed for the algebraic states at element boundaries. Furthermore, piecewise constant profiles are assumed for the **process controls**, i.e., a control variable possesses a constant value within a finite element.

By applying this collocation scheme, the dynamic optimization problem stated in Eq. (4.5) is transformed into **a standard NLP** as shown in Eq. (4.11), featuring favorable sparsity that can be efficiently exploited by NLP methods (Biegler 2007):

$$\begin{aligned}
& \min \Phi(z_N) \\
& \text{s. t.} \quad \frac{dz}{dt_{i,j}} = f(z_{i,j}, y_{i,j}, u_{i,j}, p) \\
& \quad z_{i,j} = z_{i-1} + h_i \sum_{j'=1}^K \Omega_{j'}(\tau_j) \frac{dz}{dt_{i,j}}, \\
& \quad g(z_{i,j}, y_{i,j}, u_{i,j}, p) = 0, i \in [1, \dots, N], j \in [1, \dots, K]
\end{aligned} \tag{4.11}$$

$$z_i = z_{i-1} + h_i \sum_{j=1}^K \Omega_j(1) \frac{dz}{dt_{i,j}}, \quad i \in [1, \dots, N]$$

$$g_f(z_N) = 0$$

$$z_L \leq z_{i,j} \leq z_U, \quad y_L \leq y_{i,j} \leq y_U, \quad u_L \leq u_{i,j} \leq u_U, \quad i \in [1, \dots, N], \quad j \in [1, \dots, K]$$

4.2.3 Selection of nonlinear programming algorithms

In the analysis of dynamic optimization problems with the simultaneous collocation approach, a critical consideration is the efficient solution of large nonlinear program in the form of Eq. (4.11).

To date, there exist several NLP algorithms that can be applied to solve the problem from the simultaneous formulation (Schlegel et al. 2005). Among these, the **interior point method** is able to efficiently handle large-scale problems with large numbers of degrees of freedom. Thus IPOPT (Interior Point Optimizer) is selected as the NLP solver.

IPOPT is a Newton type nonlinear optimization solver, which has proven to be quite efficient in solving NLP problems with large number of inequalities and a potentially large number of degrees of freedom (Wächter and Biegler 2006). It applies the barrier method to handle inequality constraints coupled with the filter method for global convergence. The Karush-Kuhn-Tucker conditions for optimality are satisfied at the solution after Newton iterations. For more details on the description of the algorithm, refer to (Wächter and Biegler 2006).

The software package is written in C++ language. It can be used to produce a specific library that is able to communicate with programs written in various languages, such as C++, C and Fortran. It is open source and can be accessed through <https://projects.coin-or.org/Ipopt>.

4.3 Optimization Implementation in the GAMS Platform

The optimization model is implemented and solved in the General Algebraic Modelling System (GAMS) platform, applying the solution algorithm described in the previous section.

GAMS is a state-of-the-art tool in mathematical modelling and optimization. It is specifically designed for modelling linear, nonlinear and mixed integer optimization problems, and is especially powerful in handling large-scale complex problems. It allows the user to build large maintainable models, in which the problem formulation and solver settings can be modified efficiently (Rosenthal 2012). Fig. 4.3 shows the programming environment in the GAMS platform.

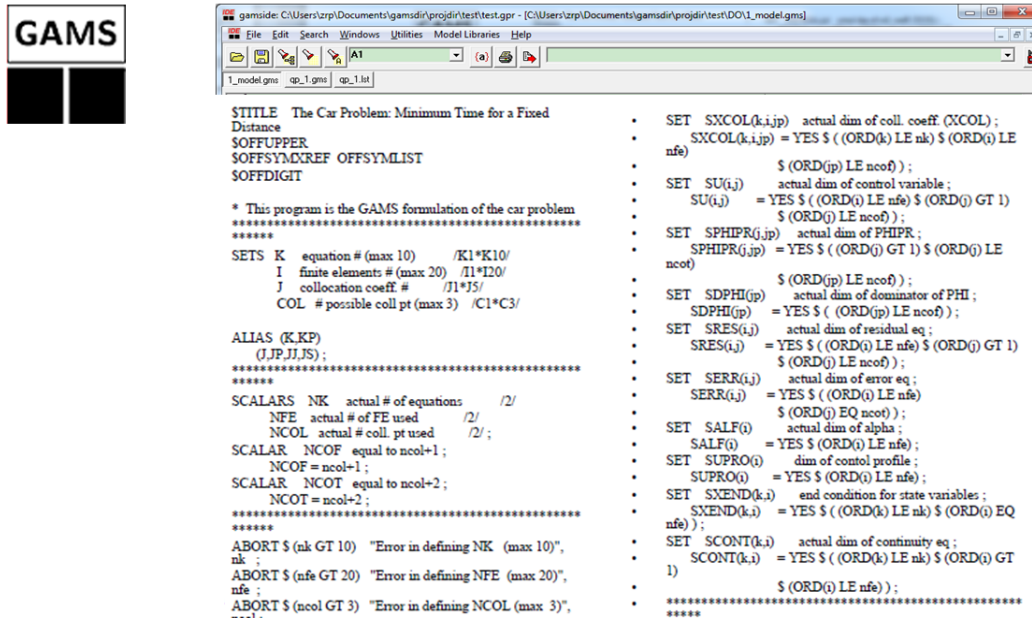


Fig. 4.3 Programming environment in the GAMS platform

GAMS provides both declarative and procedural syntax for the user to describe optimization problems. It has its own language compiler offering convenient access to alternative high-performance solvers with various optimization algorithms. The syntax has to be followed to provide the concise and exact descriptions of the model in algebraic statements in the input file, which will later be compiled by GAMS's language compiler. Then the specified solver is called and activated to work on the compiled model and find the solution to the problem, as illustrated in Fig. 4.4.

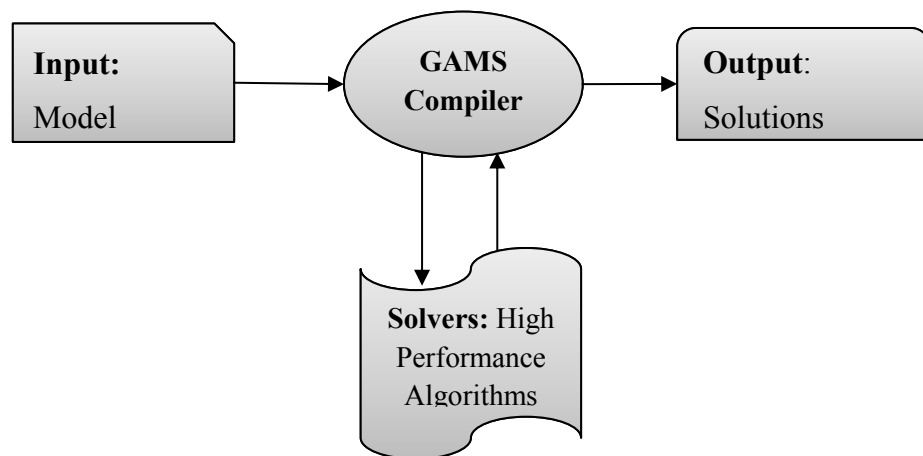


Fig. 4.4 Problem solving process in the GAMS platform

4.4 Summary of the Implementation Configurations

In the collocation scheme, 24 finite elements are used in an hourly basis, and 3 Radau points are defined in each element. The collocation coefficients of three-point Radau roots are listed in Table 4.2.

Table 4.2 Collocation coefficients of three-point Radau roots

Collocation Coefficients	1	2	3
1	0.196815433731079	0.394424288467084	0.376403042786093
2	-0.0655354025650992	0.292073492494108	0.512485883439094
3	0.0237709688340207	-0.0415487809611925	0.111111073774813

The control variables are assumed piece-wise constant over the finite elements, and therefore the degree of freedom for the optimization problem equals the product of the total number of finite elements and controls. In the daily dynamic optimization for the VAV system, the number of control variables is 5, so the degree of freedom is 120. In the optimization for the DW system, the number of control variables is 6, so the degree of freedom is 144.

After collocation, the translated NLP problem for the daily integrated VAV operation for one zone has 1605 variables, 1485 equality constraints and 280 inequality constraints. The translated NLP problem for the DW operation has 2181 variables, 2037 equality constraints and 248 inequality constraints. More details of the implementation configurations can be found in Table 4.3.

For all the daily simulations reported in this study, IPOPT is able to solve the problems to optimality within minutes on an 8-core 64-bit desktop, which illustrates the efficiency of the problem formulation.

Table 4.3 Summary of the implementation configurations for daily optimizations for a zone

Implementation Configurations	VAV	DW
No. of control variables	5	6
Degree of freedom for the optimization	120	144
Total No. of variables in NLP	1605	2181
Variables with only lower bounds	0	0
Variables with lower and upper bounds	244	240
Variables with only upper bounds	0	0
Total No. of equality constraints in NLP	1485	2037
Total No. of inequality constraints in NLP	280	248
Inequality constraints with only lower bounds	260	168
Inequality constraints with lower and upper bounds	0	0
Inequality constraints with only upper bounds	20	80
No. of non-zeros in equality constraint Jacobian	4831	6413
No. of non-zeros in inequality constraint Jacobian	540	436
No. of non-zeros in Lagrangian Hessian	960	1464

CHAPTER 5 OPTIMAL INTEGRATED OPERATION STRATEGIES AND ENERGY SAVING POTENTIAL ANALYSIS

In sections 5.1-5.5, steady periodic outdoor condition is first implemented to obtain the optimal integrated operation strategies. Such outdoor condition is more idealized and characterized than the realistic weather data containing irregular perturbations, and therefore can lead to better understanding on the optimization results.

The optimization implementing realistic meteorological weather data is then conducted in section 5.6, to explore the application of the operation design approach in actual case studies.

In section 5.7, the influence of different weather conditions on the optimization potential is investigated, the findings of which can support the architectural engineers to make more informed estimations on the operation optimization potentials under a variety of climate conditions.

5.1 Energy Saving Potentials by Dynamic Optimization

5.1.1 Steady periodic outdoor condition

Steady periodic outdoor condition is widely used in the building energy studies, especially the investigations focusing on the thermal response properties of building systems (Gagliano et al. 2014; Asan 2006) and the studies on the performance of complex building components (Ma and Wang 2012; Yam, Li, and Zheng 2003). Under steady periodic outdoor condition, both the outdoor temperature and relative humidity are assumed sinusoidal harmonic functions with an angular frequency of $\pi/12 \text{ h}^{-1}$.

In this case study, the operation time horizon of interest is set to 24 h. For the temperature, the average is 28°C, the amplitude is 6°C and the phase shift is π . For the relative humidity, the average is 75%, the amplitude is 15% and the phase shift is 0. Such conditions correspond to the warm and humid climate (Baechler et al. 2010). Other building operating conditions, including the solar radiations, internal heat and moisture generations and wind speed related coefficients, are derived from the monthly average profiles obtained from EnergyPlus simulations. The office hours are 8:00-18:00h, during which the indoor thermal comfort and air ventilation have to be satisfied by the integrated active-passive air conditioning strategies.

An iterative approach outlined in Fig. 5.1 is designed to determine the initial model conditions. Under steady periodic outdoor condition, the variations of the model state parameters are also periodic. Therefore, it is reasonable to choose the initial model conditions that can lead to similar model conditions (relative error less than 3%) at the ending of the daily simulation, in order to ensure the continuity of differential parameters at the bounds of adjacent days. The

developed approach is proven effective in determining the proper initial conditions (usually within 10 iterations) under various weather situations.

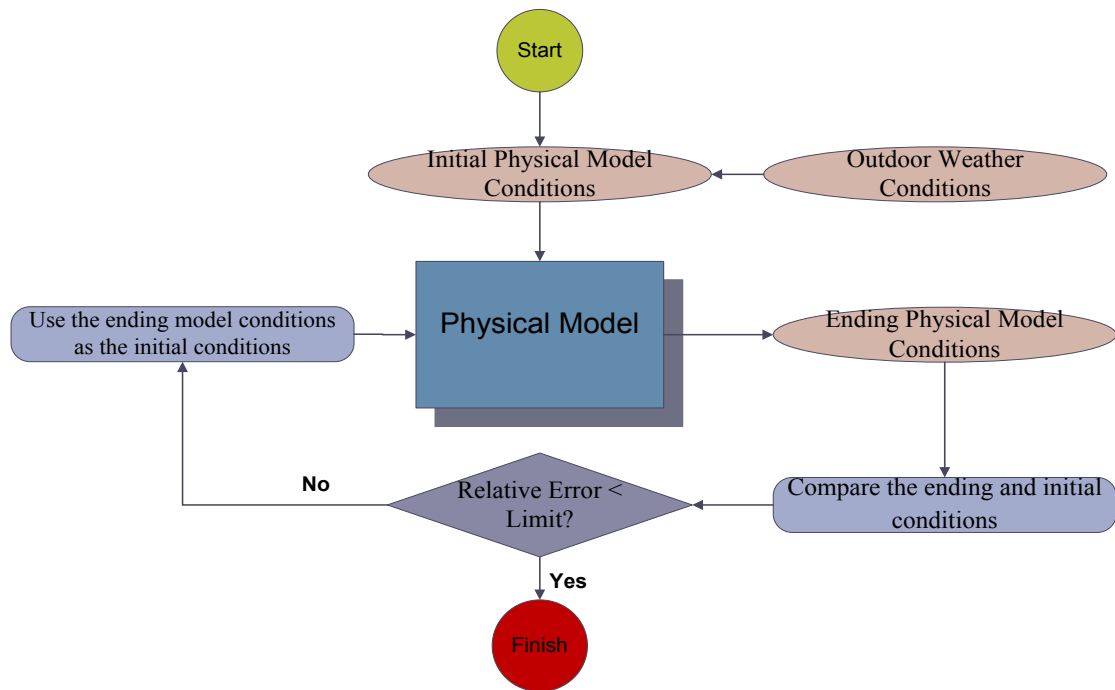


Fig. 5.1 Schematic illustration of the iterative approach for the initial model condition determination

5.1.2 Energy saving in the VAV air conditioning system

A conventional local control strategy is implemented as the baseline to compare with the optimized operation strategies derived for the VAV air conditioning system. In the local control strategy, the temperature setpoint during office hours is set to $25\text{ }^{\circ}\text{C} \pm 1\text{ }^{\circ}\text{C}$. The VAV system operates corresponding to the difference between the indoor air temperature and the setpoint. The supply air temperature and relative humidity are kept constants at $15\text{ }^{\circ}\text{C}$ and 75%, respectively. The ratio between the outdoor air and return air is kept constant as 1:4.

The comparative daily energy consumption for all the zones in the optimized operation strategy and conventional local control strategy are shown in Fig. 5.2. In the local control scheme, the average consumption of the four zones is $686.30\text{ Wh/m}^2\text{day}$, compared to $451.46\text{ Wh/m}^2\text{day}$ in the optimized scheme. An average energy saving of 34.22% is achieved by implementing the optimized operation strategy.

It can be observed that the four zones present different energy consumption due to different orientations and cooling load characteristics. In both the conventional and optimal strategies, the north zone corresponds to the lowest energy consumption while the west zone corresponds to the highest. The energy saving percentages of all the four zones are similar to each other, varying between 31.4% ~ 38.9%.

Fig. 5.3 plots the energy consumption distribution by system component in both control strategies. It can be seen that the cooling coil takes the biggest portion ($> 50\%$) of the whole energy consumption in both the strategies. Note that the portion of fan consumption in the optimal strategy is significantly increased when compared with the conventional strategy. This results from the additional operation of passive cooling ventilation at night.

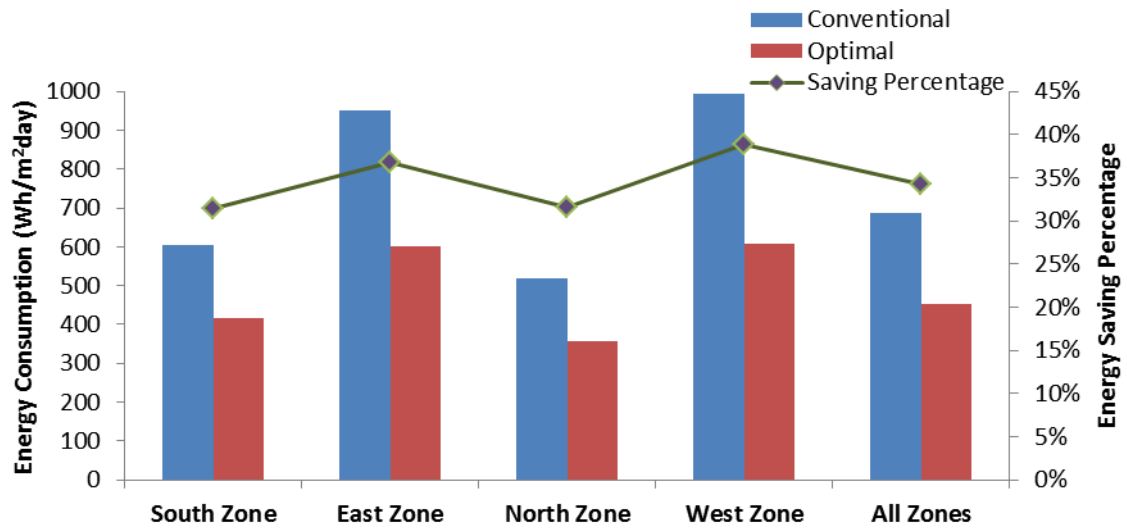


Fig. 5.2 Energy consumption of the optimized and conventional operations for VAV

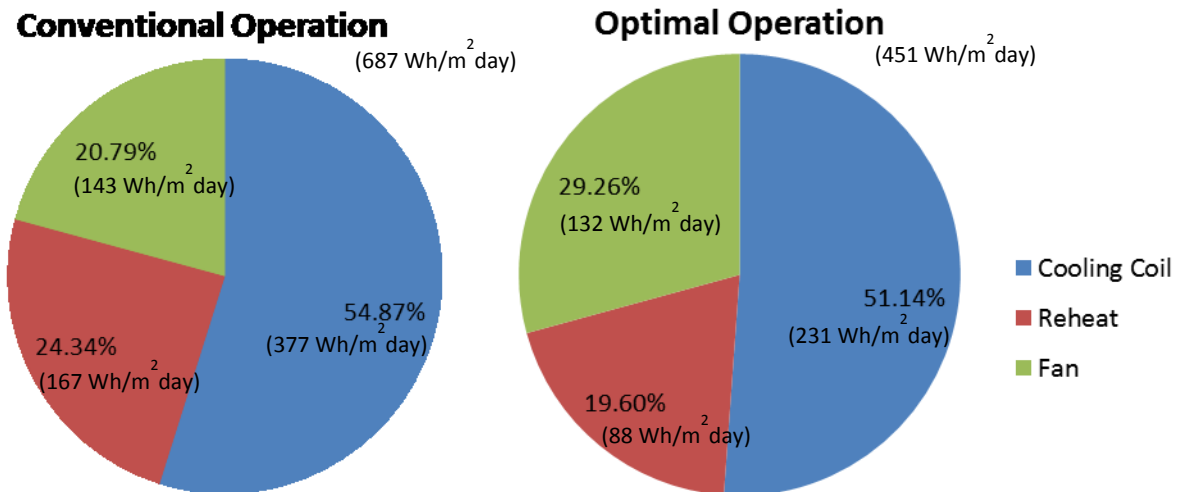


Fig. 5.3 Energy consumption distribution by system component within VAV

5.1.3 Energy saving in the DW air conditioning system

For the desiccant wheel air conditioning system, the conventional local control strategy implemented as the baseline is mostly adapted from (Zhai 2008). The ratio between the outdoor air and return air is kept constant as 1:4. Then the mixed air is processed to the moist air state of 14.5°C and 95% RH. The ratio between the air passing through the active desiccant wheel and the pass-by air is kept constant as 1:9 to generate the supply air with the moist air state of 17.5°C, 75% RH (Zhai, Archer, and Fischer 2008). The temperature setpoint during office hours is set to 25 °C \pm 1 °C.

The comparative daily energy consumption corresponding to the desiccant wheel air conditioning system are shown in Fig. 5.4. In the local control scheme, the average consumption of the four zones is 565.56 Wh/m²day, compared to 382.06 Wh/m²day in the optimized scheme. An average energy saving of 32.45% is achieved by implementing the optimized operation strategy.

Similar to the VAV system, the north zone has the lowest energy consumption while the west zone has the highest. The energy saving percentages of all the four zones are also similar to each other, varying between 31.1% ~ 34.9%.

Fig. 5.5 plots the energy consumption distribution by system component in both control strategies. It can be observed that the cooling coil also takes the biggest portion of the whole energy consumption, as with the VAV system. Compared to the conventional strategy, the portion of the desiccant wheel energy consumption in the optimal strategy presents a significant drop from 21.41% to 11.08%.

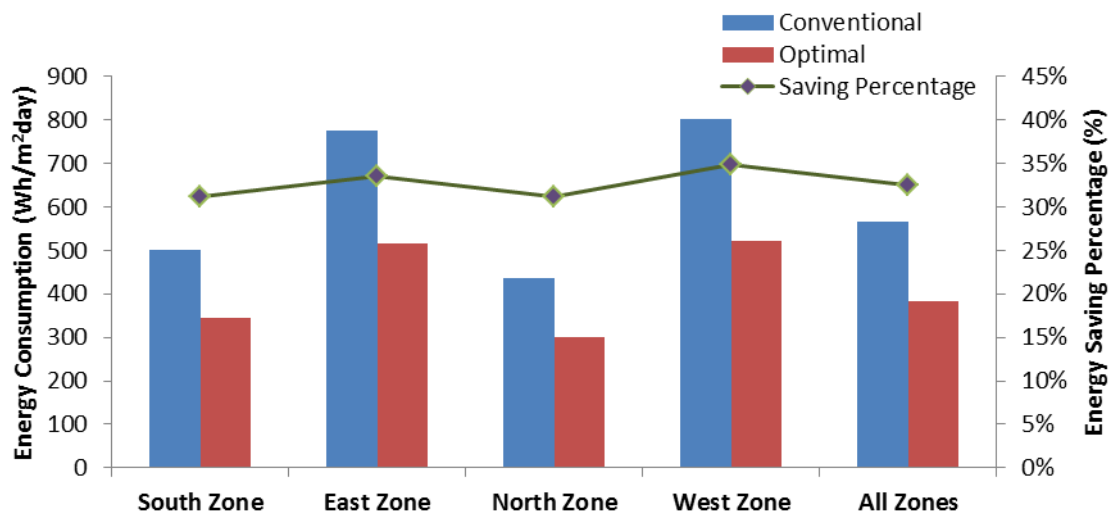


Fig. 5.4 Energy consumption of the optimized and conventional operations for DW

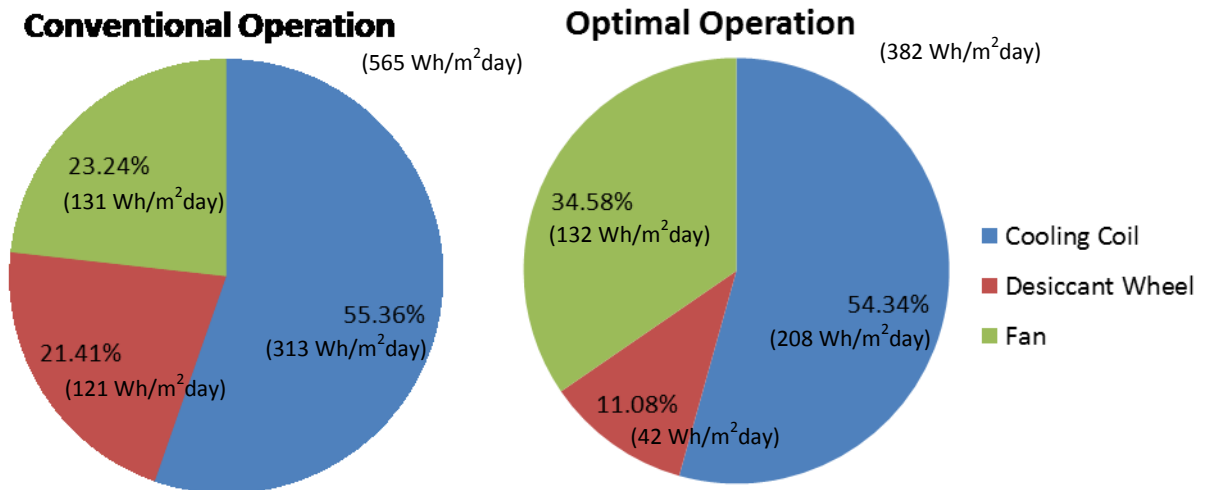


Fig. 5.5 Energy consumption distribution by system component within DW

It should be noted that idealized weather variable behaviors are assumed in the case study for both the VAV and DW systems, that is, the weather information is accurately provided during the dynamic optimization. Therefore, the achievable energy savings may vary when the designed operation strategies are implemented in the actual conditions due to the presence of uncertainties and perturbations.

5.2 Optimal Strategies for the Integrated Operation

As described in Chapter 3, the parameters to be optimized in the integrate passive-active operation can be categorized as: (1) the air flow rates via various paths (PCV, OA, RA); (2) the moist air state properties at key locations in the active air conditioning systems. The optimization results for these parameters are shown and discussed in this section from the building physics perspectives.

In general, PCV is activated when the outdoor air temperature level is sufficiently low. To obtain the optimal ventilation rates, however, the following three parameters need to be studied: (1) outdoor humidity level - high humidity may increase the energy consumption for dehumidification and consequently offset energy saving in cooling; (2) operational availability for ventilation - the effect of PCV during office hours may considerably decrease if the ventilation occurs too early before the office hours commence; (3) ventilation rates - need to be carefully manipulated to balance the energy consumption in the cooling coil and fans.

The dynamic profiles of the optimal ventilation rates and VAV airflow rates are displayed in Fig. 5.6. It is observed that the optimal PCV profiles in all the four zones share similar trends. It starts at around 1:00-2:00h, and then the ventilation rate gradually increases and achieves the maximum at 4:00-8:00h, during which the lowest outdoor air temperature occurs (see Fig. 5.7). Such profiles agree with the theoretical analysis. The specific ventilation rates for different zones are different, resulting from the different building configurations and cooling load characteristics of the zones.

Fig. 5.6 also shows that the VAV system starts to operate at 8:00h, and then the SA amount gradually rises because of the increase of the building loads. To maintain the indoor air quality during office hours, the minimum value of the sum of OA and ventilation rate is set in the optimization formulation ($2.5\text{L/s}\cdot\text{person}$) (ASHRAE 2004). This constraint is satisfied by providing ventilation during office hours and almost no OA is provided through the VAV system.

The optimal air flow profiles obtained for DW present similar trends to those in VAV (Fig. 5.6), although the specific ventilation rates are different.

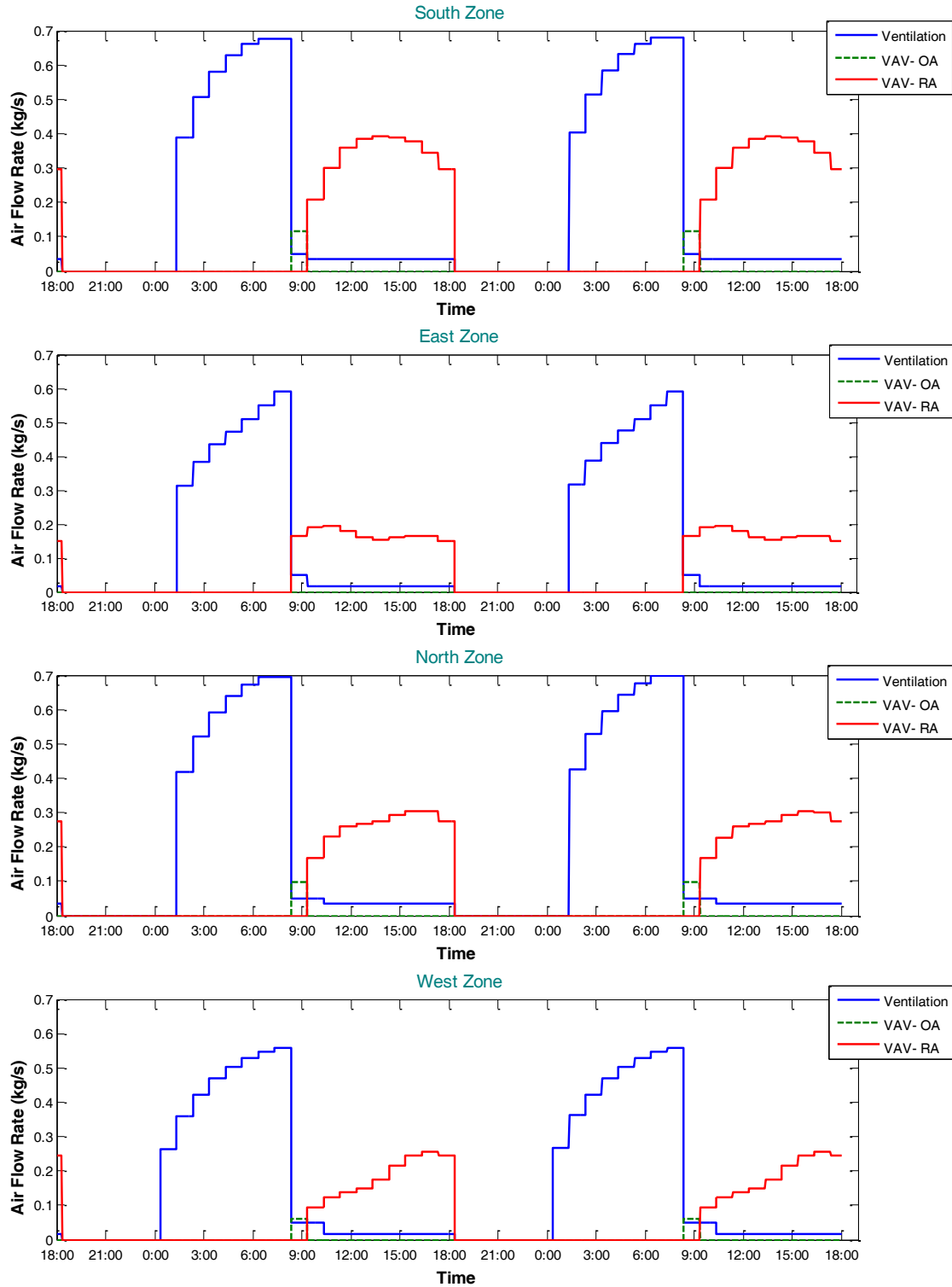


Fig. 5.6 Dynamic profiles of air flow rates in the optimized operation strategy for VAV

During the VAV operation period, the SA temperature is set to 16°C which is the required minimum value, and the humidity ratio is set to 9 g/kg which is the value of the upper bound. It indicates that the optimization solution tends to reduce the latent load of the cooling coil when balancing the energy consumption for the sensible cooling and dehumidification.

During the DW operation period, the air after DX cooling coil has a temperature level of 10°C which is the required minimum value, and its humidity ratio is set to 7.2 g/kg. The ratio between the air flow passing through the DW and the supply air is set to 0.05. All of these optimized controls eventually generate an indoor environment with acceptable thermal comfort and minimized energy consumption.

5.3 Analysis on the Indoor Temperature and Humidity Profiles

The resulting indoor air temperature and humidity conditions are discussed in this section. It is found that the indoor conditions under optimized VAV operations are very similar to those under optimized DW operations. The reason is that such indoor temperature/humidity settings can benefit the reduction of the building loads and thus the energy consumption of the active system, no matter what dehumidification approaches the system implements. Therefore, only the profiles for VAV are shown below for discussions.

Fig. 5.7 shows the indoor air temperature profiles corresponding to the optimized and conventional operations for VAV. It can be observed that there are significant time lags and magnitude dampening of the temperature profiles of indoor air and internal mass, when compared with the outdoor air temperature. In the optimized operation strategy, the indoor air temperature begins to drop at around 1:00-2:00h when the PCV starts. The decrease of the indoor air temperature lowers the temperature of the internal mass, which serves as the cooling storage material in the process. When the office hours begin at 8:00h, the internal mass temperature drops to 25.95-26.47°C, which is 4.28-9.53°C lower than that in the conventional operation strategy. The cooling effect provided by the cooled internal mass during office hours is one main contribution to the energy saving of the optimized operation strategy.

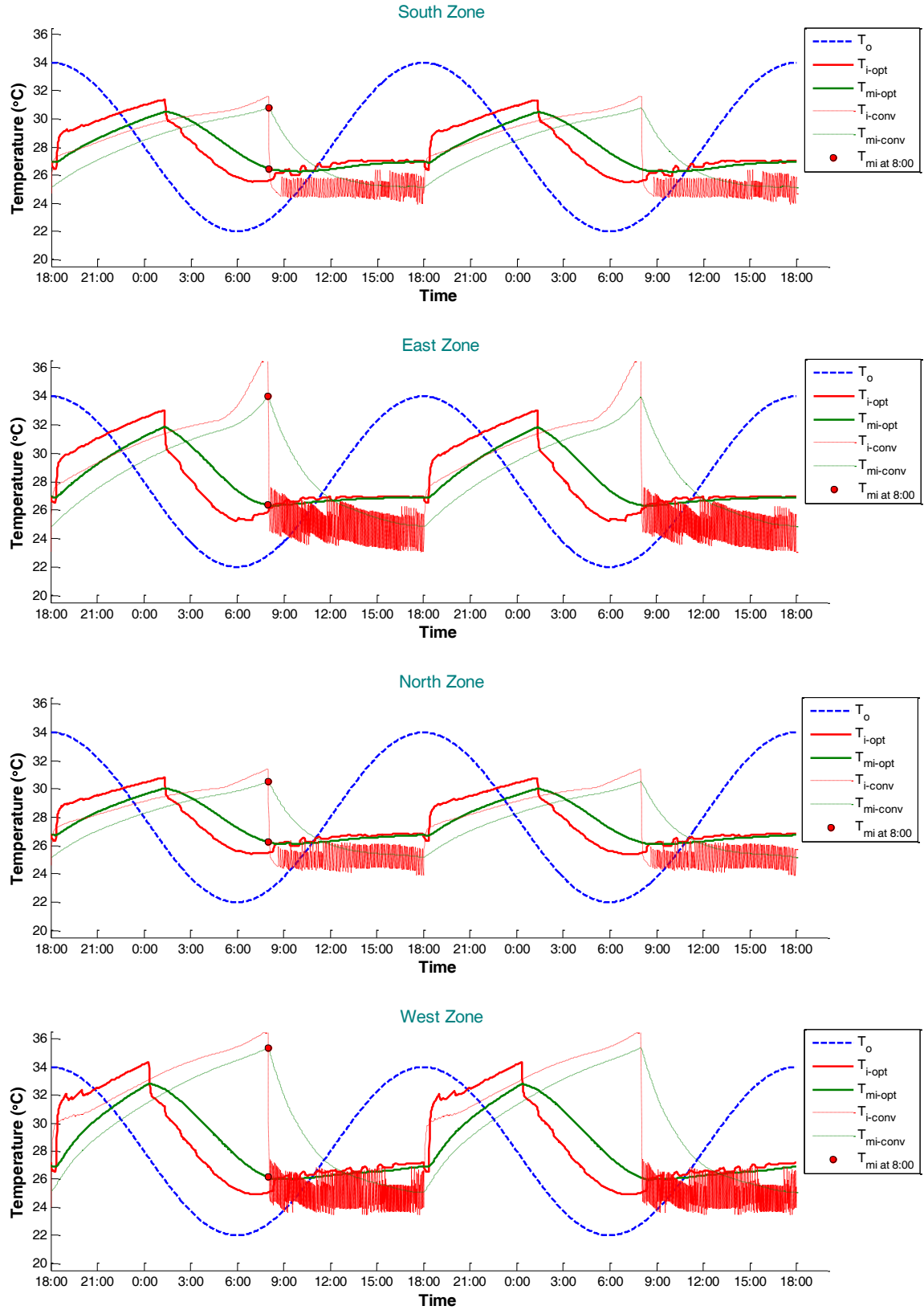


Fig. 5.7 Resulting temperature profiles in the optimized and conventional operations for VAV

Table 5.1 Comparison of the internal mass temperatures under different strategies

Unit: °C	South Zone	East Zone	North Zone	West Zone
VAV-conventional	30.80	33.58	30.54	34.90
VAV-optimal	26.47	26.36	26.26	26.14
DW-conventional	30.76	33.94	30.46	35.49
DW-optimal	26.26	25.96	25.95	25.96

Comparison of daily humidity ratio profiles is drawn in Fig. 5.8. In the conventional operation strategy, the VAV system operates according to the indoor air temperature only. Although the indoor humidity level can be implicitly controlled by the system, it may not stay within the proper range for both the energy saving and acceptable thermal comfort. In the optimized operation strategy, however, the humidity ratio of the SA is well manipulated by taking both the indoor thermal comfort and energy consumption into consideration which benefits the energy consumption reduction.

Relative humidity of the indoor air can be calculated from the air temperature and humidity ratio, using the moist air thermodynamic property model (ASHRAE 2005). Comparison of daily relative humidity profiles is shown in Fig. 5.9. Due to the significant difference in air temperature and humidity ratio, the daily relative humidity profiles in the two strategies also differ remarkably. In the optimized operation strategy, the relative humidity lies in a range between 50% and 75%, while in the conventional case it stays between 40% and 55%. The relative humidity levels further affect the indoor thermal comfort conditions as discussed in section 5.4.

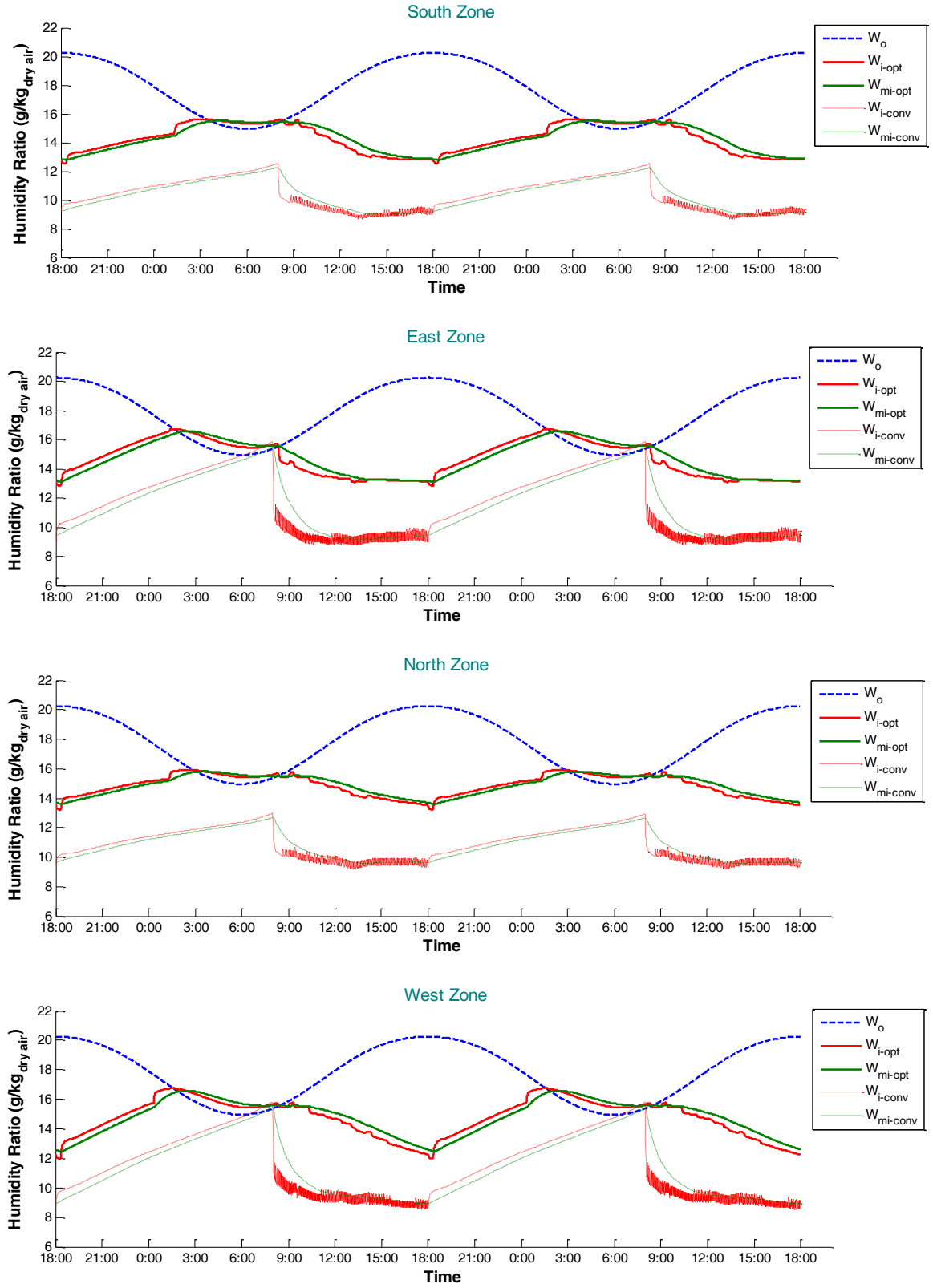


Fig. 5.8 Resulting humidity ratio profiles in the optimized and conventional operations for VAV

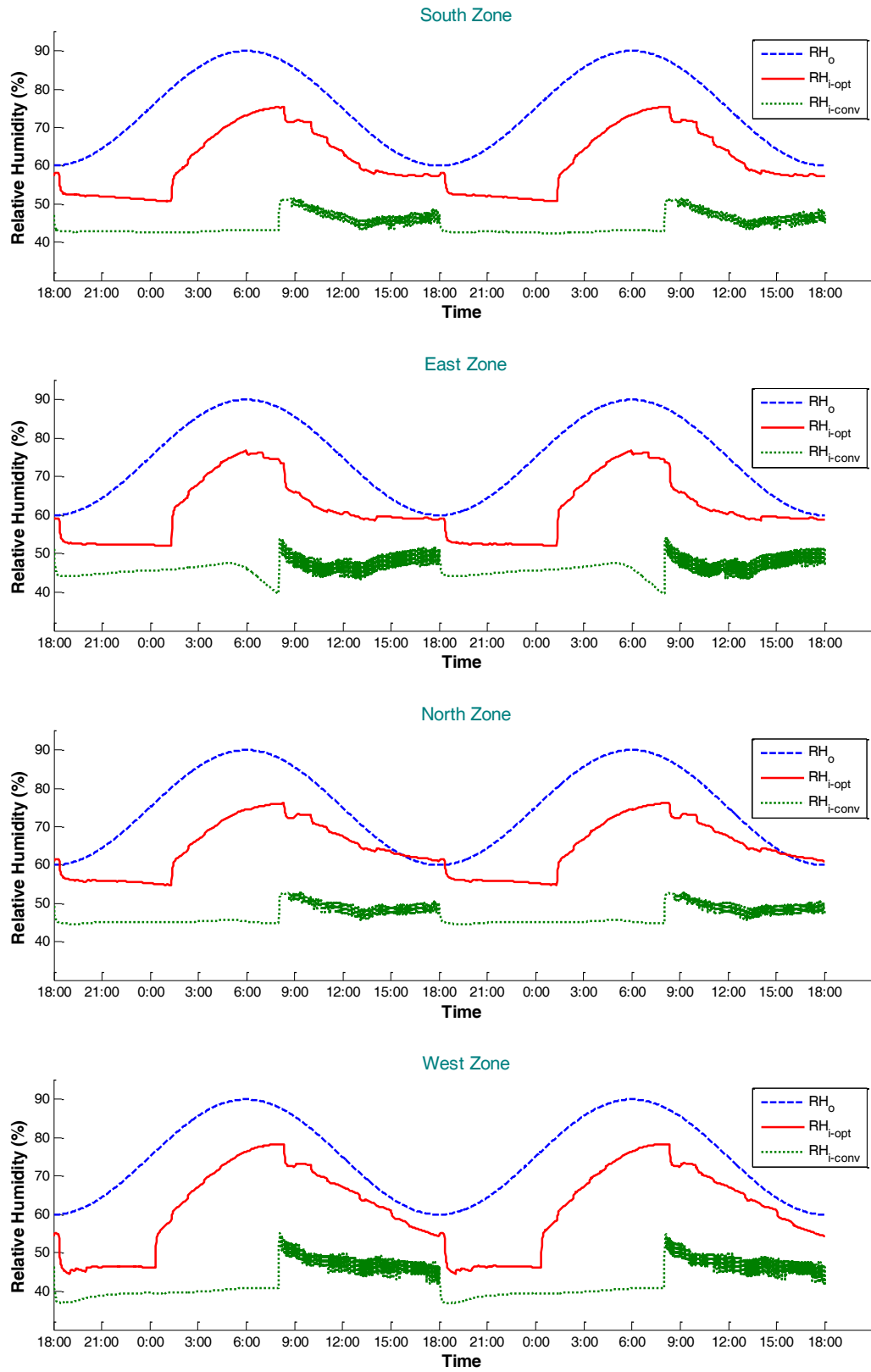


Fig. 5.9 Resulting relative humidity profiles in the optimized and conventional operations for VAV

5.4 Distribution of Predicted Percentage Dissatisfied (PPD) Index

To compare the indoor thermal environment quality provided by both operation strategies, the distribution of daily PPD values during office hours are illustrated in Fig. 5.10 for the VAV operations and Fig. 5.11 for the DW operations.

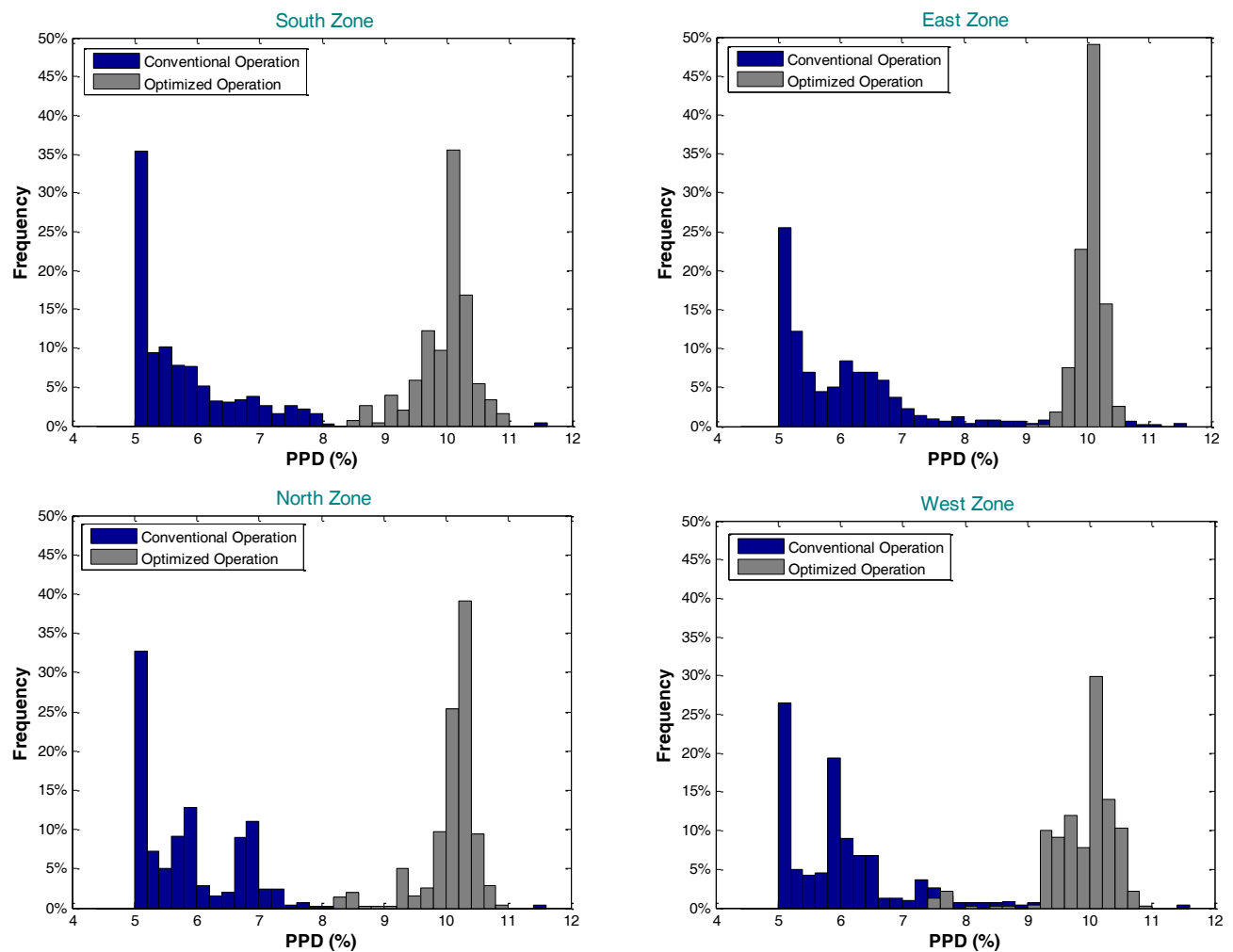


Fig. 5.10 Daily PPD distributions during office hours for the VAV operations

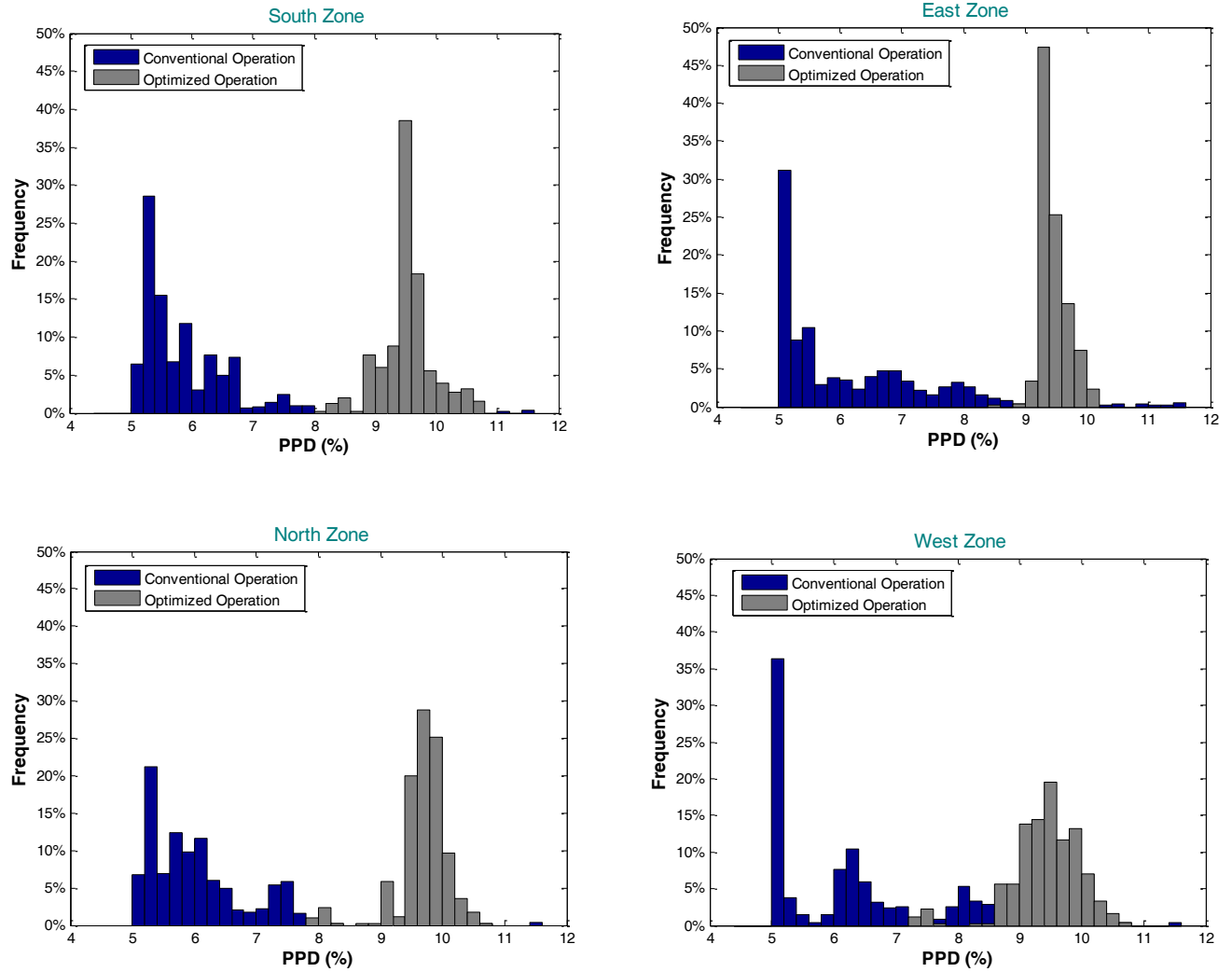


Fig. 5.11 Daily PPD distributions during office hours for the DW operations

It can be seen from the figures that, in the conventional operation strategy, the values of PPD gather around 5-8%, while in the optimized operation strategy they gather around 10% which is the upper limit of PPD. This indicates that the constraint of PPD defined in the optimization limits further reduction of the energy consumption.

To elucidate the influence of PPD constraints on the energy saving potential, different settings of the value of PPD upper limit during office hours are applied and the computed objective

function values are compared. It is found that the total optimal energy consumption drops by around 3% if the value of the PPD limit is increased by one unit between 5~15%. This can be explained from the optimization theory perspective. More specifically, a larger PPD upper bound indicates a larger feasible region for the optimization. Thus, the optimizer is able to explore more potential configurations of the system and consequently captures a better objective.

5.5 Contribution Analysis for Passive Strategy and Active Strategy

In the optimal integrated operation, the energy saving is contributed by the improvement of both the passive and active strategies. More specifically, the passive strategy improvement corresponds to the manipulation of the ventilation air flow rate, while the active strategy improvement corresponds to the manipulation of the VAV/DW system operational parameters.

Table 5.2 Control parameters corresponding to the improvement of the passive and active strategies

	Passive Strategy Improvement	Active Strategy Improvement
VAV System	Ventilation air flow rate (\dot{m}_{vent})	(1) OA air flow rate (\dot{m}_o), (2) RA air flow rate (\dot{m}_r), (3) SA temperature (T_3), (4) SA humidity ratio (W_3).
DW System	Ventilation air flow rate (\dot{m}_{vent})	(1) OA air flow rate (\dot{m}_o), (2) RA air flow rate (\dot{m}_r), (3) flow rate of the air passing through the active desiccant wheel (\dot{m}_{adw}), (4) temperature of the air after DX cooling coil (T_3), (6) humidity ratio of the air after DX cooling coil (W_3).

In this section, a third control scheme is designed in addition to the conventional local control scheme and optimized scheme, in order to explore the energy saving contributions of the

passive and active strategies. In the third control scheme, the active air conditioning system operates in the same way as the conventional local control scheme, but it implements the PCV schedule that is obtained in the optimized scheme. Therefore, the energy saving introduced by this scheme is contributed by the passive strategies only. Then the energy saving contributions of the passive and active strategies can be separated by comparing the energy saving value in this scheme with that in the optimized scheme.

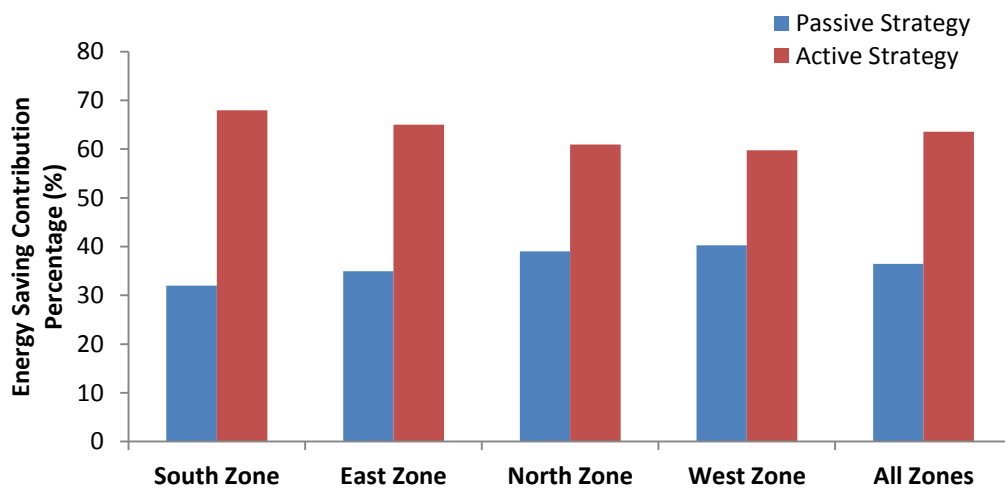


Fig. 5.12 Comparison of energy saving contributed by passive and active strategies in VAV operation

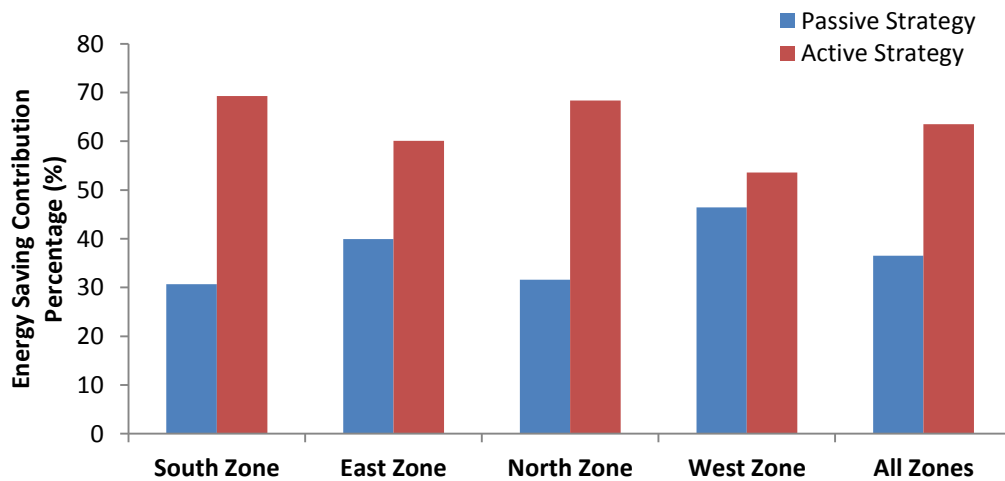


Fig. 5.13 Comparison of energy saving contributed by passive and active strategies in DW operation

The comparison of the two strategies is shown in Fig. 5.12 for the VAV system and in Fig. 5.13 for the DW system. It can be observed that the improvement of the passive strategies contributes to around 33% of the energy saving, while the improvement of the active strategies contributes to around 67%.

5.6 Integrated Operation Strategy Formulation using Realistic Weather

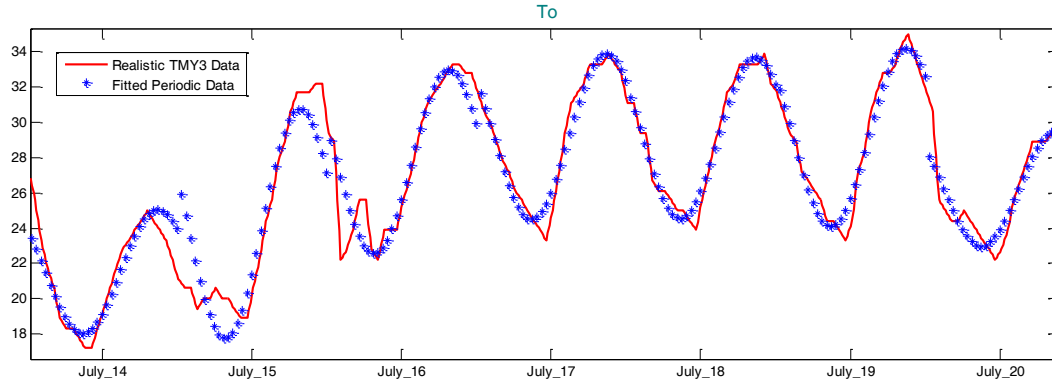
Data

Compared with the idealized periodic outdoor condition, the realistic outdoor condition presents more irregular trends due to various perturbation sources, as can be seen in Fig. 5.14. This may further challenge the dynamic optimization task and affect its energy saving performance.

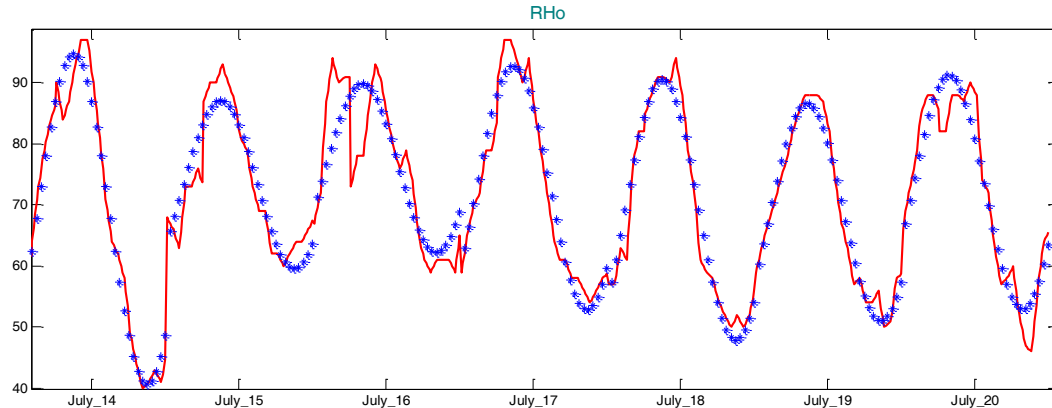
In this section, the integrated operation optimization implementing the realistic meteorological weather data is conducted, and the results are compared with those implementing the idealized periodic outdoor condition. This will test the applicability of the developed operation design approach in actual case studies.

Realistic weather data is obtained from the Typical Meteorological Year (TMY3) datasets representing typical realistic weather conditions (Wilcox and Marion 2008). A typical summer month, July, in Chicago, IL, U.S. is selected for the case study. As shown in Fig. 5.14, the daily periodic outdoor condition is first obtained by perform curve fitting to the realistic data. After that, the fitted periodic data and the realistic data are implemented separately in the

dynamic optimization to obtain two sets of operation schedules. These schedules are then deployed in the respective simulations using the same TMY3 weather conditions.



(a) Outdoor Temperature ($^{\circ}\text{C}$)

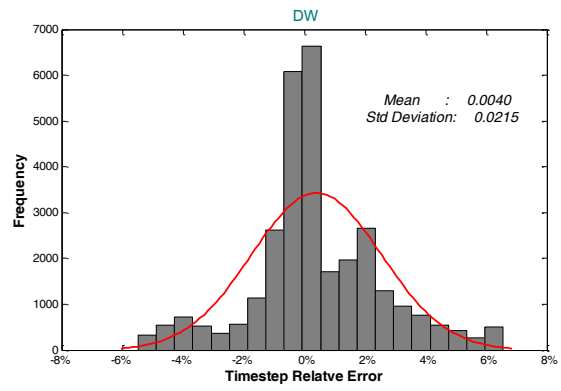
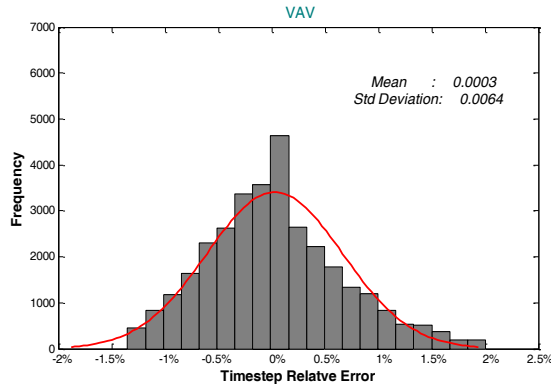


(b) Outdoor Relative Humidity (%)

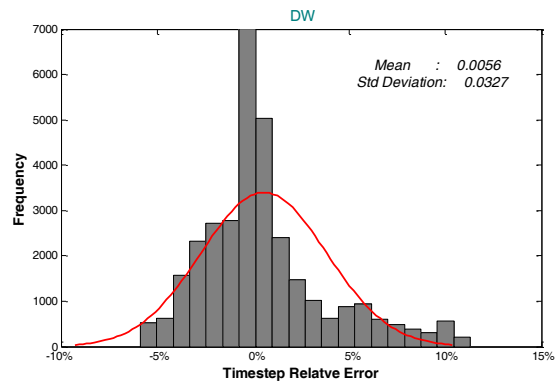
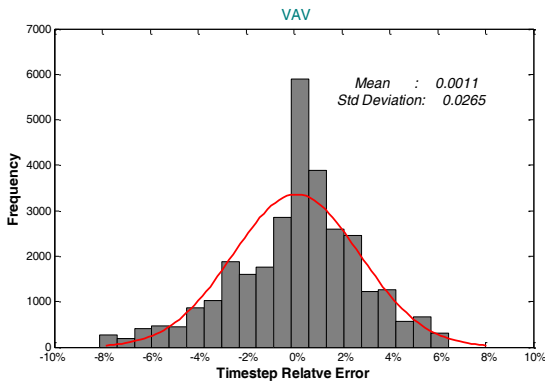
(One typical week: Jul. 14-20)

Fig. 5.14 Comparison of the realistic TMY3 weather data and the fitted periodic weather data

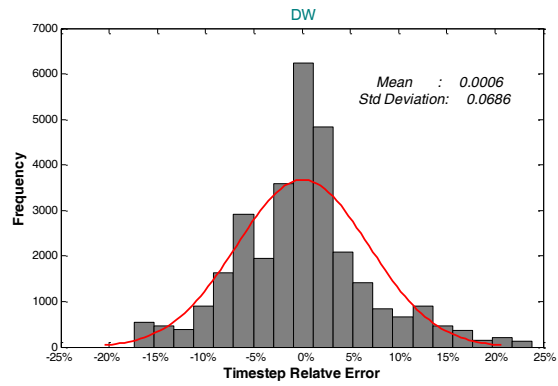
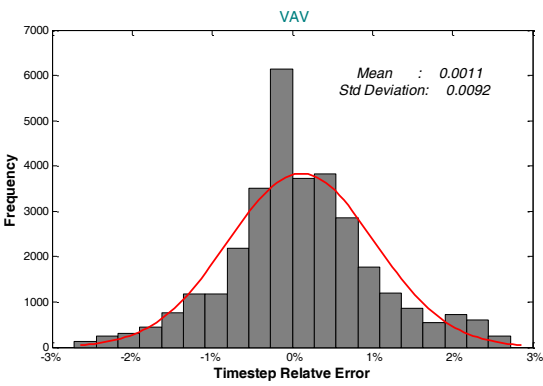
Fig. 5.15 summarizes the difference of the indoor air temperature/humidity levels and energy consumption corresponding to the two sets of operations schedules. It can be observed that the differences generally remain small: the fitted normal distributions have a mean value of less than 0.5% and standard deviation of less than 7.0%.



(a) Indoor air temperature levels



(b) Indoor air humidity levels



(c) Energy consumption

Fig. 5.15 Time-step relative error of the simulations using realistic TMY3 and fitted periodic weather data

This indicates that the dynamic optimization approach can effectively handle the perturbations in the realistic weather conditions in obtaining the optimal operation strategies. It also shows that the realistic weather data and the fitted periodic data can lead to similar operation strategies. Therefore, the simplified periodic data can be a reasonable alternative in the operation optimization, when the more detailed realistic weather data is not available.

5.7 Optimization Potential under Various Weather Conditions

Different weather conditions can significantly affect the building loads and energy consumption in both the optimized operation and conventional operation, and therefore lead to various energy saving percentages.

The influence of the weather conditions on the optimization potential is investigated in this section, in order to demonstrate the viability of the integrated approach. By illustrating the magnitude of optimization potential variations under a variety of climate conditions, the study can support the architectural engineers to make more informed estimations on the operation optimization potentials during the early phase of building retrofitting.

As shown in Table 5.3, four temperature T levels and two relative humidity RH levels are selected to represent different climate types (Baechler et al. 2010). These levels are determined based on the statistical hourly weather data in July for a number of cities located in different climate regions (DOE 2013). The energy consumption in both the local control scheme and optimized scheme are re-computed under different T/RH combinations, and then the energy saving percentages are re-calculated. Note that the initial physical model

conditions have to be re-evaluated under every weather condition, using the iterative approach described in section 5.1.1.

Table 5.3 Temperature and relative humidity levels for different climate types

Climate Type	T_mean	Representative City	Latitude	Longitude
Hot	30°C	Houston, Texas	N 30° 00'	W 95°22'
Warm	28°C	Memphis, Tennessee	N 35° 40'	W 89°58'
Mixed	26°C	Albuquerque, New Mexico	N 35° 20'	W 106°37'
Cool	24°C	Boise, Idaho	N 43° 37'	W 116°12'

Climate Type	RH_mean	Representative City	Latitude	longitude
Humid	75%	Houston, Texas	N 30° 00'	W 95°22'
Dry	40%	Albuquerque, New Mexico	N 35° 20'	W 106°37'

Study results show that the developed optimization approach works effectively in all the studied climate conditions: the optimized strategies lead to a remarkable energy saving of 29.77~48.76% for VAV compared to the traditional local control scheme, and a saving of 27.85~41.33% for DW.

The variations energy consumption of the optimized operation under different climate conditions are depicted in Fig. 5.16, and the variations of the energy saving percentage are depicted in Fig. 5.17. It can be observed that the optimized strategies yield a lower energy saving in warmer weather conditions. This can be explained by the fact that an increasing T-mean value can lead to a higher level of outdoor air temperature at night which would reduce the efficiency of PCV. It can also be observed that the dry weather conditions generally yield equal or slightly higher energy saving potentials than the humid conditions when the temperature levels are similar.

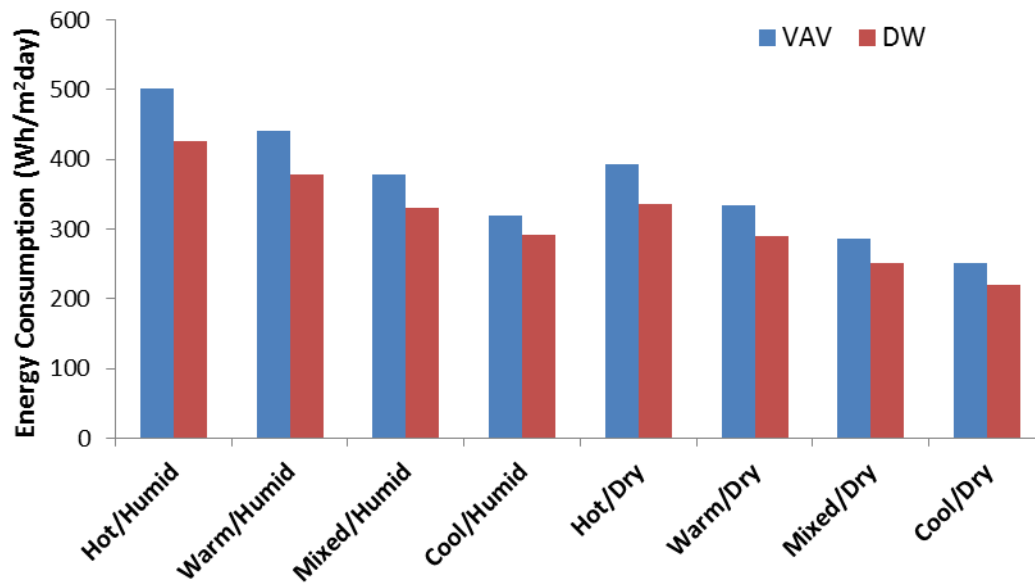


Fig. 5.16 Energy consumption of the optimized operation under different climate conditions

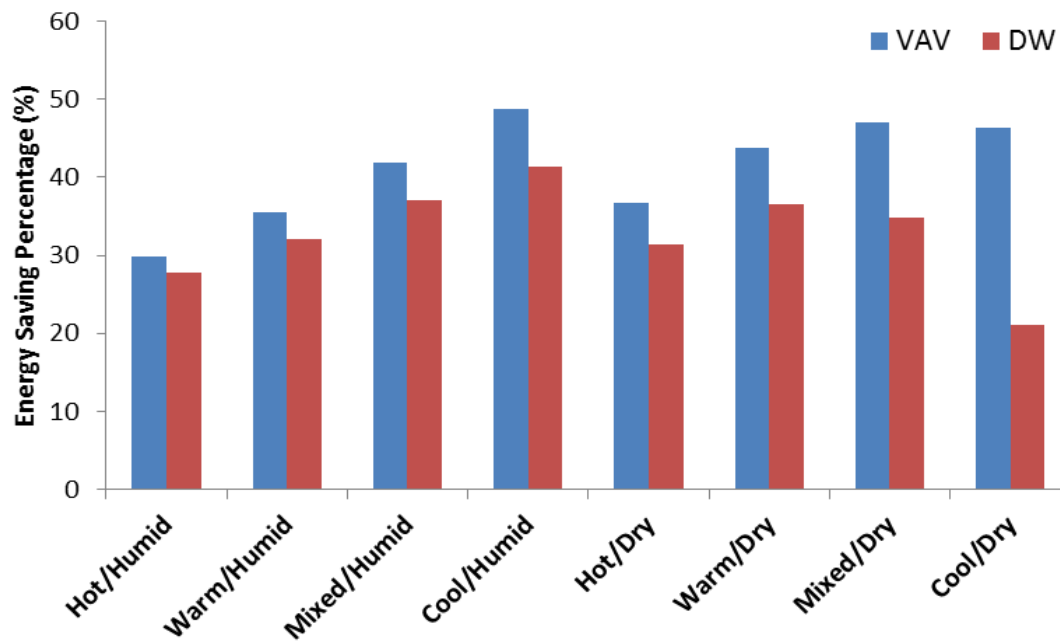
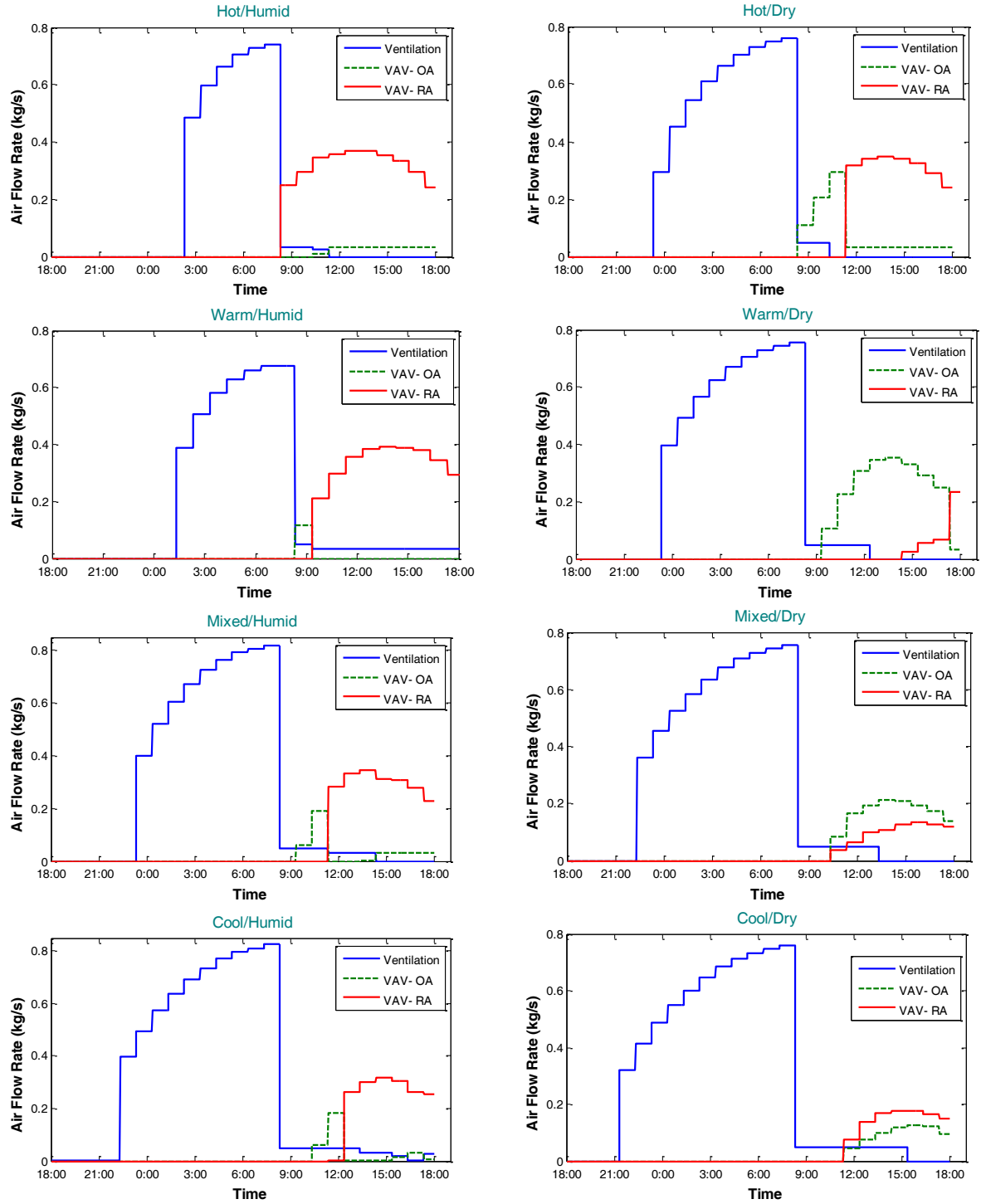


Fig. 5.17 Energy saving potential of the optimized operation under different climate conditions



(South Zone)

Fig. 5.18 Optimal air flow rate profiles for the VAV operations in different climate regions

The resulting optimal air flow rate profiles for the VAV operations in different climate regions are displayed in Fig. 5.18. It can be seen that various optimal operation strategies are derived for different climate types. In cooler weather conditions, PCV starts earlier to make better use of the outdoor cooling sources. It is also noted that the amount of OA introduced in the dry weather conditions is much more than that in the humid conditions. This is mainly because of the low humidity level of the outdoor condition, which may lead to a reduced latent load of the system. Such conclusions also apply for the optimal DW operations.

CHAPTER 6 CONCLUSIONS

6.1 Contributions

This thesis presents a systematic approach to address the dynamic optimization of the integrated active-passive strategies for building enthalpy control. More specifically:

- Develop a method to generate a differential-algebraic equations (DAEs) based physical model, by integrating a number of advanced sub-models and coupling with the high-order building energy simulations.
- Analyze the integrated active-passive operation from the process operation's point of view, and formulate it as process dynamic optimization problem.
- Introduce a powerful tool to analyze the complex integrated operations, i.e., the dynamic optimization using simultaneous collocation method.
- Interpret the optimization results from building physics perspectives to obtain in-depth understanding on the capability and applicability of the developed optimization approach in the architectural engineering fields.

The developed approach can improve the energy efficiency of the integrated building enthalpy control systems, and facilitate and supervise its design and evaluation, by:

- Making more effective use of the information on the dynamic response properties of the building system, the cooling and dehumidification features of the active air conditioning

system, and the diverse variations of the building boundary conditions over the whole operation process.

- Properly addressing the cooperation between the active-passive building enthalpy control approaches, and the numerous parameter conflicts in the integrated operations.

The method described in the thesis can be generalized to be applied to the operation design of building systems with different configurations.

6.2 Summary of Findings

The major findings achieved through the thesis work can be summarized as:

- A RTS/CTS based reduced-order model can be developed with the support of high-order building energy simulations and co-simulation programs. After the calibration procedure, the reduced-order model can predict the building thermal performance with a high level of accuracy.
- The integrated active-passive operation can be formulated as a process operation problem, which is able to concurrently address: 1) various dynamic response properties of the building system and mechanical plants, 2) diverse variations of the building boundary conditions over the whole operation process, 3) coupling effect and synergistic influence of the key operational parameters, and 4) numerous parameter conflicts in the integrated active-passive operation.
- The formulated integrated operation problem can be well handled by the advanced dynamic optimization algorithms implementing simultaneous collocation method. After collocation, the dynamic optimization problems are translated to NLP problems with 1605/2181 variables, 1485/2037 equality constraints and 280/248 inequality constraints for the daily integrated VAV/DW operation for a case zone, respectively. In the GAMS platform, IPOPT is able to solve the problems to optimality within minutes on an 8-core 64-bit desktop, which illustrates the efficiency of the problem formulation.
- The developed approach can highly improve the energy performance of the integrated active-passive operations, while maintaining acceptable indoor thermal comfort.

Compared to the conventional local control strategies, the optimized strategies can lead to remarkable energy saving percentages in different climate conditions: 29.77~48.76% for VAV and 27.85~41.33% for DW.

- The energy saving is contributed by the improvement of both the passive strategies and active strategies: the former contributes to around 33% of the energy saving while the latter contributes to around 67%.
- The constraint of PPD defined in the optimization limits further reduction of the energy consumption. The total optimal energy consumption drops by around 3% if the value of the PPD limit is increased by one unit between 5~15%.
- The developed approach can well handle the perturbations in the realistic weather conditions and work effectively in obtaining the optimal operation strategies. The fitted periodic data can lead to similar operation strategies in the dynamic optimization as the realistic weather data, and therefore can be a reasonable alternative when the more detailed realistic weather data is not available.

6.3 Future Work

The following additional research can be conducted based on the achievements of the thesis:

- Include more advanced building/system components in the physical model

The thesis implemented typical configurations in both the building and air conditioning systems. But a number of more advanced techniques are available, e.g., the phase change materials and the thermal storage system. The use of these technologies will change the response properties, dynamic hygrothermal behavior and energy performance of the building energy system, and may lead to further energy saving potentials by implementing the approach of this thesis.

- Consider the process disturbances in the dynamic optimization

In the dynamic optimization formulation, it is assumed that the building operational conditions and boundary conditions are ideally known. In reality, there exist several sources of process disturbances, such as the variability of the occupancy/lighting/equipment schedules, and the errors in the outdoor temperature/humidity level predictions. In some cities, real-time energy pricing policies are implemented, which can influence the building system operation strategies. These issues can be further studied.

- Consider the performance of the local control systems

The integrated operation design is conducted at the supervisory control level in the thesis, assuming ideal performance of the locally control components (such as fans and pumps). In reality, the capacity and controllability of these components may limit the implementation of

the optimal schedules and thus affect the energy saving. The consideration of the process disturbances as well as the local control performance can support the formulation of an on-line optimization problem based on the off-line work presented in the thesis.

- Introduce more evaluation indices in the operational design

The performance of the integrated active-passive operations can be evaluated from several other aspects besides its energy performance, such as its environmental impacts and its influence on the occupant productivity. Therefore, more evaluation indices can be introduced to the presented work according to the research interests.

- Add the chiller plant loops in the physical model development

The performance of the chiller plant loops and the corresponding local control systems are not considered in the physical model development in the thesis. The addition of the plant loop model in the dynamic optimization may lead to even higher energy saving potentials.

APPENDICES

Appendix 1 Empirical model coefficients of the implemented active desiccant wheel

$v_{nom} = 2.5;$	$TC5 = -0.105014122001509;$	$QC11 = -6.66122876558634;$
$WC0 = 0.0148880824323806;$	$TC6 = -229.668673645144;$	$QC12 = -349102295.417547;$
$WC1 = -0.000283393198398211;$	$TC7 = -0.015424703743461;$	$QC13 = 83672.179730172;$
$WC2 = -0.87802168940547;$	$TC8 = -69440.0689831847;$	$QC14 = -6059524.33170538;$
$WC3 = -0.000713615831236411;$	$TC9 = -1.6686064694322;$	$QC15 = 1220523.39525162;$
$WC4 = 0.0311261188874622;$	$TC10 = 38.5855718977592;$	$RC0 = -4.67358908091488;$
$WC5 = 1.51738892142485e-06;$	$TC11 = 0.000196395381206009;$	$RC1 = 0.0654323095468338;$
$WC6 = 0.0287250198281021;$	$TC12 = 386.179386548324;$	$RC2 = 396.950518702316;$
$WC7 = 4.94796903231558e-06;$	$TC13 = -0.801959614172614;$	$RC3 = 1.52610165426736;$
$WC8 = 24.0771139652826;$	$TC14 = -3.33080986818745;$	$RC4 = -11.3955868430328;$
$WC9 = 0.000122270283927978;$	$TC15 = -15.2034386065714;$	$RC5 = 0.00520693906104437;$
$WC10 = -0.0151657189566474;$	$QC0 = -27794046.6291107;$	$RC6 = 57.783645385621;$
$WC11 = 3.91641393230322e-08;$	$QC1 = -235725.171759615;$	$RC7 = -0.000464800668311693;$
$WC12 = 0.126032651553348;$	$QC2 = 975461343.331328;$	$RC8 = -5958.78613212602;$
$WC13 = 0.000391653854431574;$	$QC3 = -686069.373946731;$	$RC9 = -0.205375818291012;$
$WC14 = 0.002160537360507;$	$QC4 = -17717307.3766266;$	$RC10 = 5.26762675442845;$
$WC15 = 0.00132732844211593;$	$QC5 = 31482.2539662489;$	$RC11 = -8.88452553055039e-05;$
$TC0 = -38.7782841989449;$	$QC6 = 55296552.8260743;$	$RC12 = -182.382479369311;$
$TC1 = 2.0127655837628;$	$QC7 = 6195.36070023868;$	$RC13 = -0.100289774002047;$
$TC2 = 5212.49360216097;$	$QC8 = -8304781359.40435;$	$RC14 = -0.486980507964251;$
$TC3 = 15.2362536782665;$	$QC9 = -188987.543809419;$	$RC15 = -0.972715425435447.$
$TC4 = -80.4910419759181;$	$QC10 = 3933449.40965846;$	

Note:

- Process air inlet dry-bulb temperature range: 1.7°C~48.9°C;
- Process air inlet humidity ratio range: 0.002857 kg_w/kg_{air} ~0.02857 kg_w/kg_{air}.

Appendix 2 Empirical model coefficients of the implemented enthalpy recovery wheel

$V_{nom} = 1.90;$	$BE5 = -5.08E+01;$	$CE4 = -6.34E+00;$
$v_{nom} = 3.54;$	$BE6 = -1.68E-02;$	$CE5 = 9.38E-03;$
$Q_{nom} = 50.0;$	$BE7 = 5.82E+01;$	$CE6 = 5.21E-05;$
$BE1 = -7.18E+00;$	$BE8 = 5.99E-01;$	$CE7 = 6.70E-02;$
$BE2 = -1.85E+02;$	$CE1 = 3.14E-03;$	$CE8 = -1.61E-04;$
$BE3 = 1.00E+00;$	$CE2 = 1.10E+00;$	
$BE4 = 1.16E+04;$	$CE3 = -2.63E-05;$	

Note:

- Process air inlet dry-bulb temperature range: 4.58 °C ~ 21.83 °C;
- Process air inlet humidity ratio range: 0.005000 kg_w/kg_{air} ~ 0.017514 kg_w/kg_{air};
- Exhaust air inlet dry-bulb temperature range: 17.83 °C ~ 48.89 °C;
- Exhaust air inlet humidity ratio range: 0.005143 kg_w/kg_{air} ~ 0.024286 kg_w/kg_{air};
- Nominal face velocity range: 2.286m/s ~ 4.826m/s.

REFERENCES

- Abahri, K., R. Belarbi, and A. Trabelsi. 2011. Contribution to analytical and numerical study of combined heat and moisture transfers in porous building materials. *Building and Environment* 46 (7):1354-1360.
- Ahmed, MH, NM Kattab, and M Fouad. 2005. Evaluation and optimization of solar desiccant wheel performance. *Renewable Energy* 30 (3):305-325.
- Ali, Hikmat H., and Saba F. Al Nsairat. 2009. Developing a green building assessment tool for developing countries – Case of Jordan. *Building and Environment* 44 (5):1053-1064.
- Angrisani, G., A. Capozzoli, F. Minichiello, C. Roselli, and M. Sasso. 2011. Desiccant wheel regenerated by thermal energy from a microcogenerator: Experimental assessment of the performances. *Applied Energy* 88 (4):1354-1365.
- Angrisani, Giovanni, Francesco Minichiello, Carlo Roselli, and Maurizio Sasso. 2010. Desiccant HVAC system driven by a micro-CHP: experimental analysis. *Energy and Buildings* 42 (11):2028-2035.
- Artmann, N., H. Manz, and P. Heiselberg. 2007. Climatic potential for passive cooling of buildings by night-time ventilation in Europe. *Applied Energy* 84 (2):187-201.
- Artmann, N., H. Manz, and P. Heiselberg. 2008. Parameter study on performance of building cooling by night-time ventilation. *Renewable Energy* 33 (12):2589-2598.
- Asan, H. 2006. Numerical computation of time lags and decrement factors for different building materials. *Building and Environment* 41 (5):615-620.
- ASHRAE. 2004. Ventilation for Acceptable Indoor Air Quality. In ANSI/ASHRAE Standard 62.1. Atlanta: American Society of Heating, Refrigeration and Air-Conditioning Engineers, Inc.

- ASHRAE. 2005. Nonresidential cooling and heating load calculations. In ASHRAE Handbook Fundamentals Chapter 30. Atlanta, GA: American Society of Heating, Refrigerating and Air-conditioning Engineers Inc.
- ASHRAE. 2005. Psychrometrics. In ASHRAE Handbook Fundamentals Chapter 6. Atlanta, GA: American Society of Heating, Refrigerating and Air-conditioning Engineers Inc.
- ASHRAE. 2005. Thermal Comfort. In ASHRAE Handbook Fundamentals Chapter 8. Atlanta, GA: American Society of Heating, Refrigerating and Air-conditioning Engineers Inc.
- ASHRAE. 2008. Air-Cooling and Dehumidifying Coils. In HVAC Systems and Equipment Handbook Chapter 22. Atlanta, GA: American Society of Heating, Refrigerating and Air-Conditioning Engineers, Inc.
- ASHRAE. 2008. Desiccant Dehumidification and Pressure-Drying Equipment. In HVAC Systems and Equipment Handbook Chapter 23. Atlanta, GA: American Society of Heating, Refrigerating and Air-Conditioning Engineers, Inc.
- ASHRAE. 2008. Mechanical Dehumidifiers and Related Components. In HVAC Systems and Equipment Handbook Chapter 24. Atlanta, GA: American Society of Heating, Refrigerating and Air-Conditioning Engineers, Inc.
- ASHRAE. 2010. Energy Standard for Buildings Except Low-Rise Residential Buildings. In ANSI/ASHRAE/IES Standard 90.1. Atlanta: American Society of Heating, Refrigeration and Air-Conditioning Engineers, Inc.
- Baechler, Michael C. , Jennifer Williamson, Theresa Gilbride, Pam Cole, and Marye Hefty. 2010. Guide to determining climate regions by county. Pacific Northwest National Laboratory & Oak Ridge National Laboratory.
- Banks, PJ. 1985. Prediction of heat and mass regenerator performance using nonlinear analogy method. I: Basis. Journal of heat transfer 107 (1):222-229.
- Beccali, M., F. Butera, R. Guanella, and R. S. Adhikari. 2003. Simplified models for the performance evaluation of desiccant wheel dehumidification. International Journal of Energy Research 27 (1):17-29.

- Bernal, Willy, Madhur Behl, Truong X. Nghiem, and Rahul Mangharam. 2012. MLE+: a tool for integrated design and deployment of energy efficient building controls. In Proceedings of the Fourth ACM Workshop on Embedded Sensing Systems for Energy-Efficiency in Buildings. Toronto, Ontario, Canada: ACM.
- Biegler, L. T., and S. Kameswaran. 2006. Simultaneous dynamic optimization strategies: Recent advances and challenges. *Computers and Chemical Engineering* 30 (10-12):1560-75.
- Biegler, L.T., ed. 2010. *Nonlinear Programming: Concepts, Algorithms, and Applications to Chemical Processes*. Philadelphia, PA: Society for Industrial and Applied Mathematics.
- Biegler, Lorenz T. 2007. An overview of simultaneous strategies for dynamic optimization. *Chemical Engineering and Processing: Process Intensification* 46 (11):1043-1053.
- Blondeau, P., M. Spérandio, and F. Allard. 1997. Night ventilation for building cooling in summer. *Solar Energy* 61 (5):327-335.
- Bock, H.G. , and K.J. Plitt. 1984. A multiple shooting algorithm for direct solution of optimal control problems. *Proceedings 9th IFAC World Congress Budapest XLII* (2):243-247.
- Bornehag, CG, J Sundell, and L Hägerhed. 2003. Dampness in dwellings and sick building symptoms among adults: A cross-sectional study on 8918 Swedish homes. Paper read at Proceedings of 7th International Conference on Health Buildings.
- Brandemuehl, MJ, MJ Lepore, and JF Kreider. 1990. Modeling and testing the interaction of conditioned air with building thermal mass. *ASHRAE Transactions* 96 (2):871-875.
- Braun, James E. 1990. Reducing energy costs and peak electrical demand through optimal control of building thermal storage. *ASHRAE Transactions* 96 (2):876-888.
- Breesch, H., and A. Janssens. 2010. Performance evaluation of passive cooling in office buildings based on uncertainty and sensitivity analysis. *Solar Energy* 84 (8):1453-1467.
- Brown, S, I Cole, V Daniel, S King, and C Pearson. 2002. Guidelines for environmental control in cultural institutions.
- BSL. 1999. *BLAST 3.0 Users Manual*. Urbana-Champaign, IL: Building Systems Laboratory, University of Illinois.

- Calvino, Francesco, Maria La Gennusa, Massimo Morale, Gianfranco Rizzo, and Gianluca Scaccianoce. 2010. Comparing different control strategies for indoor thermal comfort aimed at the evaluation of the energy cost of quality of building. *Applied Thermal Engineering* 30 (16):2386-2395.
- Capozzoli, A., P. Mazzei, F. Minichiello, and D. Palma. 2006. Hybrid HVAC systems with chemical dehumidification for supermarket applications. *Applied Thermal Engineering* 26 (8-9):795-805.
- Cerolini, S., M. D'Orazio, C. Di Perna, and A. Stazi. 2009. Moisture buffering capacity of highly absorbing materials. *Energy and Buildings* 41 (2):164-168.
- Charoensupaya, D., and W. M. Worek. 1988. Effect of adsorbent heat and mass transfer resistances on performance of an open-cycle adiabatic desiccant cooling system. *Heat Recovery Systems and CHP* 8 (6):537-548.
- Chong, Adrian , Weili Xu, Chao Ding, and Khee Poh Lam. 2014. Parametric analysis on the performance of various HVAC systems configuration. In *EEB Hub BP3 Task 2.1 Report*. Pittsburgh, PA: Carnegie Mellon University.
- Chung, Jae Dong, Dae-Young Lee, and Seok Mann Yoon. 2009. Optimization of desiccant wheel speed and area ratio of regeneration to dehumidification as a function of regeneration temperature. *Solar Energy* 83 (5):625-635.
- Corgnati, Stefano Paolo, and Andrea Kindinis. 2007. Thermal mass activation by hollow core slab coupled with night ventilation to reduce summer cooling loads. *Building and Environment* 42 (9):3285-3297.
- Crawley, Drury B., Linda K. Lawrie, Frederick C. Winkelmann, W. F. Buhl, Y. Joe Huang, Curtis O. Pedersen, Richard K. Strand, Richard J. Liesen, Daniel E. Fisher, Michael J. Witte, and Jason Glazer. 2001. EnergyPlus: creating a new-generation building energy simulation program. *Energy and Buildings* 33 (4):319-331.
- Cunningham, M. J. 1988. The moisture performance of framed structures—A mathematical model. *Building and Environment* 23 (2):123-135.

- Cunningham, M.J. 1992. Effective penetration depth and effective resistance in moisture transfer. *Building and Environment* 27 (3):379-386.
- Daou, K., RZ Wang, and ZZ Xia. 2006. Desiccant cooling air conditioning: a review. *Renewable and Sustainable Energy Reviews* 10 (2):55-77.
- De Antonellis, Stefano, Cesare Maria Joppolo, and Luca Molinaroli. 2010. Simulation, performance analysis and optimization of desiccant wheels. *Energy and Buildings* 42 (9):1386-1393.
- De Freitas, V. P., V. Abrantes, and P. Crausse. 1996. Moisture migration in building walls—Analysis of the interface phenomena. *Building and Environment* 31 (2):99-108.
- Deru, M, B Griffith, and P Torcellini. 2006. Establishing Benchmarks for DOE Commercial Building R&D and Program Evaluation. California: National Renewable Energy Laboratory.
- DOE. 2011. Buildings Energy Data Book. Washington D.C.: Office of energy efficiency and renewable energy, U.S. Department of Energy.
- DOE. 2013. EnergyPlus Engineering Reference Version 8.0. Washington, D.C.: Department of Energy.
- DOE. 2013. Weather Data for EnergyPlus Energy Simulation. Office of Energy Efficiency and Renewable Energy, Department of Energy, US.
- Duffy, M.J. , M. Hiller , D.E. Bradley, W. Keilholz, and J.W. Thornton. 2009 TRNSYS: features and functionality for building simulation. In Eleventh International IBPSA Conference Glasgow, Scotland
- EIA. 2010. International Energy Outlook 2010. Washington, DC: U.S. Energy Information Administration.
- El Diasty, R., P. Fazio, and I. Budaiwi. 1992. Modelling of indoor air humidity: the dynamic behaviour within an enclosure. *Energy and Buildings* 19 (1):61-73.
- El Diasty, R., P. Fazio, and I. Budaiwi. 1993. The dynamic modelling of air humidity behaviour in a multi-zone space. *Building and Environment* 28 (1):33-51.

- El Diasty, R., P. Fazio, and I. Budaiwi. 1993. Dynamic modelling of moisture absorption and desorption in buildings. *Building and Environment* 28 (1):21-32.
- EnergyStar. Top 12 ways to decrease the energy consumption of your data center. Energy Star 2013. Available from <http://www.energystar.gov/index.cfm>.
- Enshen, Long. 2005. Research on the influence of air humidity on the annual heating or cooling energy consumption. *Building and Environment* 40 (4):571-578.
- EPC. 2010. Directive 2010/31/EU of the European Parliament and of the Council of 19 May 2010 on the energy performance of buildings. *Official Journal of the European Union* L153:13–35.
- Esteban-Bravo, M. 2008. An interior-point algorithm for computing equilibria in economies with incomplete asset markets. *Journal of Economic Dynamics and Control* 32 (3):677-694.
- Evins, Ralph, Philip Pointer, Ravi Vaidyanathan, and Stuart Burgess. 2012. A case study exploring regulated energy use in domestic buildings using design-of-experiments and multi-objective optimisation. *Building and Environment* 54 (0):126-136.
- Fang, Lei, Geo Clausen, and Povl Ole Fanger. 2000. Temperature and humidity: important factors for perception of air quality and for ventilation requirements. *ASHRAE Transactions* 106 (Pt. 2):503-510.
- Fanger, P O, ed. 1970. *Thermal comfort: analysis and applications in environmental engineering*. Copenhagen: Danish Technical Press.
- Feehery, W. F., and P. I. Barton. 1998. Dynamic optimization with state variable path constraints. Paper read at European Symposium on Computer Aided Process Engineering -6. ESCAPE-6, 26-29 May 1996, at UK.
- Fischer, J. C., and C. W. Bayer. 2003. Failing grade for most schools - Report card on humidity control. *ASHRAE Journal* 45 (5):30-39.
- Fisk, William J, Quanhong Lei-Gomez, and Mark J Mendell. 2007. Meta-analyses of the associations of respiratory health effects with dampness and mold in homes. *Indoor Air* 17 (4):284-296.

- Fowler, K. M., and E.M. Rauch. 2006. Sustainable Building Rating Systems. Pacific Northwest National Laboratory.
- Gagge A.P. , A.P. Fobelets, L.G. Berglund. 1994. A standard predictive index of human response to the thermal environment. ASHRAE Transactions 92 (2B).
- Gagliano, A., F. Patania, F. Nocera, and C. Signorello. 2014. Assessment of the dynamic thermal performance of massive buildings. *Energy and Buildings* 72 (0):361-370.
- Ge, T. S., Y. Li, R. Z. Wang, and Y. J. Dai. 2008. A review of the mathematical models for predicting rotary desiccant wheel. *Renewable & Sustainable Energy Reviews* 12 (6):1485-1528.
- Geros, V., M. Santamouris, S. Karatasou, A. Tsangrassoulis, and N. Papanikolaou. 2005. On the cooling potential of night ventilation techniques in the urban environment. *Energy and Buildings* 37 (3):243-257.
- Gondzio, Jacek, and Andreas Grothey. 2007. Parallel interior-point solver for structured quadratic programs: Application to financial planning problems. *Annals of Operations Research* 152:319-339.
- Grossmann, I. 2005. Enterprise-wide optimization: A new frontier in process systems engineering. *Aiche Journal* 51 (7):1846-1857.
- Hamdi, Maher, Gérard Lachiver, and François Michaud. 1999. A new predictive thermal sensation index of human response. *Energy and Buildings* 29 (2):167-178.
- Hameury, Stéphane. 2005. Moisture buffering capacity of heavy timber structures directly exposed to an indoor climate: a numerical study. *Building and Environment* 40 (10):1400-1412.
- Harriman, Lewis G, Dean Plager, and Douglas Kosar. 1999. Dehumidification and cooling loads from ventilation air. *Energy engineering* 96 (6):31-45.
- Hatami, Zahra, Mohammad Hassan Saidi, Masoud Mohammadian, and Cyrus Aghanajafi. 2012. Optimization of solar collector surface in solar desiccant wheel cycle. *Energy and Buildings* 45 (0):197-201.

- Häupl, P., J. Grunewald, H. Fechner, and H. Stopp. 1997. Coupled heat air and moisture transfer in building structures. *International Journal of Heat and Mass Transfer* 40 (7):1633-1642.
- Henninger, Robert H., and Michael J. Witte. 2013. *EnergyPlus Testing with Building Thermal Envelope and Fabric Load Tests from ANSI/ASHRAE Standard 140-2011* Arlington Heights, IL: University of Central Florida.
- IBP. 2012 *Computer Simulation with the WUFI Model*. Holzkirchen, Germany: Fraunhofer Institute for Building Physics.
- ISO. 2005. 7730: Ergonomics of the thermal environment - Analytical determination and interpretation of thermal comfort using calculation of the PMV and PPD indices and local thermal comfort criteria. Switzerland.
- Jeong, Jae-Weon, and Stanley A. Mumma. 2005. Practical thermal performance correlations for molecular sieve and silica gel loaded enthalpy wheels. *Applied Thermal Engineering* 25 (5–6):719-740.
- Kameswaran, Shivakumar, and Lorenz Biegler. 2008. Convergence rates for direct transcription of optimal control problems using collocation at Radau points. *Computational Optimization and Applications* 41 (1):81-126.
- Karaguzel, Omer T, Rongpeng Zhang, Haopeng Wang, and Khee Poh Lam. 2013. *Instructions for the Web-Based Industry Product Data Acquisition and Schema Mapping Tool*. Pittsburgh, PA: Carnegie Mellon University.
- Karaguzel, Omer T., Rongpeng Zhang, and Khee Poh Lam. 2012. Integrated Simulation Based Design Optimization of Office Building Envelopes for the Minimization of Life Cycle Costs. In *Proceedings of the Second International Conference on Building Energy and Environment (COBEE 2012)*. Boulder, USA.
- Kerestecioglu, A. , M. Swami, R. Dabir, N. Razzaq, and P. Fairey. 1988. *Theoretical and Computational Investigation of Algorithms for Simultaneous Heat and Moisture Transport in Buildings*. Cape Canaveral, FL.

- Kerestecioglu, A., M. Swami, and A. Kamel. 1989. Theoretical and Computational Investigation of Simultaneous Heat and Moisture Transfer in Buildings: Effective Penetration Depth Theory. In ASHRAE Winter Meeting. Atlanta, GA.
- Khudhair, Amar M., and Mohammed M. Farid. 2004. A review on energy conservation in building applications with thermal storage by latent heat using phase change materials. *Energy Conversion and Management* 45 (2):263-275.
- Kishi, R, Y Saijo, A Kanazawa, M Tanaka, T Yoshimura, H Chikara, T Takigawa, K Morimoto, K Nakayama, and E Shibata. 2009. Regional differences in residential environments and the association of dwellings and residential factors with the sick house syndrome: a nationwide cross-sectional questionnaire study in Japan. *Indoor Air* 19 (3):243-254.
- Kolokotroni, M., and A. Aronis. 1999. Cooling-energy reduction in air-conditioned offices by using night ventilation. *Applied Energy* 63 (4):241-253.
- Kolokotroni, M., M. D. Perera, D. Azzi, and G. S. Virk. 2001. An investigation of passive ventilation cooling and control strategies for an educational building. *Applied Thermal Engineering* 21 (2):183-199.
- Kosar, D. 2006. Dehumidification system enhancements. *ASHRAE Journal* 48 (2):48-58.
- Kosny, Jan, Elisabeth Kossecka, Andre O Desjarlais, and Jeffrey E Christian. 1998. Dynamic thermal performance of concrete and masonry walls. *Proceedings, Thermal Performance of the Exterior Envelopes of Buildings VII*:629-643.
- Künzel, H. M. 1995. Simultaneous Heat and Moisture Transport in Building Components. PhD Dissertation, Fraunhofer Institute of Building Physics, Holzkirchen, Germany.
- Künzel, H. M., A. Holm, D. Zirkelbach, and A. N. Karagiozis. 2005. Simulation of indoor temperature and humidity conditions including hygrothermal interactions with the building envelope. *Solar Energy* 78 (4):554-561.
- Kuznik, Frédéric, Joseph Virgone, and Jean Noel. 2008. Optimization of a phase change material wallboard for building use. *Applied Thermal Engineering* 28 (11-12):1291-1298.

- La, D., Y. J. Dai, Y. Li, T. S. Ge, and R. Z. Wang. 2010. Study on a novel thermally driven air conditioning system with desiccant dehumidification and regenerative evaporative cooling. *Building and Environment* 45 (11):2473-2484.
- Lam, Khee Poh, Stephen R Lee, Gregory M Dobbs, CQ Zhai, and YC Huang. 2005. Simulation of the Effect of an Energy Recovery Ventilator on Indoor Thermal Conditions and System Performance. Paper read at Ninth International IBPSA Conference, edited by I Beausoleil-Morrison and M Bernier.
- Lapinskiene, Vilune, and Vytautas Martinaitis. 2013. The Framework of an Optimization Model for Building Envelope. *Procedia Engineering* 57 (0):670-677.
- LBNL. 2012. ENERGYPLUS™ Energy Management System User Guide. Berkeley, CA: Lawrence Berkeley National Laboratory.
- Lee, Jeong Hoe. 2007. Optimization of indoor climate conditioning with passive and active methods using GA and CFD. *Building and Environment* 42 (9):3333-3340.
- Lengsfeld, Kristin, Andreas Holm, and Martin Krus. 2007. Moisture-buffering effect - Experimental investigations and validation. Paper read at 6th International Conference on Indoor Air Quality, Ventilation and Energy Conservation in Buildings: Sustainable Built Environment, IAQVEC 2007, October 28, 2007 - October 31, 2007, at Sendai, Japan.
- Levermore, G. J. 2000. *Building Energy Management Systems: Applications to Low-energy HVAC and Natural Ventilation Control*. New York, NY: E & FN Spon.
- Li, Kangji, Wenping Xue, Chao Xu, and Hongye Su. 2013. Optimization of ventilation system operation in office environment using POD model reduction and genetic algorithm. *Energy and Buildings* 67 (0):34-43.
- Li, Yang, Paul Fazio, and Jiwoo Rao. 2012. An investigation of moisture buffering performance of wood paneling at room level and its buffering effect on a test room. *Building and Environment* 47 (1):205-216.

- Li, Yang, Paul Fazio, and Jiwu Rao. 2012. An investigation of moisture buffering performance of wood paneling at room level and its buffering effect on a test room. *Building and Environment* 47 (0):205-216.
- Liesen, R.J. . 1994. Development of a Response Factor Approach for Modeling the Energy Effects of Combined Heat and Mass Transfer with Vapor Adsorption in Building Elements, Mechanical Engineering Department, University of Illinois, Champaign, IL.
- Lin, Weijie. 2011. Modeling and Optimization of a Semi-Interpenetrating Polymer Network Process, Carnegie Mellon University, Pittsburgh, Pennsylvania, USA.
- Lund, Berit Floor, and Bjarne A. Foss. 2008. Parameter ranking by orthogonalization—Applied to nonlinear mechanistic models. *Automatica* 44 (1):278-281.
- Ma, Peizheng, and Lin-Shu Wang. 2012. Effective heat capacity of exterior Planar Thermal Mass (ePTM) subject to periodic heating and cooling. *Energy and Buildings* 47 (0):394-401.
- Ma, Peizheng, and Linshu Wang. 2012. Effective heat capacity of interior planar thermal mass (iPTM) subject to periodic heating and cooling. *Energy and Buildings* 47 (0):44-52.
- Ma, Zhenjun, Paul Cooper, Daniel Daly, and Laia Ledo. 2012. Existing building retrofits: Methodology and state-of-the-art. *Energy and Buildings* 55 (0):889-902.
- MacLaine-Cross, IL, and PJ Banks. 1972. Coupled heat and mass transfer in regenerators—prediction using an analogy with heat transfer. *International Journal of Heat and Mass Transfer* 15 (6):1225-1242.
- Majumdar, P, and WM Worek. 1989. Combined heat and mass transfer in a porous adsorbent. *Energy* 14 (3):161-175.
- Majumdar, P., and W. M. Worek. 1989. Combined heat and mass transfer in a porous adsorbent. *Energy* 14 (3):161-175.
- MathWorks. 2013. MATLAB Tutorial. Natick, MA: The MathWorks, Inc.
- MathWorks. 2013. Optimization Toolbox™ User's Guide Natick, MA: The MathWorks, Inc.
- Mazzei, P., F. Minichiello, and D. Palma. 2005. HVAC dehumidification systems for thermal comfort: a critical review. *Applied Thermal Engineering* 25 (5-6):677-707.

- McQuiston, Faye C , Jerald D Parker, and Jeffery D Spitler. 2005. Heating, Ventilating and Air Conditioning Analysis and Design. John Wiley & Sons, Inc.
- Mendes, N., F. C. Winkelmann, R. Lamberts, and P. C. Philippi. 2003. Moisture effects on conduction loads. *Energy and Buildings* 35 (7):631-644.
- Nia, F. E., D. van Paassen, and M. H. Saidi. 2006. Modeling and simulation of desiccant wheel for air conditioning. *Energy and Buildings* 38 (10):1230-1239.
- NIBS. 2007. National Building Information Modeling Standard Part 1: Overview, Principles, and Methodology. National Institute of Building Sciences.
- Nie, Yisu, Lorenz T. Biegler, and John M. Wassick. 2012. Integrated scheduling and dynamic optimization of batch processes using state equipment networks. *Aiche Journal* 58 (11):3416-3432.
- Niu, J. L., and L. Z. Zhang. 2002. Effects of wall thickness on the heat and moisture transfers in desiccant wheels for air dehumidification and enthalpy recovery. *International Communications in Heat and Mass Transfer* 29 (2):255-268.
- Ogoli, David Mwale. 2003. Predicting indoor temperatures in closed buildings with high thermal mass. *Energy and Buildings* 35 (9):851-862.
- Pfafferott, Jens, Sebastian Herkel, and Martina Jäschke. 2003. Design of passive cooling by night ventilation: evaluation of a parametric model and building simulation with measurements. *Energy and Buildings* 35 (11):1129-1143.
- Poel, Bart, Gerelle van Cruchten, and Constantinos A. Balaras. 2007. Energy performance assessment of existing dwellings. *Energy and Buildings* 39 (4):393-403.
- Qin, Menghao, Rafik Belarbi, Abdelkarim Aït-Mokhtar, and Francis Allard. 2009. Simulation of coupled heat and moisture transfer in air-conditioned buildings. *Automation in Construction* 18 (5):624-631.
- Rhodes, Clyde L. 1996. The process simulation revolution: Thermophysical property needs and concerns. *Journal of Chemical & Engineering Data* 41 (5):947-950.

- Rode, Carsten, Ruut Peuhkuri, Berit Time, Kaisa Svennberg, and Tuomo Ojanen. 2007. Moisture buffer value of building materials. ASTM Special Technical Publication 1495:33-44.
- Rosenthal, Richard E. 2012. GAMS - A User's Guide. Washington DC, USA: GAMS Development Corporation.
- San, Jung-Yang. 1993. Heat and mass transfer in a two-dimensional cross-flow regenerator with a solid conduction effect. International Journal of Heat and Mass Transfer 36 (3):633-643.
- Sato, Mikiya, Shingo Fukayo, and Eiji Yano. 2003. Adverse environmental health effects of ultra-low relative humidity indoor air. Journal of occupational health 45 (2):133-136.
- Schlegel, Martin, Klaus Stockmann, Thomas Binder, and Wolfgang Marquardt. 2005. Dynamic optimization using adaptive control vector parameterization. Computers and Chemical Engineering 29 (8):1731-1751.
- Sheikhi, A., A. M. Ranjbar, and H. Oraee. 2012. Financial analysis and optimal size and operation for a multicarrier energy system. Energy and Buildings 48:71-78.
- Simonson, Carey J, and Robert W Besant. 1997. Heat and moisture transfer in desiccant coated rotary energy exchangers: Part I. Numerical model. HVAC&R Research 3 (4):325-350.
- Slayzak, Steven J, and Joseph P Ryan. 2000. Desiccant dehumidification wheel test guide: National Renewable Energy Laboratory.
- Smolka, Jacek. 2013. Genetic algorithm shape optimisation of a natural air circulation heating oven based on an experimentally validated 3-D CFD model. International Journal of Thermal Sciences 71 (0):128-139.
- Snyder, ME, and TA Newell. 1990. Cooling cost minimization using building mass for thermal storage. ASHRAE Transactions (American Society of Heating, Refrigerating and Air-Conditioning Engineers);(United States) 96 (CONF-9006117--).

- Sphaier, L. A., and W. M. Worek. 2004. Analysis of heat and mass transfer in porous sorbents used in rotary regenerators. *International Journal of Heat and Mass Transfer* 47 (14-16):3415-3430.
- Sphaier, LA, and WM Worek. 2004. Analysis of heat and mass transfer in porous sorbents used in rotary regenerators. *International Journal of Heat and Mass Transfer* 47 (14):3415-3430.
- Spitler, Jeffrey D., and Daniel E. Fisher. 2000. On the relationship between the Radiant Time Series and Transfer Function Methods for design cooling load calculations. Paper read at 2000 ASHRAE Winter Meeting, Feb 5 - Feb 9 2000, at Dallas, TX, United states.
- Spitler, Jeffrey D., Daniel E. Fisher, and Curtis O. Pedersen. 1997. Radiant time series cooling load calculation procedure. Paper read at Proceedings of the 1997 ASHRAE Annual Meeting, June 28, 1997 - July 2, 1997, at Boston, MA, USA.
- Spitler, Jeffrey D., and Bereket A. Nigusse. 2010. Refinements and improvements to the radiant time series method. Paper read at 2010 ASHRAE Winter Conference, January 23, 2010 - January 27, 2010, at Orlando, FL, United states.
- Steeman, H. J., A. Janssens, J. Carmeliet, and M. De Paepe. 2009. Modelling indoor air and hygrothermal wall interaction in building simulation: Comparison between CFD and a well-mixed zonal model. *Building and Environment* 44 (3):572-583.
- Tariku, Fitsum, Kumar Kumaran, and Paul Fazio. 2010. Integrated analysis of whole building heat, air and moisture transfer. *International Journal of Heat and Mass Transfer* 53 (15-16):3111-3120.
- Tariku, Fitsum, Kumar Kumaran, and Paul Fazio. 2011. Determination of indoor humidity profile using a whole-building hygrothermal model. *Building Simulation* 4 (3):277-277.
- Thornton, B.A., M.I. Rosenberg, E.E. Richman, W. Wang, Y. Xie, J.L. Zhang, and H. Cho. 2011. Energy and Cost savings of ASHRAE Standard 90.1-2010. Richland, WA: PNNL.

- Vu, Dinh-Hieu, Kuen-Sheng Wang, Bui Hoang Bac, and Bui Xuan Nam. 2013. Humidity control materials prepared from diatomite and volcanic ash. *Construction and Building Materials* 38 (0):1066-1072.
- Wächter, Andreas, and Lorenz T. Biegler. 2006. On the implementation of an interior-point filter line-search algorithm for large-scale nonlinear programming. *Mathematical Programming* 106 (1):25-57.
- Wang, Weimin, Radu Zmeureanu, and Hugues Rivard. 2005. Applying multi-objective genetic algorithms in green building design optimization. *Building and Environment* 40 (11):1512-1525.
- Wang, Zhaojun, Lingli Yi, and Fusheng Gao. 2009. Night ventilation control strategies in office buildings. *Solar Energy* 83 (10):1902-1913.
- WBCSD. 2009. *Transforming the Market: Energy Efficiency in Buildings*. World Business Council for Sustainable Development.
- Wetter, Michael 2011. *GenOpt: Generic Optimization Program User Manual*. Berkeley, CA Lawrence Berkeley National Laboratory.
- Wilcox, S. , and W. Marion. 2008. User's Manual for TMY3 Data Sets. In NREL/TP-581-43156. Golden, Colorado: National Renewable Energy Laboratory.
- Winkelmann, F.C. , B.E. Birdsall, W.F. Buhl, K.L. Ellington, A.E. Erdem, J.J. Hirsch, and S. Gates. 1993. DOE-2 Supplement Version 2.1E. Springfield, VA Lawrence Berkeley National Laboratory.
- Woloszyn, Monika, Carsten Rode, Angela Sasic Kalagasidis, Arnold Janssens, and Michel De Paepe. 2009. From EMPD to CFD - Overview of different approaches for heat air and moisture modeling in IEA annex 41. Paper read at 2009 ASHRAE Annual Conference, June 20, 2009 - June 24, 2009, at Louisville, KY, United states.
- Wong, Samuel P. W., and S. K. Wang. 1990. Fundamentals of simultaneous heat and moisture transfer between the building envelope and the conditioned space air. Paper read at 1990 Annual Meeting of the American Society of Heating, Refrigerating and

Air-Conditioning Engineers, Technical and Symposium Papers, June 10, 1990 - June 13, 1990, at St. Louis, MO, USA.

- Wu, Yang, Paul Fazio, and Mavinkal K. Kumaran. 2008. Moisture buffering capacities of five North American building materials. *Journal of Testing and Evaluation* 36 (1):34-40.
- Yam, Jimmy, Yuguo Li, and Zuohuan Zheng. 2003. Nonlinear coupling between thermal mass and natural ventilation in buildings. *International Journal of Heat and Mass Transfer* 46 (7):1251-1264.
- Yan, Da, Jianjun Xia, Waiyin Tang, Fangting Song, Xiaoliang Zhang, and Yi Jiang. 2008. DeST — An integrated building simulation toolkit Part I: Fundamentals. *Building Simulation* 1 (2):95-110.
- Yang, Lina, and Yuguo Li. 2008. Cooling load reduction by using thermal mass and night ventilation. *Energy and Buildings* 40 (11):2052-2058.
- Yang, Xiangjin, Paul Fazio, Hua Ge, and Jiwu Rao. 2012. Evaluation of moisture buffering capacity of interior surface materials and furniture in a full-scale experimental investigation. *Building and Environment* 47 (1):188-196.
- Yao, K Zhen, Benjamin M Shaw, Bo Kou, Kim B McAuley, and DW Bacon. 2003. Modeling Ethylene/Butene Copolymerization with Multi-site Catalysts: Parameter Estimability and Experimental Design. *Polymer Reaction Engineering* 11 (3):563-588.
- Yoshino, H., T. Mitamura, and K. Hasegawa. 2009. Moisture buffering and effect of ventilation rate and volume rate of hygrothermal materials in a single room under steady state exterior conditions. *Building and Environment* 44 (7):1418-1425.
- Zavala, Victor M., Emil M. Constantinescu, Theodore Krause, and Mihai Anitescu. 2009. On-line economic optimization of energy systems using weather forecast information. *Journal of Process Control* 19 (10):1725-1736.
- Zhai, C. 2008. Performance modeling of desiccant wheel design and operation. 3309580, Carnegie Mellon University, Pittsburgh, Pennsylvania, USA.

- Zhai, C., X. Liao, R. Radermacher, K.P. Lam, and V. Hartkopf. 2005. Simulation Analysis of Building Humidity Control and Energy Consumption for Different System Configurations. In Ninth International IBPSA Conference. Montreal, Canada.
- Zhai, Chaoqin, David H Archer, and John C Fischer. 2008. Integration of the Active Desiccant Wheel in CHP System Design. Paper read at ASME 2008 2nd International Conference on Energy Sustainability collocated with the Heat Transfer, Fluids Engineering, and 3rd Energy Nanotechnology Conferences.
- Zhai, Chaoqin, David H. Archer, and Jhon C. Fischer. 2008. Performance Modeling of Desiccant Wheels (1): Model Development. Paper read at Energy Sustainability, August 10-14, at Jacksonville, Florida, USA.
- Zhang, Huibo, Hiroshi Yoshino, and Kenichi Hasegawa. 2012. Assessing the moisture buffering performance of hygroscopic material by using experimental method. *Building and Environment* 48 (0):27-34.
- Zhang, L. Z., and J. L. Niu. 2002. Performance comparisons of desiccant wheels for air dehumidification and enthalpy recovery. *Applied Thermal Engineering* 22 (12):1347-1367.
- Zheng, W, WM Worek, and D Novosel. 1995. Performance optimization of rotary dehumidifiers. *Journal of solar energy engineering* 117 (1).
- Zhou, Junli, Guoqiang Zhang, Yaolin Lin, and Yuguo Li. 2008. Coupling of thermal mass and natural ventilation in buildings. *Energy and Buildings* 40 (6):979-986.
- Zhou, Junli, Guoqiang Zhang, Yaolin Lin, and Hanqing Wang. 2011. A new virtual sphere method for estimating the role of thermal mass in natural ventilated buildings. *Energy and Buildings* 43 (1):75-81.
- Zhu, L., R. Hurt, D. Correia, and R. Boehm. 2009. Detailed energy saving performance analyses on thermal mass walls demonstrated in a zero energy house. *Energy and Buildings* 41 (3):303-310.